

Sampling and Quantization for Optimal Reconstruction

by

Shay Maymon

Submitted to the Department of Electrical Engineering and Computer Science

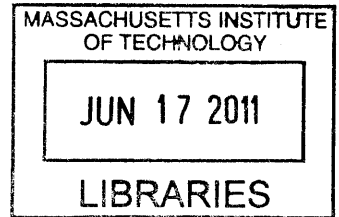
in partial fulfillment of the requirements for the degree of

Doctor of Philosophy in Electrical Engineering

at the

MASSACHUSETTS INSTITUTE OF TECHNOLOGY

June 2011




ARCHIVES

© Massachusetts Institute of Technology 2011. All rights reserved.

Author

Department of Electrical Engineering and Computer Science
May 17, 2011

Certified by ..

 Alan V. Oppenheim
Ford Professor of Engineering
Thesis Supervisor

Accepted by

 Professor Leslie A. Kolodziej
Chairman, Department Committee on Graduate Theses

Sampling and Quantization for Optimal Reconstruction

by

Shay Maymon

Submitted to the Department of Electrical Engineering and Computer Science
on May 17, 2011, in partial fulfillment of the
requirements for the degree of
Doctor of Philosophy in Electrical Engineering

Abstract

This thesis develops several approaches for signal sampling and reconstruction given different assumptions about the signal, the type of errors that occur, and the information available about the signal. The thesis first considers the effects of quantization in the environment of interleaved, oversampled multi-channel measurements with the potential of different quantization step size in each channel and varied timing offsets between channels. Considering sampling together with quantization in the digital representation of the continuous-time signal is shown to be advantageous. With uniform quantization and equal quantizer step size in each channel, the effective overall signal-to-noise ratio in the reconstructed output is shown to be maximized when the timing offsets between channels are identical, resulting in uniform sampling when the channels are interleaved. However, with different levels of accuracy in each channel, the choice of identical timing offsets between channels is in general not optimal, with better results often achievable with varied timing offsets corresponding to recurrent nonuniform sampling when the channels are interleaved. Similarly, it is shown that with varied timing offsets, equal quantization step size in each channel is in general not optimal, and a higher signal-to-quantization-noise ratio is often achievable with different levels of accuracy in the quantizers in different channels.

Another aspect of this thesis considers nonuniform sampling in which the sampling grid is modeled as a perturbation of a uniform grid. Perfect reconstruction from these nonuniform samples is in general computationally difficult; as an alternative, this work presents a class of approximate reconstruction methods based on the use of time-invariant lowpass filtering, i.e., sinc interpolation. When the average sampling rate is less than the Nyquist rate, i.e., in sub-Nyquist sampling, the artifacts produced when these reconstruction methods are applied to the nonuniform samples can be preferable in certain applications to the aliasing artifacts, which occur in uniform sampling. The thesis also explores various approaches to avoiding aliasing in sampling. These approaches exploit additional information about the signal apart from its bandwidth and suggest using alternative pre-processing instead of the traditional linear time-invariant anti-aliasing filtering prior to sampling.

Thesis Supervisor: Alan V. Oppenheim
Title: Ford Professor of Engineering

Acknowledgments

I am fortunate to have had the privilege of being supervised and mentored by Professor Alan Oppenheim, and I am most grateful for his guidance and support throughout the course of this thesis. Working with Al has been an invaluable experience for me; I have benefited tremendously from his dedication to my intellectual and personal growth. Encouraging me to unconventional thinking and to creativity, stimulating me, and providing me with unlimited freedom, he has made this journey enjoyable and rewarding. I look forward to collaborating with him in the future.

I wish to express my warm and sincere thanks to Professor Ehud Weinstein of Tel-Aviv University. I had a unique opportunity of working with Udi while co-teaching the graduate level course "Detection and Estimation Theory," when we also collaborated on several research problems. Working and interacting with him has been invaluable to my development personally, professionally, and academically: Udi has become my friend and mentor.

I would also like to express my sincere appreciation to Professors Vivek Goyal and Lizhong Zheng for serving as readers on the thesis committee and for their valuable comments and suggestions throughout this thesis work.

I am grateful to have been part of the Digital Signal Processing Group (DSPG) at MIT. For providing a stimulating and enjoyable working environment, I would like to acknowledge past and present members of DSPG: Tom Baran, Ballard Blair, Petros Boufounos, Sefa Demirtas, Sourav Dey, Dan Dudgeon, Xue Feng, Zahi Karam, John Paul Kitchens, Jeremy Leow, Joseph McMichael, Martin McCormick, Milutin Pajovic, Charles Rohrs, Melanie Rudoy, Joe Sikora, Archana Venkataraman, and Dennis Wei. The intellectual atmosphere of the group as well as the willingness to share ideas and to collaborate on research problems has made it a very exciting and enriching experience. Special thanks to Eric Strattman and Kathryn Fischer for providing administrative assistance, for running the group smoothly and efficiently, and for always being friendly and willing to help.

No words can fully convey my gratitude to my family. I am deeply grateful to my parents for their ever present love, their support throughout my education, and their encouraging me to strive for the best. I sincerely thank my sisters, brother, nephews, and nieces for the continuous love and support. I appreciate my wife's family for their care and encouragement. Finally, my deep gratitude to my best friend and wife, Keren, for her many sacrifices during the last four years, unconditional love, boundless patience, encouragement, and for being there for me every step in the way. Ending my doctoral training and looking forward with Keren to our new roles as parents, I am as excited about earning the title ABBA as I am about receiving my Ph.D.

The Thesis Ends;

Research Continues Forever

Contents

1	Introduction	19
1.1	Background	19
1.1.1	Sampling Theory - A Historical Overview	19
1.1.2	Extensions of the Sampling Theorem	20
1.1.3	Error and Aliasing	25
1.2	Objectives	27
1.3	Outline	28
2	Perfect Reconstruction in Multi-channel Nonuniform Sampling	29
2.1	Introduction	29
2.2	Multi-channel Sampling and Reconstruction	31
2.2.1	Perfect Reconstruction	33
2.2.2	Optimal Reconstruction in the Presence of Quantization Error	38
2.2.3	Optimal Signal-to-Quantization-Noise Ratio (SQNR)	45
2.2.4	Simulations	50
2.3	Differential Uniform Quantization	57
3	MMSE Reconstruction in Multi-channel Nonuniform Sampling	63
3.1	Reconstruction Error	63
3.2	Optimal Reconstruction Filters	66
3.2.1	Optimal Reconstruction for the Case of Uniform Sampling	68
3.3	Illustrative Examples & Simulations	69

4	Sinc Interpolation of Nonuniform Samples	75
4.1	Introduction	75
4.2	Reconstruction of Bandlimited Signals from Nonuniform Samples	77
4.3	Sinc Interpolation of Nonuniform Samples	79
4.3.1	Mathematical Formulation	80
4.3.2	Randomized Sinc Interpolation	82
4.3.3	Uniform Sinc Interpolation	83
4.3.4	Nonuniform Sinc Interpolation	86
4.3.5	Independent Sinc Interpolation	86
4.3.6	RSI - Minimum Mean Square Reconstruction Error	88
4.3.7	Discussion	91
5	Timing Errors in Discrete-time Processing of Continuous-time Signals	93
5.1	Introduction	93
5.2	The Effects of Timing Errors in Discrete-time Processing of Continuous-time Signals	95
5.3	Jitter Compensation	99
6	Sub-Nyquist Sampling - Aliasing Mitigation	101
6.1	Introduction	101
6.2	Sinc Interpolation of sub-Nyquist Samples	103
6.2.1	Randomized Sinc Interpolation	103
6.2.2	Uniform Sinc Interpolation	104
6.2.3	Nonuniform Sinc Interpolation	105
6.2.4	Independent Sinc Interpolation	107
6.3	Simulations	108
7	Sub-Nyquist Sampling & Aliasing	111
7.1	Introduction	111
7.2	Sampling a Non-negative Bandlimited Signal	111
7.2.1	Bandlimited Square-roots	113

7.2.2	Signals with Real Bandlimited Square-roots	116
7.2.3	Nonlinear Anti-aliasing	118
7.2.4	Generalization	126
7.3	Inphase and Quadrature Anti-aliasing	127
7.3.1	Inphase and Quadrature Decomposition	127
7.3.2	IQ Anti-aliasing	130
7.4	Co-sampling	134
7.4.1	Perfect Reconstruction	135
7.4.2	Blind Co-sampling	137
Appendices		139
A Optimal Constrained Reconstruction filters		141
B Derivation of $S_{ee}(e^{j\omega})$		143
C Optimal MMSE Reconstruction Filters		149
D Randomized Sinc Interpolation - MSE Derivation		151
E The Autocorrelation Function of a Bandlimited Signal		153
F Time Jitter in Discrete-time Processing of Continuous-time Signals		155
G Randomized Sinc Interpolation - Sub-Nyquist Sampling		159

List of Figures

2-1	Multi-channel sampling.	32
2-2	Interleaving the output samples of the multi-channel sampling system of Figure 2-1 obtains either uniform or recurrent nonuniform sampling.	32
2-3	An example of recurrent nonuniform sampling of $x(t)$ where $M = 3$ and $L = 2$	32
2-4	Multi-channel reconstruction.	33
2-5	Interleaving followed by sampling rate conversion.	34
2-6	Multi-channel sampling rate conversion.	35
2-7	Multi-channel sampling and quantization.	38
2-8	Single channel in the reconstruction system of Figure 2-4.	39
2-9	The k^{th} branch of the polyphase implementation of the system in Figure 2-4.	42
2-10	The reduction factor γ in the average noise power at the output of the reconstruction of Figure 2-4 achieves its maximum value at $\tau_1 = -\tau_2 = \pm(2/3) \cdot T_N$, i.e., when the multi-channel sampling is equivalent to uniform sampling. Since this curve is based on the additive noise model of the quantization error, which assumes uncorrelated errors, it is less accurate in the vicinity of $\tau_1 = 0$, $\tau_2 = 0$, and $\tau_1 = \tau_2$	51
2-11	The reduction factor γ in the average noise power at the output of the reconstruction system of Figure 2-4 where actual quantizers are applied to the multi-channel output samples with accuracy of 10 bits.	52

2-12	Each vector represents a channel whose time delay τ_m is determined by the vector's phase ω_m according to the transformation $\omega_m = 2\pi\tau_m/(LT_N)$, which maps the region $\tau_m \in [-T_N, T_N]$ into the region $\omega_m \in [-\pi, \pi]$. The numbers associated with each of the vectors are the optimal bit allocations for the case of $\tau_0 = 0$, $\tau_1 = T_N/8$, and $\tau_2 = -3T_N/4$	54
2-13	With bit allocation $N_0 = 3$, $N_1 = 4$, and $N_2 = 4$, the optimal choice of time delays is $\tau_1 = -\tau_2 = \pm 0.54T_N$, for which the multi-channel sampling system is equivalent to recurrent nonuniform sampling.	54
2-14	The relative performance compared to uniform sampling as a function of τ_1 and τ_2 when $\tau_0 = 0$, $N_0 = 3$, $N_1 = 4$, and $N_2 = 4$. Since this curve is based on the additive noise model of the quantization error, which assumes uncorrelated errors, it is less accurate in the vicinity of $\tau_1 = 0$, $\tau_2 = 0$, and $\tau_1 = \tau_2$	55
2-15	Optimal time delays for different choices of N_2 (a) based on the additive noise model, (b) based on simulations with actual quantizers.	56
2-16	Block diagram of differential quantization: coder and decoder.	58
3-1	Optimal reconstruction is equivalent to interleaving of the multi-channel samples followed by Wiener filtering.	69
3-2	Interleaving followed by sampling rate converter and Wiener filtering.	73
3-3	The relative gain of $d(\omega_1, \omega_2)$ as compared to the case of uniform sampling when $N_0 = 3$, $N_1 = 4$, $N_2 = 4$	74
4-1	Reconstruction using sinc interpolation.	81
4-2	A second-order statistics model for nonuniform sampling followed by Randomized Sinc Interpolation for the case where $T \leq T_N$	82
4-3	$Q(\Omega)$ for the case where $\xi_n \sim u[-T/2, T/2]$ and $T = T_N = 1$	91
4-4	The optimal choice of β that minimizes σ_{eR}^2 as a function of B_x for the case where $T = T_N = 1$	91
5-1	Discrete-time processing of continuous-time signals.	93

5-2	Time jitter in discrete-time processing of continuous-time signals.	95
5-3	A second-order statistics model for the system of Figure 5-2.	96
5-4	A second-order statistics model for the system of Figure 5-2 with $G(e^{j\omega}) = G(\frac{\omega}{T})$, $ \omega < \pi$ and where $\xi_n = 0$	98
5-5	A second-order statistics model for the system of Figure 5-2 with $G(e^{j\omega}) = G(\frac{\omega}{T})$, $ \omega < \pi$ and where $\zeta_n = 0$	98
6-1	Anti-aliasing followed by nonuniform sampling and Lagrange interpolation.	102
6-2	Reconstruction from nonuniform samples for the case $T > T_N$ using sinc interpolation.	103
6-3	A second-order-statistics equivalent of nonuniform sampling followed by Uniform Sinc Interpolation for the case where $T > T_N$	105
6-4	A second-order-statistics equivalent of nonuniform sampling followed by Nonuniform Sinc Interpolation for the case where $T > T_N$	106
6-5	A second-order-statistics equivalent of nonuniform sampling followed by Independent Sinc Interpolation for the case where $T > T_N$	107
6-6	Pole-zero diagram of the transfer function $H_c(s)$	108
6-7	Artifacts with sub-Nyquist sampling. (a) The estimated power spectrum of $x(t)$. The estimated power spectrum vs. analytic results in the case of (b) Uniform Sampling, (c) USI applied to nonuniform sampling, (d) NSI applied to nonuniform sampling, and (e) ISI applied to nonuniform sampling. (f) The estimated power spectrum of $x(t)$ and of its approximations.	110
7-1	A sampling-reconstruction scheme of a non-negative bandlimited signal. The sampling system consists of non-linear pre-processing whose output signal $x(t)$ is bandlimited to $\pm\pi/T$ and satisfies the relation $y(t) = x(t) ^2$	112
7-2	The region within which all possible $ Y(\Omega) $ that satisfy (7.21) lie.	117
7-3	Non-linear anti-aliasing.	118
7-4	The frequency response $H(\Omega)$ of the LTI system in Figure 7-3.	119

7-5	Complex anti-aliasing applied to $y(t)$ from (7.35) where $a = -\pi/2$ and $\Omega_x = \pi/T$. (a) The spectrums of the complex bandlimited square roots. (b) The partial energies of the complex bandlimited square roots. (c) The frequency responses of $y(t)$ and of its approximations $\hat{y}(t) = \hat{x}(t) ^2$ where the cut-off frequency of $H(\Omega)$ is $\gamma = \pi/(2T)$. (d) The frequency responses of $y(t)$ and of its approximations $\hat{y}(t) = \hat{x}(t) ^2$ where the cut-off frequency of $H(\Omega)$ is $\gamma = \pi/(4T)$	123
7-6	An example for which the bandwidth of $y(t)$ is equal to the sum of the bandwidths of $x_1(t)$ and $x_2(t)$	126
7-7	An example for which the bandwidth of $y(t)$ is greater than the sum of the bandwidths of $x_1(t)$ and $x_2(t)$	126
7-8	An example for which the bandwidth of $y(t)$ is less than the sum of the bandwidths of $x_1(t)$ and $x_2(t)$	126
7-9	Decomposing $Y(\Omega)$ into $Y_1(\Omega)$ and $Y_2(\Omega)$	129
7-10	Iterative decomposition of $y(t)$ into its inphase and quadrature components after two iterations ($N = 2$).	131
7-11	A comparison between LTI anti-aliasing filtering and IQ anti-aliasing applied to a signal whose spectrum is triangular to reduce its bandwidth to 0.3 times its original bandwidth. (a) LTI anti-aliasing (original signal dashed). (b) IQ anti-aliasing with $N = 4$ iterations (original signal dashed).	132
7-12	Generating $y_1(t)$ and $y_2(t)$ through sub-Nyquist sampling of $y(t)$ followed by lowpass filtering. The Nyquist interval $T_N = \pi/\Omega_c$	133
7-13	The multi-channel model.	134
7-14	Reconstruction of $x_1(t)$ and $x_2(t)$ from uniform samples of $y_1(t)$ and $y_2(t)$. .	135

List of Tables

- 2.1 The performance gain for different bit allocations. 53
- 2.2 Examples of overall improvement in SQNR when replacing uniform quantization with differential uniform quantization 61
- 4.1 Sinc Interpolation Reconstruction Methods 82

CHAPTER 1

INTRODUCTION

1.1 Background

1.1.1 Sampling Theory - A Historical Overview

Sampling theory is a fundamental concept in signal processing and its applications. It plays an important role as a connecting link between continuous-time and discrete-time signals as it allows representation, without loss of information, of continuous-time bandlimited signals by discrete-time sequences, which can then be processed digitally. The most commonly used sampling theorem asserts that a bandlimited signal, observed over the entire time axis, can be perfectly reconstructed from its equally spaced samples taken at a rate which exceeds twice the highest frequency present in the signal. The sampling theorem was first introduced in information theory and communication engineering by C. E. Shannon in 1940. However, it did not appear in the engineering literature until after World War II in 1949 [79]. Shannon states the sampling theorem in the following terms: "*Theorem 1: If a function $f(t)$ contains no frequencies higher than W cps, it is completely determined by giving its ordinates at a series of points spaced $1/(2W)$ seconds apart.*" Shannon did not claim it as his own, and in fact following the theorem he notes: "*This is a fact which is common knowledge in the communication art.*" However, later he adds, "*Theorem 1 has been given previously in other forms by mathematicians but in spite of its evident importance seems not to have appeared explicitly in the literature of communication theory.*"

The sampling theorem has been attributed in the literature to numerous different authors including E. T. Whittaker [92], H. Nyquist [67], J. M. Whittaker [93, 94], V. A. Kotelnikov

[50], D. Gabor [28], and C. E. Shannon [79], and its historical roots have been often discussed. The Mathematician E. T. Whittaker [92] is considered to be the first to address the sampling theorem in 1915 in his study of the cardinal functions. The sampling theorem introduced by Shannon is very close to the more refined statement in 1935 of J. M. Whittaker [94], concerning the relation between the cardinal functions and the finite-limit Fourier integral. Shannon was aware of the mathematical work of J. M. Whittaker and he acknowledged it in his paper. Nyquist [67] (1928) did not explicitly consider the problem of sampling and reconstruction of continuous-time bandlimited signals, but a different problem which has some mathematical similarities. Considering the problem of distortionless transmission of telegraphic signals, Nyquist showed that up to $2W$ independent pulse samples could be sent through a system of bandwidth W . When Shannon stated the sampling theorem, he referred to the critical sampling interval $T = 1/(2W)$ as the Nyquist interval corresponding to the band W , in recognition of Nyquist's discovery of the fundamental importance of this interval in connection with telegraphy. In the late fifties, it became known that Kotel'nikov [50] introduced the sampling theorem in the Russian literature to communications theory in 1933.

Sampling theory has found application in many fields including signal analysis, system theory, information theory, spectroscopy and image processing, radar, sonar, acoustics, optics, holography, meteorology, oceanography, crystallography, physical chemistry, medical imaging, and there are important connections with multi-resolution analysis and wavelets.

1.1.2 Extensions of the Sampling Theorem

Many extensions and generalizations of the Nyquist-Shannon sampling theorem exist. Kohlenberg [49] (1953) extended the sampling theorem to bandpass signals. For a bandpass signal to be accurately represented by a set of its equally spaced samples at the minimum possible rate, the lowest frequency occupied by the signal must be an integer multiple of the signal's bandwidth. Introducing "second-order sampling," which involves two interleaved sequences of uniformly spaced sampling points, Kohlenberg proved that perfect reconstruction of bandpass signals is possible at a rate equal to twice the bandwidth of the signal, with

no restrictions on the range of frequencies that the signal occupies.

The first to extend the Nyquist-Shannon sampling theorem to bandlimited signals in higher dimensions was Parzen [72] in 1956. Petersen and Middleton [74] show that in the case of multidimensional sampling, the most efficient lattice is in general not rectangular. Hexagonal sampling and its higher dimensional generalizations are shown in [63, 64] to yield a lower sampling density. Sampling expansions for radially symmetric functions that are bandlimited to the unit sphere in R^N have also been obtained [42].

When the Nyquist-Shannon sampling theorem is applied to the autocorrelation function of a bandlimited wide-sense stationary stochastic process, the optimal linear estimator, in the mean square sense, of the stochastic process based on its Nyquist-rate samples achieves zero mean square error, as shown by A. V. Balakrishnan [2] in 1957. Generalization to bandpass or multipass stochastic processes is presented in [56]. Extension of stochastic sampling to n -dimensional processes is introduced in [66]. Sampling theorems for nonstationary random processes are also presented [29, 75, 101].

Another interesting extension involves the reconstruction of a bandlimited signal from samples of the signal and its derivatives. When Shannon [79] introduced the sampling theorem, he also remarked that a bandlimited signal could be reconstructed from uniform samples of the signal and its derivative at half the Nyquist rate. He then generalized his remark to higher derivatives. The details were later worked out and Shannon's statements were mathematically formulated and proved by L. Fogel [27], D. Jagerman and L. Fogel [39], D. Linden [54], and D. Linden and N. Abramson [55]. Specifically, it was shown that a bandlimited signal can be perfectly reconstructed from equally spaced samples of the signal and its first $M - 1$ derivatives taken at a rate that is M times lower than the Nyquist rate of the signal. The importance of this result lies in its application. For example, the velocity and the position of an aircraft are sampled at half the Nyquist rate to determine a continuous course of its path. Linden [55] also showed that for large M , the expansion approaches a Taylor-type series weighted by a Gaussian density function centered about each sample point.

Papoulis' generalized sampling expansion [71] (1977) is a further generalization of the sampling theorem which suggests reconstructing a bandlimited signal using data other

than the sampled values of the signal and its derivatives. Papoulis has shown that under certain conditions on multi-channel systems for which the input is bandlimited, the bandlimited input signal can be perfectly reconstructed from samples of the responses of M linear time-invariant (LTI) systems, each sampled at $1/M$ times the Nyquist rate. The sampling expansion introduced by Linden [55] can be viewed as a special case of Papoulis' generalized sampling expansion, in which the LTI systems of the multi-channel system are chosen so the multi-channel outputs correspond to the signal and its first $M - 1$ derivatives.

The generalized sampling expansion of Papoulis suggests various ways to split a signal into different channels in which the analog-to-digital (A/D) converter in each channel provides different information about the signal. This parallelism is one possibility for improving data acquisition systems whose performance is limited by the A/D converters, which work at their limits and cannot be pushed further. A very common method for splitting a signal into different channels is the use of time-interleaved A/D converters [46], in which the input signal in each of the M channels is first time-delayed and then sampled at a rate which is M times lower than the signal's Nyquist rate. With the time-delays appropriately designed, interleaving the multi-channel output samples produces uniform samples of the input signal at the Nyquist rate. Thus, sampling with an ideal time-interleaved A/D converter with M channels is equivalent to sampling with an ideal A/D converter with a sampling rate M times higher. In practice, however, channel mismatches limit the performance of time-interleaved A/D converters.

Papoulis [70] also generalizes the sampling theorem for the case in which the sampling rate exceeds the Nyquist rate, i.e., oversampling. He shows that in this case the demands on the reconstruction filter can be considerably relaxed. Reconstructing the signal from its Nyquist rate samples requires an ideal lowpass filter, which is, of course, impossible to realize. Alternatively, by increasing the sampling rate above Nyquist, the requirement of a sharp cut-off of the interpolation filter is removed due to the existence of a free attenuation interval. There are other advantages of oversampling. When a signal is oversampled, its samples become dependent and the signal reconstruction is not affected when losing an arbitrarily large but finite number of sampled values. Oversampling can also improve the performance in the presence of quantization error [15, 69]. Specifically, a high-resolution

A/D converter can be achieved by oversampling a low-resolution A/D converter followed by discrete-time processing of the digital oversampled signal.

The sampling expansions discussed so far assumed that the entire signal is observed. Brown [13] considers the problem of predicting bandlimited signals from their past values. He shows that a bandlimited signal can be approximated fairly well by a linear combination of past samples, provided that the sampling rate exceeds twice the Nyquist rate of the signal.

The first to extend the sampling theorem for the analysis of signals specified by a time-varying spectrum with time-varying bands was Horiuchi [35]. In this expansion, the coefficients are in general not the same as the samples of the continuous-time signal.

Reconstruction of a bandlimited signal from nonuniform samples has also been extensively explored in the literature. J. R. Higgins [33] suggests that irregular sampling is a norm: *"Irregular sampling arises mathematically by simply asking the question "What is special about equidistantly spaced sample points?"; and then finding that the answer is "Within certain limitations, nothing at all". In practice it is often said that irregular sampling is the norm rather than the exception."* In a variety of contexts, nonuniform sampling naturally arises or is preferable to uniform sampling. Uniform sampling with missing samples or with time-jitters can be regarded as nonuniform sampling. In the spatial domain, non-uniformity of the spacing of the array elements in an antenna or acoustic sensor array is often part of the array design as a trade off between the length of the array and the number of elements. A signal specified by time-varying spectrum is another example for which nonuniform sampling is more natural than uniform sampling. When the signal is varying rapidly it is more appropriate to sample it at a higher rate than when it is varying slowly. Reconstruction from nonuniform sampling has been used in many fields including Computed Tomography (CT), Magnetic Resonance Imaging (MRI), optical and electronic imaging systems. H. S. Black [7] credits Cauchy [16] for the origin of nonuniform sampling in 1841 and offers the following translation to Cauchy's statement: *"If a signal is a magnitude-time function, and if time is divided into equal intervals such that each subdivision comprises an interval T seconds long, where T is less than half the period of the highest significant frequency component of the signal, and if one instantaneous sample is taken from each sub-interval in any manner, then a knowledge of the instantaneous mag-*

nitude of each sample plus a knowledge of the instant within each sub-interval at which the sample is taken, contains all the information of the original signal.” J. R. Higgins [32], however, notes that such a statement was not included in the paper by Cauchy.

With unequal spacing of the sampling instants, the reconstruction process is often more involved. Yen [100] (1956) considers the reconstruction of a bandlimited signal from its nonuniform samples for various special cases which possess simple reconstruction formulas. Specifically, he treats the case of uniform sampling where a finite number of samples migrate to distinct new positions. He also provides an explicit reconstruction formula for the case in which an infinite number of samples are shifted by the same amount, resulting in a gap in an otherwise uniform sampling grid. The case of recurrent nonuniform sampling, in which the nonuniform sampling grid has a periodic structure, is also analyzed by Yen, who provides an exact reconstruction formula. The sampling instants in this case can be divided into groups of M samples each, where each group has a recurrent period, which is M times the Nyquist period of the input signal. Recurrent nonuniform sampling can also be viewed as a special case of the generalized sampling expansion of Papoulis [71], in which the LTI systems are pure delays. Comparing the reconstruction formulas for the different cases of nonuniform sampling with that of uniform sampling, Yen remarks that it is evident that the composing functions become more and more complicated as the sampling grid deviates more and more from a uniform grid.

More generally, Beutler [5] (1966) proved that a bandlimited signal can be perfectly reconstructed from its nonuniform samples, under certain conditions on the nonuniform grid and provided that the average sampling rate exceeds the Nyquist rate, i.e., that the number of samples per unit time exceeds (on the average) twice the highest frequency present in the signal. This result, which is shown for deterministic signals as well as for wide-sense stationary stochastic signals, depends most directly on some closure theorems first obtained by Levinson [53]. Yao and Thomas [98, 99] later derived a sampling expansion for nonuniform samples of a bandlimited signal for the case, in which each of the sampling instants deviates less than $(1/\pi)\ln 2$ from the corresponding uniform grid. They also considered the question of stable reconstruction and showed that Lagrange interpolation is stable when the deviation of the sampling instants from a uniform sampling grid is less than $1/4$.

Landau [51] considers the question of whether the Nyquist rate can be improved if the sampling instants are chosen differently; or the signals are bandpass or multi-band; or at the cost of more computing than is required by sinc interpolation. He proves that stable sampling cannot be performed at a rate lower than the Nyquist, regardless of the location of sampling instants, the nature of the set of frequencies which the signals occupy, or the method of construction.

There are also other extensions of the sampling theorem in which the sampling instants are dependent on the signal. Representing a bandlimited signal by its zero crossings or by its crossings with a cosine function are just a few examples. This kind of sampling is referred to as *implicit* sampling and it was first considered by Bond and Cahn [9]. Since nonlinear transformation may increase the signal's bandwidth, this sampling approach may be advantageous in reconstructing a bandlimited signal that was processed through a nonlinear zero-crossing-preserving transformation.

A comprehensive review of literature concerning other extensions and generalizations of the sampling theorem can be found in [33, 38, 43, 88, 102].

1.1.3 Error and Aliasing

The sampling theorem assumes that the signal is bandlimited, it is observed over the entire time axis, its exact sampled values are accurately known, and the sampling instants are uniformly spaced. However, in many cases of practical interest, the underlying signal is not strictly band-limited, it is observed only over a finite time interval, its exact sampled values are not known, and jitter occurs in acquiring the samples. These deviations from the ideal scenario influence the accuracy of the signal reconstruction and result in interpolation error.

When the signal is not band-limited or, alternatively, it is bandlimited but sampled at a rate lower than its Nyquist rate, frequency components of the original signal that are higher than half the sampling rate are folded into lower frequencies resulting in aliasing. The aliasing error is defined as the difference between the original signal and the series constructed using the signal's samples. A classical result giving an upper bound on the

aliasing error was stated originally by P. Weiss [91] in 1963 and proved in 1967 by J. L. Brown [12], who also obtained an upper bound for the aliasing error of bandpass signals.

To avoid aliasing in sampling, the continuous-time signal must be forced to be bandlimited to frequencies below one-half the desired sampling rate. This aim is often accomplished by processing the continuous-time signal through an LTI anti-aliasing low-pass filter prior to sampling it. There is a variety of other contexts, in which the alias of the signal is preferable to the original signal. This is the case, for example, with band-pass signals, in which the aliasing is exploited for modulating the signal into baseband frequencies. Another example in the same category is a sampling oscilloscope. This instrument is intended for observing very high-frequency waveforms, and it exploits the principles of sampling to alias these frequencies into ones that are more easily displayed. In other cases, aliasing is deliberately distributed to various channels in such a way that when they are combined properly, aliasing is cancelled and perfect recovery is achieved. This is the case, for example, with interlaced sampling as in interleaved A/D converters or more generally with Papoulis' generalized sampling expansion.

When the signal is observed over a finite time interval, only a finite number of samples can be used for the signal reconstruction. Since the sampling expansion requires an infinite number of terms to exactly interpolate a bandlimited signal from its samples, an interpolation error, referred to as a truncation error, occurs. Several results concerning the truncation error were obtained by several authors including B. Tsybakov and V. Iakovlev, [87], Helms and Thomas [31], and Papoulis [70].

The amplitude error arises when the exact sampled values are not accurately known and their approximations are used for the interpolation of the signal. Round-off and quantization errors may be considered as special cases of amplitude error. Papoulis [70] shows that even if the errors in the sampled values are bounded, the amplitude error may exceed all bounds for some values of t .

Deviations of the sampling instants from the uniform sampling grid also occur in practice, and the problem is to determine the original signal based on these samples. This error is referred to as a time-jitter error and is similar in its treatment to the amplitude error. Assuming that the timing errors are known, Papoulis [70] derives an approximation of the

reconstructed signal from these samples. Butzer [14] provides a bound for the time-jitter error which is similar to the bound obtained on the amplitude error.

In practice, more than one of the errors mentioned above can occur. Butzer [14] provides an upper bound for the error caused by approximating a not-necessarily band-limited signal by a truncated series with quantized sampled values taken at jittered time instants.

1.2 Objectives

This thesis considers the problem of reconstructing a bandlimited signal from its sampled values. It develops various methods for optimal reconstruction given different assumptions about the signal, the sampling grid and the type of errors that arise. The thesis also explores the benefits of nonuniform sampling over uniform sampling in the presence of quantization error and when aliasing occurs as a result of sub-Nyquist sampling.

The work discusses optimal reconstruction of the continuous-time bandlimited signal in the environment of interleaved multi-channel measurements in the presence of quantization error. A new approach for mitigating the effects of quantization error on the reconstructed signal is introduced. This approach involves time-varying quantization whose time-dependent parameters are specified according to the relative timing between adjacent samples. In a broader view, this approach suggests the benefits of considering sampling together with quantization in the digital representation of the continuous-time signal.

The thesis also considers an extension of the Nyquist-Shannon sampling theorem, in which additional information is available about the continuous-time signal apart from its bandwidth. Utilizing this additional information can result in perfect reconstruction of the bandlimited signal from samples taken at a rate lower than the Nyquist rate.

In the context of sub-Nyquist sampling, the thesis also suggests various methods for mitigating or avoiding aliasing, which may be preferable in some contexts to the traditional LTI anti-aliasing filtering. Among these methods are non-linear methods, linear time-varying methods and methods in which aliasing mitigation is accomplished by perturbation of the uniform sampling grid. In the scenario of multiple correlated signals, co-sampling is introduced as a way to possibly reduce the overall sampling rate by distributing

co-aliasing in sampling so that it gets cancelled in reconstruction.

1.3 Outline

The thesis is organized as follows. Chapter 2 considers the case of multi-channel measurements as may arise in interleaved A/D converter or in distributed sensor networks. We consider the case of oversampling and design optimal reconstruction filters under the constraint of perfect reconstruction in the absence of errors. Chapter 3 takes a different approach to the design of the reconstruction filters in which the constraints of perfect reconstruction are relaxed. In both approaches, the effects of quantization error on the reconstructed output are analyzed, and optimal design of the relative timing between the channels and the quantizer step size in each of the channels is discussed.

Chapter 4 considers the case in which the nonuniform sampling grid is modeled as a perturbation of a uniform grid. The exact reconstruction in this case is computationally difficult, and a class of simple approximate reconstruction methods based on the use of LTI low-pass filtering is suggested and analyzed. Chapter 5 analyzes the effects of timing errors in processing continuous-time bandlimited signals using discrete-time systems. It also discusses the design of a discrete-time system which compensates for the timing errors. In Chapter 6 we use the class of approximate reconstruction methods developed in Chapter 4 for the reconstruction from nonuniform samples at a rate lower than the Nyquist rate. We show that the artifacts due to sub-Nyquist sampling can be controlled so that aliasing is traded off with uncorrelated noise, which may be beneficial in various contexts.

In Chapter 7, we assume that additional information about the signal apart from its bandwidth is available and suggest a sampling-reconstruction scheme which exploits this information for reducing the sampling rate. In this chapter we also discuss various alternative methods to avoid aliasing in sampling.

PERFECT RECONSTRUCTION IN MULTI-CHANNEL NONUNIFORM SAMPLING

This chapter considers interleaved, multi-channel measurements as arise for example in time-interleaved analog-to-digital (A/D) converters and in distributed sensor networks. Such systems take the form of either uniform or recurrent nonuniform sampling, depending on the relative timing between the channels. Uniform quantization in each channel results in an effective overall signal-to-quantization-error ratio (SQNR) in the reconstructed output which is dependent on the quantizer step size in each channel, the relative timing between the channels and the oversampling ratio. It is shown that in the multi-channel sampling system when the quantization step size is not restricted to be the same in each channel and the channel timing is not constrained to correspond to uniform sampling, it is often possible to reduce the SQNR relative to the uniform case.

2.1 Introduction

High bandwidth signals or the use of large oversampling ratios often require the use of time-interleaved A/D converters [46]. Similarly in a sensor network environment, separate sensors might independently sample a shifted version of an underlying signal with the sensor outputs then transmitted to a fusion center for interleaving and processing. The relative timing of the channels is typically chosen so that simple interleaving results in uniform

sampling. More generally, the interleaved samples correspond to recurrent nonuniform sampling [23, 43, 61, 71, 100].

When interleaving is assumed to correspond to uniform sampling but fails to do so because of timing errors, the channel timing is often referred to as mismatched; if not accounted for, this mismatch can lead to significant degradation in performance. A variety of methods have been suggested in the literature to mitigate these problems. To reduce the errors introduced by timing mismatches it is first required to detecting the timing errors. In general, there exist two approaches for detection of timing errors: one which does not assume prior knowledge and is based on the output samples of the time-interleaved A/D converter [21, 22, 36, 37, 59, 78, 83, 90], and another which incorporates a known signal at the input to the system [41, 44]. Once the timing errors have been measured, the correction can be done either by adjusting the sampling clock in each A/D converter to eliminate the timing errors, or by digital processing of the output samples to obtain uniform samples.

In single or multi-channel sampling systems for A/D conversion, quantization effects must also be taken into account. Oversampling is a well established approach to mitigating the effects of quantization, effectively trading off between the oversampling ratio and the required quantization step size for a fixed signal-to-quantization-error ratio. This trade-off can be accomplished in a direct way by following the quantizer with a sampling rate converter or by using noise-shaping techniques as in delta-sigma A/D converters [15, 69]. A systematic alternative approach is introduced in [47, 48] to derive the time-interleaved equivalent structure for an arbitrary delta-sigma converter. A vector quantization approach is used in [85] to develop a lower bound on the mean squared reconstruction error for periodic bandlimited signals from the quantized oversampled signal.

The multi-channel sampling system which we consider is presented in section 2.2, where we also suggest a multi-channel reconstruction scheme. In section 2.2.1 we design the multi-channel reconstruction filters to achieve perfect reconstruction of the input signal in the absence of quantization error. In sections 2.2.2 we consider the effects of uniform quantization in the environment of interleaved, oversampled multi-channel measurements and the design of the optimal reconstruction filters, which compensate for the nonuniform spacing of the channel offsets and for the quantization error. Modeling quantization er-

ror with an additive noise model, we show in section 2.2.3 that for the multi-channel case, when the quantizer step size is not constrained to be the same in each channel and the channel timing is not constrained to result in uniform sampling, it is often possible to reduce the SQNR relative to the uniform case. Specifically, we show that timing mismatches between channels can be compensated for by appropriate choice of quantization step size in each channel rather than attempting to correct the timing mismatch. Alternatively, the choice of using different quantizer step size in each channel can be matched by appropriate choice of the relative timing between channels together with properly designed compensation filters. The concept of having different levels of accuracy in different channels is similar to the approach in sub-band coding [19, 76, 89], in which each sub-band is quantized with an accuracy based upon appropriate criteria. Replacing uniform quantization with differential uniform quantization, it is shown in section 2.3 that higher performance gain is achieved when the channel offsets are nonuniformly spaced.

2.2 Multi-channel Sampling and Reconstruction

The basic multi-channel sampling which we consider is shown in Figure 2-1¹. In this system, the Nyquist rate of the bandlimited input signal $x(t)$ is denoted by $1/T_N$, and each of the M channels is sampled at a rate of $1/T = 1/(LT_N)$ with $M > L$, corresponding to an effective oversampling factor of $\rho = M/L > 1$. We assume the usual Nyquist-Shannon sampling model but with the sampling done in a multi-channel structure. The notation C/D in Figure 2-1 represents continuous-to-discrete-time conversion and refers to ideal sampling, i.e., $x_m[n] = x(nT - \tau_m)$ with τ_m as the time delay of the m^{th} channel.

Interleaving the outputs of the multi-channel sampling system, as shown in Figure 2-2, we obtain either uniform or recurrent nonuniform samples of $x(t)$, depending on the relative timing between the channels. Specifically, when

$$\tau_m = (m/M) \cdot T, \quad m = 0, 1, \dots, M-1, \quad (2.1)$$

¹This system can be viewed as a special case of the multi-channel case discussed by Papoulis [71].

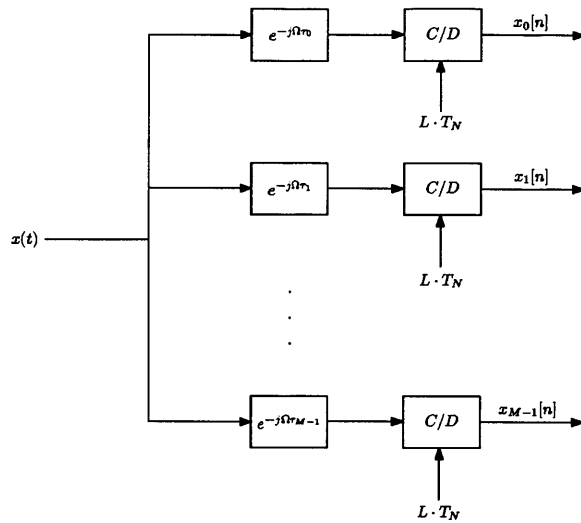


Figure 2-1: Multi-channel sampling.

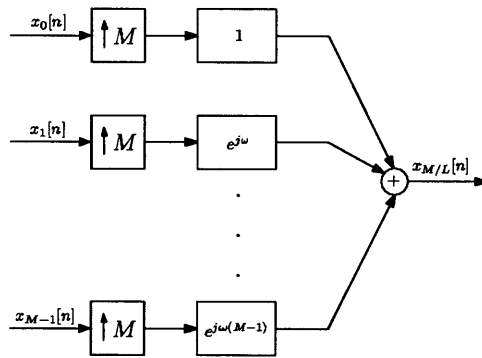


Figure 2-2: Interleaving the output samples of the multi-channel sampling system of Figure 2-1 obtains either uniform or recurrent nonuniform sampling.

the interleaved sequence $x_{M/L}[n]$ will correspond to uniform samples of $x(t)$ at a rate of M/L times its Nyquist rate. Otherwise, with nonuniform spacing of the time delays, $x_{M/L}[n]$ will correspond to recurrent nonuniform samples of $x(t)$, as shown for example in Figure 2-3.

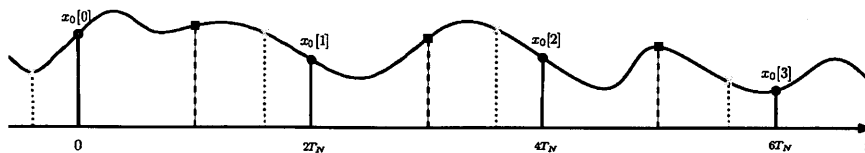


Figure 2-3: An example of recurrent nonuniform sampling of $x(t)$ where $M = 3$ and $L = 2$.

2.2.1 Perfect Reconstruction

In [71], Papoulis has shown that under certain conditions on multi-channel systems for which the input is bandlimited, the bandlimited input signal can be perfectly reconstructed from samples of the responses of M linear time-invariant (LTI) systems, each sampled at $1/M$ times the Nyquist rate. Specifically, perfect reconstruction is possible when the condition in (2.2) on the frequency response $H_m(\Omega)$ of each channel in the multi-channel systems is satisfied.

$$\left| \begin{array}{ccc} H_0(\Omega) & \dots & H_{M-1}(\Omega) \\ \vdots & \ddots & \vdots \\ H_0\left(\Omega - k \cdot \frac{2\pi}{MT_N}\right) & \dots & H_{M-1}\left(\Omega - k \cdot \frac{2\pi}{MT_N}\right) \\ \vdots & \ddots & \vdots \\ H_0\left(\Omega - (M-1) \cdot \frac{2\pi}{MT_N}\right) & \dots & H_{M-1}\left(\Omega - (M-1) \cdot \frac{2\pi}{MT_N}\right) \end{array} \right| \neq 0, \quad \Omega \in \left[\frac{\pi}{T_N} - \frac{2\pi}{MT_N}, \frac{\pi}{T_N} \right]. \quad (2.2)$$

Similarly, perfect reconstruction of $x(t)$ is possible from the multi-channel outputs of Figure 2-1, provided that the effective sampling rate meets or exceeds the Nyquist rate of the input signal $x(t)$. For example, perfect reconstruction can be accomplished by combining the sequences $x_m[n]$ to form uniform Nyquist samples of $x(t)$, as shown in Figure 2-4, from which $x(t)$ is obtained by sinc interpolation.

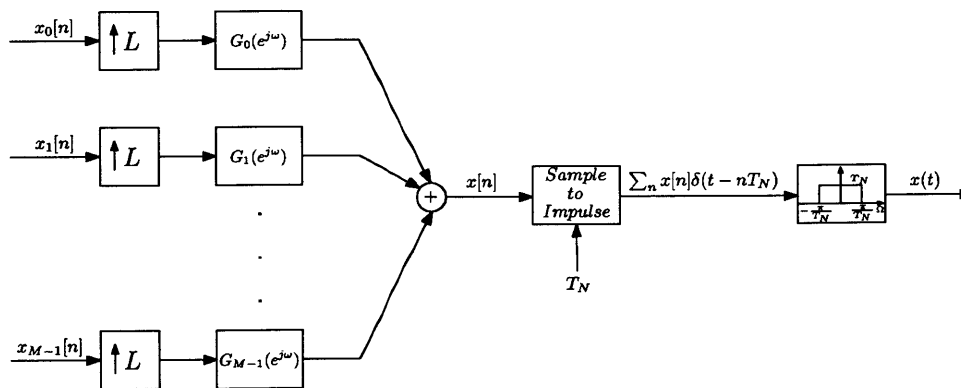


Figure 2-4: Multi-channel reconstruction.

2.2.1.1 Uniform spacing of the time delays

When the time delays of the multi-channel system of Figure 2-1 are uniformly spaced as in (2.1), choosing the reconstruction filters in the system of Figure 2-4 as

$$G_m(e^{j\omega}) = \frac{L}{M} e^{j\omega \frac{L}{M} m}, \quad |\omega| < \pi, \quad m = 0, 1, \dots, M-1, \quad (2.3)$$

results in perfect reconstruction of $x(t)$. With this choice of $G_m(e^{j\omega})$, the discrete-time processing in the multi-channel reconstruction of Figure 2-4 is equivalent to interleaving the outputs of the multi-channel sampling system followed by sampling rate conversion by a noninteger factor of L/M , as shown in Figure 2-5.

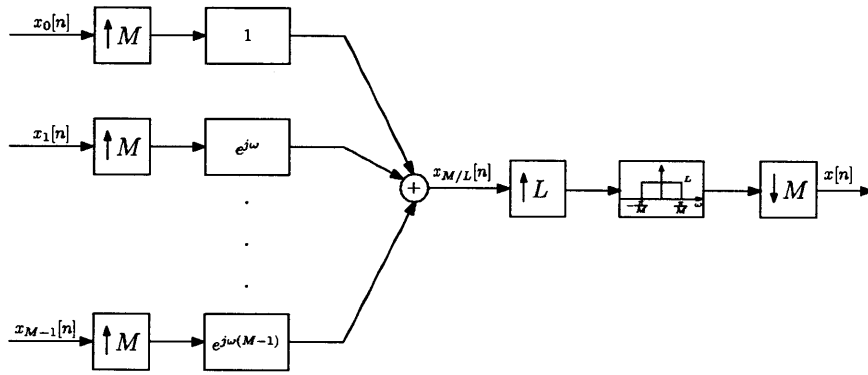


Figure 2-5: Interleaving followed by sampling rate conversion.

This follows by first noting that interchanging the sampling rate expanders with filtering in the system of Figure 2-5 resulting in the system of Figure 2-6. Then, the reconstruction filters in (2.3) can be shown to be equivalent to the processing follows the sampling rate expanders in Figure 2-6.

More generally, the filters $G_m(e^{j\omega})$ are chosen to compensate for the nonuniform spacing of the channel offsets τ_m so that $x[n]$ represents uniform samples of $x(t)$.

2.2.1.2 Nonuniform spacing of the time delays

Perfect reconstruction of $x(t)$ is obtained in the system of Figure 2-4 when

$$\sum_{m=0}^{M-1} G_m(e^{j\omega}) X_m(e^{j\omega L}) = \frac{1}{T_N} X\left(\frac{\omega}{T_N}\right), \quad |\omega| < \pi, \quad (2.4)$$

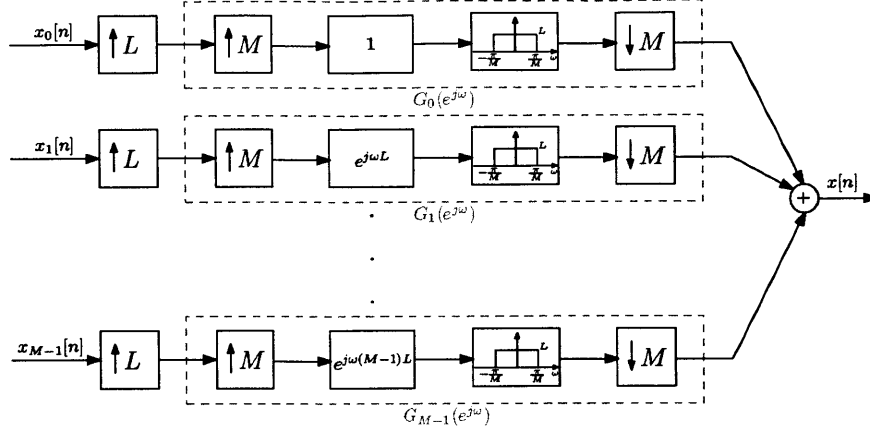


Figure 2-6: Multi-channel sampling rate conversion.

or equivalently when

$$\sum_{m=0}^{M-1} G_m(e^{j\omega}) \cdot \left[\frac{1}{T} \sum_{k=-(L-1)}^{L-1} X \left(\frac{\omega - \frac{2\pi}{L}k}{T_N} \right) \cdot e^{-j(\omega - \frac{2\pi}{L}k) \frac{\tau_m}{T_N}} \right] = \frac{1}{T_N} X \left(\frac{\omega}{T_N} \right), \quad |\omega| < \pi. \quad (2.5)$$

Since the sampling rate in each channel is $1/L$ times the Nyquist rate of the input signal, only L shifted replicas of the spectrum of $x(t)$ contribute to each frequency ω in the spectrum of each signal $x_m[n]$ in Figure 2-1. Consequently, at each frequency ω , equation (2.5) imposes L constraints on the M reconstruction filters $G_m(e^{j\omega})$. Of these constraints we impose $L-1$ to remove the aliasing components and one to preserve $X(\Omega)$.

Rearranging eq. (2.5), we obtain

$$\frac{1}{T} \sum_{k=-(L-1)}^{L-1} X \left(\frac{\omega - \frac{2\pi}{L}k}{T_N} \right) \cdot \left(\sum_{m=0}^{M-1} G_m(e^{j\omega}) \cdot e^{-j(\omega - \frac{2\pi}{L}k) \frac{\tau_m}{T_N}} \right) = \frac{1}{T_N} X \left(\frac{\omega}{T_N} \right), \quad |\omega| < \pi, \quad (2.6)$$

which results in the following set of constraints:

$$\sum_{m=0}^{M-1} G_m(e^{j\omega}) \cdot e^{-j(\omega - \frac{2\pi}{L}k) \frac{\tau_m}{T_N}} = L \cdot \delta[k] \quad \omega \in \Delta\omega_i, \quad (2.7)$$

$$k = -i, -i+1, \dots, L-1-i, \quad i = 0, 1, \dots, L-1,$$

where $\Delta\omega_i = \left[\pi - (i+1) \frac{2\pi}{L}, \pi - i \frac{2\pi}{L} \right]$.

2.2.1.3 Nyquist-rate Sampling

With no oversampling, i.e, when $M = L$, eqs. (2.8) uniquely determine the reconstruction filters $G_m(e^{j\omega})$. To obtain the reconstruction filters in this case, we first write the set of equations in (2.8) in a matrix form, i.e.,

$$V \cdot \begin{bmatrix} e^{-j\omega_0 i} \cdot G_0(e^{j\omega}) \cdot e^{-j\omega\tau_0/T_N} \\ e^{-j\omega_1 i} \cdot G_1(e^{j\omega}) \cdot e^{-j\omega\tau_1/T_N} \\ \vdots \\ e^{-j\omega_{M-1} i} \cdot G_{M-1}(e^{j\omega}) \cdot e^{-j\omega\tau_{M-1}/T_N} \end{bmatrix} = L \cdot \underline{e}_i, \quad \omega \in \Delta\omega_i, \quad i = 0, 1, \dots, L-1, \quad (2.8)$$

where \underline{e}_i is an indicator vector whose i^{th} entry is 1 and all other entries are zero, and V is in general an $L \times M$ Vandermonde matrix of the form

$$V = \begin{pmatrix} 1 & 1 & \dots & 1 \\ \alpha_1 & \alpha_2 & \dots & \alpha_M \\ \alpha_1^2 & \alpha_2^2 & \dots & \alpha_M^2 \\ \dots & \ddots & \ddots & \dots \\ \alpha_1^{L-1} & \alpha_2^{L-1} & \dots & \alpha_M^{L-1} \end{pmatrix}, \quad (2.9)$$

with $\alpha_{m+1} = e^{j\omega_m}$, $m = 0, 1, \dots, M-1$. When $M = L$ and all α_m are distinct, V is invertible. Using the explicit formula in [57] for the inverse of a square Vandermonde matrix, the solution to the set of eqs. in (2.8) for the case $M = L$ becomes

$$G_m(e^{j\omega}) = L \cdot e^{j\omega_m i} \cdot e^{j\omega\tau_m/T_N} \cdot \frac{(-1)^{L-1-i}}{\prod_{l=0, l \neq m}^{L-1} (\alpha_{m+1} - \alpha_{l+1})} \cdot \sigma_{L-1-i, L-1}^{m+1}, \quad \omega \in \Delta\omega_i, \quad i = 0, 1, \dots, L-1, \quad m = 0, 1, \dots, L-1, \quad (2.10)$$

where the coefficients $\{\sigma_{L-1-i, L-1}^{m+1}\}_{i=0}^{L-1}$ are determined by the following expansion

$$\prod_{l=1, l \neq m+1}^L (x - \alpha_l) = \sum_{i=0}^{L-1} (-1)^{L-1-i} x^i \sigma_{L-1-i, L-1}^{m+1}. \quad (2.11)$$

Denoting by $g_m(t)$ the impulse response corresponding to the frequency response

$$G_m(\Omega) = \begin{cases} T_N \cdot G_m(e^{j\Omega T_N}) & |\Omega| < \pi/T_N \\ 0 & \text{otherwise} \end{cases}, \quad m = 0, 1, \dots, M-1, \quad (2.12)$$

it follows from eqs. (2.10) and (2.11) that

$$\begin{aligned} g_m(t - \tau_m) &= \frac{1}{2\pi} \int_{-\pi/T_N}^{\pi/T_N} T_N G_m(e^{j\Omega T_N}) e^{j\Omega(t - \tau_m)} d\Omega \\ &= \frac{\left(\sum_{i=0}^{L-1} (-1)^{L-1-i} (\alpha_{m+1} e^{-j\frac{2\pi}{LT_N}t})^i \cdot \sigma_{L-1-i, L-1}^{m+1} \right)}{\prod_{l=0, l \neq m}^{L-1} (\alpha_{m+1} - \alpha_{l+1})} \cdot \text{sinc}(\pi t/T) \cdot e^{j\frac{\pi}{T_N}(\frac{L-1}{L})t} \\ &= \prod_{l=0, l \neq m}^{L-1} \frac{(\alpha_{m+1} e^{-j\frac{2\pi}{LT_N}t} - \alpha_{l+1})}{(\alpha_{m+1} - \alpha_{l+1})} \cdot \text{sinc}(\pi t/T) \cdot e^{j\frac{\pi}{T_N}(\frac{L-1}{L})t}, \quad m = 0, 1, \dots, L-1. \end{aligned} \quad (2.13)$$

Substituting $\alpha_{m+1} = e^{j\omega_m}$ in (2.13) results in

$$g_m(t) = \text{sinc}\left(\frac{\pi}{T}(t + \tau_m)\right) \cdot \left(\prod_{l=0, l \neq m}^{L-1} \frac{\sin\left(\frac{\pi}{T}(t + \tau_l)\right)}{\sin\left(\frac{\pi}{T}(\tau_l - \tau_m)\right)} \right) \quad m = 0, 1, \dots, L-1. \quad (2.14)$$

Consequently, with the reconstruction filters corresponding to $g_m(t)$ in (2.14), the output of the system in Figure 2-4 is a perfect reconstruction of the continuous-time signal $x(t)$.

Specifically,

$$\begin{aligned} x(t) &= \sum_{m=0}^{M-1} \sum_{n=-\infty}^{\infty} x_m[n] \cdot g_m(t - nT) \\ &= \sum_{m=0}^{M-1} \sum_{n=-\infty}^{\infty} x_m[n] \text{sinc}\left(\frac{\pi}{T}(t - nT + \tau_m)\right) \cdot \left(\prod_{l=0, l \neq m}^{L-1} \frac{\sin\left(\frac{\pi}{T}(t - nT + \tau_l)\right)}{\sin\left(\frac{\pi}{T}(\tau_l - \tau_m)\right)} \right). \end{aligned} \quad (2.15)$$

The reconstruction formula in (2.15) is consistent with [100] and [23]. While the derivation in [23] is based on the Lagrange interpolation formula, the derivation here is carried out by forcing the conditions for perfect reconstruction.

2.2.2 Optimal Reconstruction in the Presence of Quantization Error

In this section we consider uniform quantization applied to the multi-channel output samples of Figure 2-1, i.e., $\tilde{x}_m[n] = Q(x_m[n])$, and we analyze its effect on the reconstructed signal at the output of the system in Figure 2-4. With $M > L$, i.e., with oversampling, and with L constraints for perfect reconstruction, there remain $M - L$ degrees of freedom for the design of the reconstruction filters. These degrees of freedom can be used to minimize the average noise power at the output of the reconstruction system due to quantization of the multi-channel output samples, as shown in Figure 2-7.

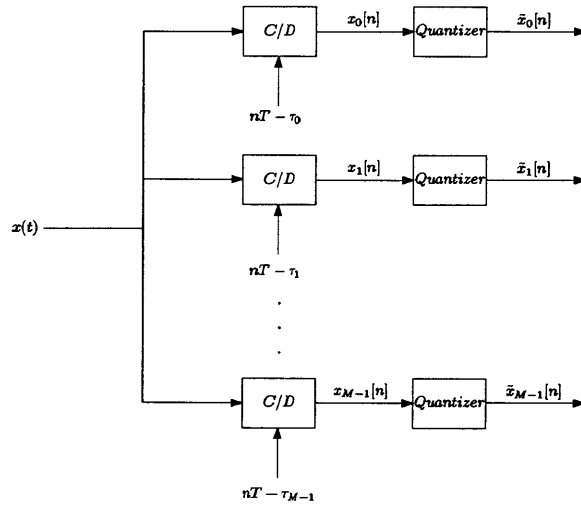


Figure 2-7: Multi-channel sampling and quantization.

2.2.2.1 Quantization Noise Analysis

In our analysis we represent the error due to the uniform quantizer in each channel of Figure 2-7 through an additive noise model [4, 81, 95, 96]. Specifically, the quantizer output $\tilde{x}_m[n]$ in the m^{th} channel is represented as

$$\tilde{x}_m[n] = x_m[n] + q_m[n], \quad (2.16)$$

where $q_m[n]$ is assumed to be a white-noise process uniformly distributed between $\pm\Delta_m/2$ and uncorrelated with $x_m[n]$, where Δ_m denotes the quantizer step size. Correspondingly, the variance of $q_m[n]$ is $\sigma_m^2 = \Delta_m^2/12$.

To analyze the effect of each channel of Figure 2-4 on the corresponding quantization noise we consider the system of Figure 2-8 whose output $\tilde{q}_m(t)$ is

$$\begin{aligned}
\tilde{q}_m(t) &= \sum_{k=-\infty}^{\infty} \tilde{q}_m[k] \operatorname{sinc}\left(\frac{\pi}{T_N}(t - kT_N)\right) \\
&= \sum_{k=-\infty}^{\infty} \left(\sum_{n=-\infty}^{\infty} q_m[n] g_m[k - nL] \right) \operatorname{sinc}\left(\frac{\pi}{T_N}(t - kT_N)\right) \\
&= \sum_{n=-\infty}^{\infty} q_m[n] \left(\sum_{k=-\infty}^{\infty} g_m[k - nL] \operatorname{sinc}\left(\frac{\pi}{T_N}(t - kT_N)\right) \right) \\
&= \sum_{n=-\infty}^{\infty} q_m[n] \left(\sum_{k=-\infty}^{\infty} g_m[k] \operatorname{sinc}\left(\frac{\pi}{T_N}(t - n(LT_N) - kT_N)\right) \right) \\
&= \sum_{n=-\infty}^{\infty} q_m[n] g_m(t - nT).
\end{aligned} \tag{2.17}$$

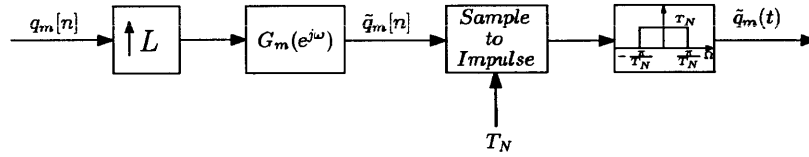


Figure 2-8: Single channel in the reconstruction system of Figure 2-4.

Under the assumption that $q_m[n]$ is a zero-mean white-noise process with variance σ_m^2 , the autocorrelation function of $\tilde{q}_m(t)$ is

$$R_{\tilde{q}_m \tilde{q}_m}(t, t - \tau) = \sigma_m^2 \cdot \sum_{k=-\infty}^{\infty} g_m(t - kT) g_m(t - \tau - kT), \tag{2.18}$$

which is periodic in t with period $T = LT_N$, and $\tilde{q}_m(t)$ is therefore a wide-sense cyclostationary random process. Alternatively, $R_{\tilde{q}_m \tilde{q}_m}(t, t - \tau)$ can be expressed as

$$R_{\tilde{q}_m \tilde{q}_m}(t, t - \tau) = \frac{1}{2\pi} \int_{-\pi/T_N}^{\pi/T_N} S_{\tilde{q}_m \tilde{q}_m}(\Omega; t) \cdot e^{j\Omega\tau} d\Omega, \tag{2.19}$$

where

$$\begin{aligned}
S_{\tilde{q}_m \tilde{q}_m}(\Omega; t) &= \int_{-\infty}^{\infty} R_{\tilde{q}_m \tilde{q}_m}(t, t - \tau) \cdot e^{-j\Omega\tau} d\tau \\
&= \sigma_m^2 \cdot \sum_{k=-\infty}^{\infty} g_m(t - kT) \int_{-\infty}^{\infty} g_m(t - \tau - kT) \cdot e^{-j\Omega\tau} d\tau \\
&= \sigma_m^2 \cdot G_m^*(\Omega) \cdot \sum_{k=-\infty}^{\infty} g_m(t - kT) e^{-j\Omega(t - kT)} \\
&= \begin{cases} \sigma_m^2 \cdot T_N G_m^*(e^{j\Omega T_N}) \cdot \sum_{k=-\infty}^{\infty} g_m(t - kT) e^{-j\Omega(t - kT)} & |\Omega| < \frac{\pi}{T_N} \\ 0 & \text{otherwise} \end{cases}
\end{aligned} \tag{2.20}$$

We denote by $e(t)$ the total noise component due to quantization in the system of Figure 2-4, i.e.,

$$e(t) = \sum_{m=0}^{M-1} \tilde{q}_m(t). \tag{2.21}$$

With the assumption that the quantization noise is uncorrelated between channels,

$$R_{ee}(t, t - \tau) = \sum_{m=0}^{M-1} R_{\tilde{q}_m \tilde{q}_m}(t, t - \tau), \tag{2.22}$$

from which it follows that $e(t)$ is also a wide-sense cyclo-stationary random process. Thus, the ensemble average power $E(e^2(t))$ of $e(t)$ is periodic with period T . Averaging also over time and denoting by σ_e^2 the time and ensemble average power of $e(t)$, we obtain

$$\sigma_e^2 = \frac{1}{T} \int_0^T E(e^2(t)) dt = \frac{1}{T} \int_0^T R_{ee}(t, t) dt = \sum_{m=0}^{M-1} \frac{1}{T} \int_0^T R_{\tilde{q}_m \tilde{q}_m}(t, t) dt. \tag{2.23}$$

Expressing $R_{\tilde{q}_m \tilde{q}_m}(t, t)$ in terms of $S_{\tilde{q}_m \tilde{q}_m}(\Omega; t)$ as in (2.20), eq. (2.23) becomes

$$\begin{aligned}
\sigma_e^2 &= \sum_{m=0}^{M-1} \frac{\sigma_m^2}{2\pi L} \cdot \int_{-\pi/T_N}^{\pi/T_N} G_m^*(e^{j\Omega T_N}) \cdot \left(\sum_{k=-\infty}^{\infty} \int_0^T g_m(t - kT) e^{-j\Omega(t - kT)} dt \right) d\Omega \\
&= \frac{1}{2\pi} \int_{-\pi}^{\pi} \sum_{m=0}^{M-1} (\sigma_m^2/L) \cdot |G_m(e^{j\omega})|^2 d\omega.
\end{aligned} \tag{2.24}$$

2.2.2.2 Optimal reconstruction filters

In general, the design of $G_m(e^{j\omega})$ can be formulated in a variety of ways, one of which is to use all degrees of freedom to minimize the reconstruction error (Chapter 3). However, in the specific approach taken in this chapter, the only characteristic of the signal assumed to be known is its bandwidth. Consequently, we choose the optimal reconstruction filters $G_m(e^{j\omega})$ to minimize σ_e^2 under the set of constraints in (2.8), which guarantees perfect reconstruction in the absence of error due to quantization. As shown in Appendix A, the reconstruction filters $G_m(e^{j\omega})$ that minimize σ_e^2 under the set of constraints in (2.8) are

$$\begin{aligned} G_m(e^{j\omega}) &= 1/\sigma_m^2 \cdot e^{j\omega\tau_m/T_N} \left(\sum_{l=-i}^{L-1-i} \lambda_l^{(i)} \cdot e^{-j2\pi(\tau_m/LT_N)l} \right) \\ &= 1/\sigma_m^2 \cdot e^{j\omega\tau_m/T_N} \cdot \Lambda^{(i)}(e^{j\omega_m}) \end{aligned} \quad (2.25a)$$

$$\begin{aligned} &= 1/\sigma_m^2 \cdot e^{j\omega\tau_m/T_N} \cdot \left(\underline{v}_m^H \underline{\lambda}^{(i)} \right) e^{j\omega_m i}, \quad \omega \in \Delta\omega_i \\ &i = 0, 1, \dots, L-1, \quad m = 0, 1, \dots, M-1, \end{aligned} \quad (2.25b)$$

where $\Lambda^{(i)}(e^{j\omega_m})$ is the discrete-time Fourier transform of the finite-length sequence $\{\lambda_k^{(i)}\}_{k=-i}^{L-1-i}$ sampled in frequency at

$$\omega_m = 2\pi\tau_m/(LT_N), \quad (2.26)$$

and

$$\underline{v}_m^H = \left[1, e^{-j2\pi\frac{\tau_m}{LT_N}}, \dots, e^{-j2\pi\frac{\tau_m}{LT_N}(L-1)} \right]. \quad (2.27)$$

For each $i = 0, 1, \dots, L-1$, the sequence $\underline{\lambda}^{(i)} = \{\lambda_k^{(i)}\}_{k=-i}^{L-1-i}$ is defined as the solution to the following set of equations:

$$A_M \cdot \underline{\lambda}^{(i)} = L \cdot \underline{e}_i, \quad (2.28)$$

with \underline{e}_i an indicator vector whose i^{th} entry is 1 and all other entries are zeros, and A_M is an $L \times L$ Hermitian Toeplitz matrix such that

$$A_M = \sum_{m=0}^{M-1} (\underline{v}_m \cdot \underline{v}_m^H) / \sigma_m^2. \quad (2.29)$$

2.2.2.3 Polyphase Implementation of the reconstruction filters

If the reconstruction filters in Figure 2-4 are designed as finite impulse response (FIR) filters, considerable gain in computational efficiency can be achieved by utilizing a polyphase decomposition of $G_m(e^{j\omega})$ and rearranging the operations so that the filtering is done at the low sampling rate. Specifically, $G_m(e^{j\omega})$ can be expressed as

$$G_m(e^{j\omega}) = \sum_{n=0}^{L-1} E_m^{(n)}(e^{j\omega L}) \cdot e^{-j\omega n}, \quad (2.30)$$

where $E_m^{(n)}(e^{j\omega})$ are the discrete-time Fourier transforms of the polyphase components $e_m^{(n)}[k]$ of $g_m[n]$ defined as

$$e_m^{(n)}[k] = g_m[n + kL] \quad n = 0, 1, \dots, L-1, \quad k = 0, \pm 1, \dots \quad (2.31)$$

Interchanging filtering with the sampling rate expanders using the noble identity [69], $\tilde{x}[n]$ is obtained from a superposition of L sub-systems of the form of Figure 2-9 in which the filters are implemented at the low sampling rate.

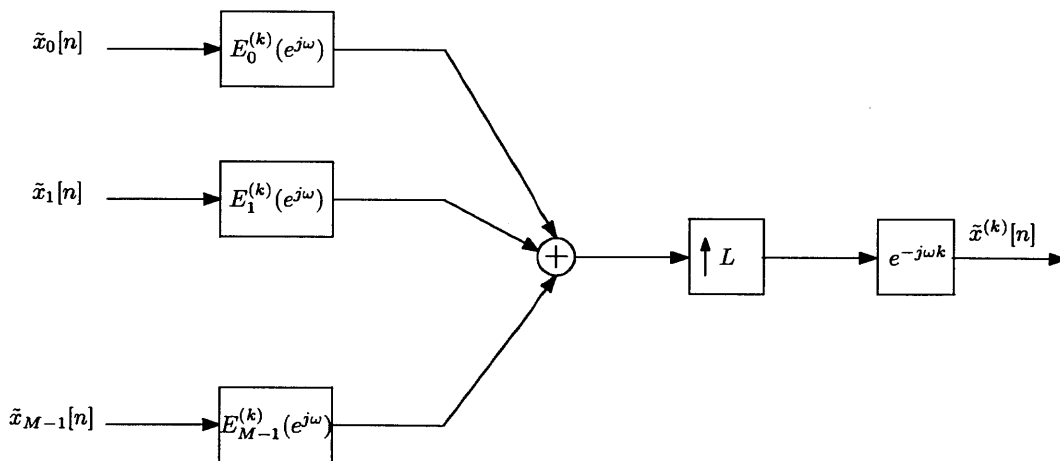


Figure 2-9: The k^{th} branch of the polyphase implementation of the system in Figure 2-4.

2.2.2.4 Minimum average quantization noise power

Substituting the expression for $G_m(e^{j\omega})$ from (2.25a) into (2.24) we obtain for the minimum achievable value of σ_e^2

$$\begin{aligned}\sigma_{e_{min}}^2 &= \frac{1}{L} \sum_{i=0}^{L-1} \frac{1}{2\pi} \int_{\pi-(i+1)\frac{2\pi}{L}}^{\pi-i\frac{2\pi}{L}} \sum_{m=0}^{M-1} (1/\sigma_m^2) \cdot |\Lambda^{(i)}(e^{j\omega_m})|^2 d\omega \\ &= \frac{1}{L} \sum_{i=0}^{L-1} \left(\frac{1}{L} \sum_{m=0}^{M-1} |\Lambda^{(i)}(e^{j\omega_m})|^2 / \sigma_m^2 \right).\end{aligned}\quad (2.32)$$

Alternatively, using the expression for $G_m(e^{j\omega})$ from (2.25b), the integrand in eq. (2.24) can be expressed as

$$\begin{aligned}\sum_{m=0}^{M-1} (\sigma_m^2/L) \cdot |G_m(e^{j\omega})|^2 &= \frac{1}{L} \cdot (\underline{\lambda}^{(i)})^H \left(\sum_{m=0}^{M-1} (\underline{v}_m \cdot \underline{v}_m^H) / \sigma_m^2 \right) \underline{\lambda}^{(i)} \\ &= \frac{1}{L} \cdot (\underline{\lambda}^{(i)})^H A_M \underline{\lambda}^{(i)} \\ &= (\underline{\lambda}^{(i)})^H \cdot \underline{e}_i, \quad \omega \in \Delta\omega_i, \quad i = 0, 1, \dots, L-1.\end{aligned}\quad (2.33)$$

Since $V = [\underline{v}_1, \underline{v}_2, \dots, \underline{v}_{M-1}]$ is a full-rank matrix, it follows from (2.29) that

$$\underline{c}^H A_M \underline{c} = \sum_{m=0}^{M-1} \frac{|\underline{v}_m^H \underline{c}|^2}{\sigma_m^2} > 0, \quad \forall \underline{c} \neq \underline{0},\quad (2.34)$$

and thus A_M is a positive-definite matrix. Using (2.33) together with (2.34), an equivalent expression for the minimum value of σ_e^2 follows

$$\sigma_{e_{min}}^2 = \frac{1}{L} \sum_{i=0}^{L-1} (\underline{\lambda}^{(i)})^H \cdot \underline{e}_i = \sum_{i=0}^{L-1} \underline{e}_i^H A_M^{-1} \underline{e}_i = tr(A_M^{-1}).\quad (2.35)$$

With no oversampling, i.e., when $M = L$, it is intuitively reasonable and straight forward to show that the optimal filters in (2.25) are consistent with $g_m(t)$ in (2.14). In addition, A_L can be represented as

$$A_L = V \Sigma^{-1} V^H,\quad (2.36)$$

where V is given by (2.9) and $\Sigma = \text{diag}[\sigma_0^2, \sigma_1^2, \dots, \sigma_{L-1}^2]$. Since V is invertible, the minimum achieved output average noise power can be written as

$$\sigma_{e,L}^2 = \text{tr}(A_L^{-1}) = \text{tr}(U\Sigma U^H) = \sum_{m=0}^{L-1} \sigma_m^2 |\underline{u}_m|^2, \quad (2.37)$$

where $U^H = V^{-1}$ and \underline{u}_m denotes the m^{th} column of U . Using the formula in [57] for the inverse of V in calculating the norm of \underline{u}_m , we obtain

$$|\underline{u}_m|^2 = \sum_{i=0}^{L-1} |u_{i,m}|^2 = \frac{\sum_{i=0}^{L-1} \left| (-1)^{L-1-i} \cdot \sigma_{L-1-i,L-1}^{m+1} \right|^2}{\prod_{l=0, l \neq m}^{L-1} (\alpha_{m+1} - \alpha_{l+1})}. \quad (2.38)$$

Substituting $x = e^{-j\frac{2\pi}{L}k}$ in (2.11) results in the Discrete Fourier Transform of the sequence $\{(-1)^{L-1-i} \cdot \sigma_{L-1-i,L-1}^{m+1}\}_{i=0}^{L-1}$. Specifically,

$$\sum_{i=0}^{L-1} (-1)^{L-1-i} \cdot \sigma_{L-1-i,L-1}^{m+1} e^{-j\frac{2\pi}{L}ki} = \prod_{l=0, l \neq m}^{L-1} \left(e^{-j\frac{2\pi}{L}k} - \alpha_{l+1} \right), \quad k = 0, 1, \dots, L-1, \quad (2.39)$$

from which the numerator of the expression in (2.38) can be calculated using Parseval relation and the output average noise power in eq. (2.37) becomes

$$\sigma_{e,L}^2 = \sum_{m=0}^{L-1} \sigma_m^2 \cdot \frac{\frac{1}{2\pi} \int_{-\pi}^{\pi} \prod_{l=0, l \neq M}^{L-1} \sin^2\left(\frac{\omega_l - \omega}{2}\right) d\omega}{\prod_{l=0, l \neq M}^{L-1} \sin^2\left(\frac{\omega_m - \omega_l}{2}\right)}. \quad (2.40)$$

When $M > L$, eq. (2.35) together with the Woodbury matrix identity [97] suggest a simple recursive formula for the update of the output average noise power $\sigma_{e,min}^2$. Specifically,

$$A_n^{-1} = A_{n-1}^{-1} - A_{n-1}^{-1} \underline{v}_n \underline{v}_n^H A_{n-1}^{-1} / (\sigma_n^2 + \underline{v}_n^H A_{n-1}^{-1} \underline{v}_n), \quad n = L+1, \dots, M, \quad (2.41)$$

$$\sigma_{e,n}^2 = \text{tr}(A_n^{-1}) = \sigma_{e,n-1}^2 - \frac{\underline{v}_n^H A_{n-1}^{-2} \underline{v}_n}{\sigma_n^2 + \underline{v}_n^H A_{n-1}^{-1} \underline{v}_n}, \quad n = L+1, \dots, M. \quad (2.42)$$

2.2.3 Optimal Signal-to-Quantization-Noise Ratio (SQNR)

In previous sections, the effects of quantization in the multi-channel sampling system of Figure 2-7 were analyzed, and optimal reconstruction filters were designed to compensate for the nonuniform spacing of the channel offsets and for the quantization error. It was shown that the effective overall signal-to-noise ratio in the reconstructed output depends on the quantizer step size, the relative timing between the channels and the oversampling ratio. We next discuss how to appropriately choose these parameters for optimal overall SQNR.

Noting that the i^{th} equation in (2.28) corresponds to

$$\sum_{m=0}^{M-1} 1/\sigma_m^2 \cdot \Lambda^{(i)}(e^{j\omega_m}) = L, \quad (2.43)$$

and applying the Cauchy-Schwartz inequality to (2.43) results in

$$\sum_{n=0}^{M-1} 1/\sigma_n^2 \cdot \sum_{m=0}^{M-1} |\Lambda^{(i)}(e^{j\omega_m})|^2 / \sigma_m^2 \geq L^2, \quad (2.44)$$

for each $i = 0, 1, \dots, L-1$. Combining eqs. (2.32) and (2.44) it follows that

$$\sigma_{e_{min}}^2 \geq \frac{L}{\sum_{m=0}^{M-1} 1/\sigma_m^2}, \quad (2.45)$$

where equality is achieved if and only if the following condition is satisfied

$$\sum_{m=0}^{M-1} 1/\sigma_m^2 \cdot e^{j\omega_m l} = 0 \quad l = 1, 2, \dots, L-1. \quad (2.46a)$$

This condition is equivalent to each of the following conditions:

$$\Lambda^{(i)}(e^{j\omega_m}) = \frac{L}{\sum_{n=0}^{M-1} 1/\sigma_n^2} \quad \begin{array}{l} i = 0, 1, \dots, L-1 \\ m = 0, 1, \dots, M-1, \end{array} \quad (2.46b)$$

$$\lambda_k^{(i)} = \frac{L}{\sum_{m=0}^{M-1} 1/\sigma_m^2} \delta[k] \quad k = -i, -i+1, \dots, L-1-i. \quad (2.46c)$$

To show the equivalence between the conditions in (2.46), we first show that (2.46a) implies (2.46c). The condition in (2.46c) is then shown to imply (2.46b), from which (2.46a) is implied. To show that (2.46a) implies (2.46c), we note that when $\sum_{m=0}^{M-1} 1/\sigma_m^2 \cdot e^{j\omega_m l} = 0$ $l = 1, 2, \dots, L-1$, the matrix A_M in (2.29) becomes

$$A_M = \left(\sum_{m=0}^{M-1} 1/\sigma_m^2 \right) \cdot I_{L \times L}, \quad (2.47)$$

and (2.46c) follows from (2.28) together with (2.47). Using the equality in (2.46c) in the definition of $\Lambda^{(i)}(e^{j\omega_m})$, we obtain (2.46b), i.e.,

$$\begin{aligned} \Lambda^{(i)}(e^{j\omega_m}) &= \sum_{l=-i}^{L-1-i} \left(\frac{L}{\sum_{m=0}^{M-1} 1/\sigma_m^2} \delta[l] \right) \cdot e^{-j\omega_m l} \\ &= \frac{L}{\sum_{n=0}^{M-1} 1/\sigma_n^2}, \quad i = 0, 1, \dots, L-1, \quad m = 0, 1, \dots, M-1. \end{aligned} \quad (2.48)$$

Finally, it follows from (2.28) together with (2.46b) that

$$\begin{aligned} L \cdot \underline{e}_i &= \left(\sum_{m=0}^{M-1} 1/\sigma_m^2 \cdot \underline{v}_m \underline{v}_m^H \right) \cdot \underline{\lambda}^{(i)} = \sum_{m=0}^{M-1} 1/\sigma_m^2 \cdot \underline{v}_m \cdot (\underline{v}_m^H \cdot \underline{\lambda}^{(i)}) = \\ &= \sum_{m=0}^{M-1} 1/\sigma_m^2 \cdot \underline{v}_m \cdot \Lambda^{(i)}(e^{j\omega_m}) e^{-j\omega_m i} = \frac{L \cdot (\sum_{m=0}^{M-1} 1/\sigma_m^2 e^{-j\omega_m i} \cdot \underline{v}_m)}{\sum_{m=0}^{M-1} 1/\sigma_m^2}, \quad i = 0, 1, \dots, L-1, \end{aligned} \quad (2.49)$$

from which (2.46a) follows.

2.2.3.1 Optimal time delays with uniform quantization step size

When the quantizers in Figure 2-7 all have the same step size, we next show that τ_m as given by eq. (2.1) is optimal, i.e., the relative timing between adjacent channels is a constant. The optimal reconstruction filters in (2.25) then reduce to the noninteger delays in (2.3). Also in this case,

$$\sigma_{emin}^2 = (L/M) \cdot \sigma^2, \quad (2.50)$$

where σ^2 denotes the variance of the quantization noise source in each channel. To show this, we note that with $\sigma_m^2 = \sigma^2$, the condition of eq. (2.46a) becomes

$$\sum_{m=0}^{M-1} e^{j\omega_m l} = 0 \quad l = 1, 2, \dots, L-1, \quad (2.51)$$

which is clearly satisfied for any L and M when the values $e^{j\omega_m}$ are uniformly spaced on the unit circle, corresponding to uniform sampling. However, this is in general not a unique solution as there are other distributions of ω_m which satisfy eq. (2.51).

In summary, it follows from eq. (2.45) that for the reconstruction structure suggested in Figure 2-4 and with the quantization step size the same in each channel, the uniform sampling grid achieves the minimum average quantization noise power $(L/M) \cdot \sigma^2$. Any other choice of τ_m , for which (2.51) is not satisfied, results in a higher average quantization noise power.

2.2.3.2 Optimal time delays with nonuniform quantization step size

As we next show, by allowing the quantization step size to be chosen separately for each channel, so that quantization noise sources $q_m[n]$ in the different channels have different variances σ_m^2 , better SQNR can often be achieved. For comparison purposes, we will assume that the quantization noise power averaged over all channels is equal to a pre-specified fixed value σ^2 , i.e.,

$$\frac{1}{M} \sum_{m=0}^{M-1} \sigma_m^2 = \sigma^2. \quad (2.52)$$

Applying the Cauchy-Schwartz inequality to the identity $\sum_{m=0}^{M-1} \sigma_m \cdot 1/\sigma_m = M$, it follows that

$$\sum_{n=0}^{M-1} \sigma_n^2 \cdot \sum_{m=0}^{M-1} 1/\sigma_m^2 \geq M^2, \quad (2.53)$$

and equivalently

$$\frac{L}{\sum_{m=0}^{M-1} 1/\sigma_m^2} \leq (L/M) \cdot \sigma^2, \quad (2.54)$$

with equality if and only if

$$\sigma_m^2 = \sigma^2, \quad m = 0, 1, \dots, M-1. \quad (2.55)$$

Together with (2.45), we conclude that by having different levels of accuracy in the quantizers in the different channels, there is the possibility of reducing the average quantization noise power. This suggests a way to compensate for the mismatched timing in the channels of Figure 2-7 and increase the total SQNR. Alternatively, we can deliberately introduce timing mismatch so that with appropriate design of the quantizers, we will achieve better SQNR as compared to the equivalent uniform sampling with equal quantizer step size in each channel. The analysis and conclusions of course rely on the validity of the additive noise model used for the quantizer, which becomes less appropriate as the quantizer step size increases or the relative timing between adjacent channels decreases.

A similar result to that in (2.54) can be shown under other normalizations. Specifically, instead of fixing the average power of the quantization noise sources in each of the channels, we now fix the total number of bits used to quantize the samples, i.e.,

$$N_T = \sum_{m=0}^{M-1} N_m,$$

where N_m represents the number of bits allocated in channel m . Consequently,

$$\Delta_m = \frac{2X}{2^{N_m}} \quad (2.56)$$

and

$$\sigma_m^2 = \frac{\Delta_m^2}{12} = \underbrace{(X^2/3)}_{\alpha} \left(\frac{1}{4}\right)^{N_m}, \quad (2.57)$$

where X represents the full scale level of the A/D converter. It then follows from (2.57)

that

$$\frac{L}{\sum_{m=0}^{M-1} 1/\sigma_m^2} = \frac{L}{(1/\alpha) \cdot \sum_{m=0}^{M-1} 4^{N_m}}. \quad (2.58)$$

Using convexity arguments to show $\frac{1}{M} \sum_{m=0}^{M-1} 4^{N_m} \geq 4^{N_T/M}$, it follows that

$$\frac{L}{\sum_{m=0}^{M-1} 1/\sigma_m^2} \leq (L/M) \cdot \sigma^2, \quad (2.59)$$

where $\sigma^2 = \alpha \cdot (\frac{1}{4})^{N_T/M}$ represents the variance of the quantization error of an $\frac{N_T}{M}$ -bit quantizer, based on the additive noise model.

Another important aspect in comparing systems is the total number of comparators used in the implementation of the A/D converters. With flash architecture used for the design of the converters, $2^n - 1$ comparators are required for an n -bit quantizer. With M channels and an N_m -bit quantizer in the m^{th} channel, the total number of comparators N_c in the multi-channel system is

$$N_c = \sum_{m=0}^{M-1} (2^{N_m} - 1). \quad (2.60)$$

The number of bits N_{Ave} allocated to each of the channels in an equivalent system, all of whose quantizers are the same and whose total number of comparators is identical to N_c in (2.60), is obtained by solving

$$2^{N_{Ave}} - 1 = \frac{1}{M} \sum_{m=0}^{M-1} (2^{N_m} - 1), \quad (2.61)$$

which results in $N_{Ave} = \log_2 (\frac{1}{M} \sum_{m=0}^{M-1} 2^{N_m})$. Using the following inequality,

$$\frac{1}{M} \sum_{m=0}^{M-1} 4^{N_m} \geq \left(\frac{1}{M} \sum_{m=0}^{M-1} 2^{N_m} \right)^2, \quad (2.62)$$

which follows from Cauchy-Schwartz inequality, or the equivalent form of (2.62)

$$\frac{1}{M} \sum_{m=0}^{M-1} 4^{N_m} \geq 2^{\log_2 \left(\frac{1}{M} \sum_{m=0}^{M-1} 2^{N_m} \right)^2} = 4^{N_{Ave}}, \quad (2.63)$$

we obtain

$$\frac{L}{\sum_{m=0}^{M-1} 1/\sigma_m^2} = \frac{L/M}{\frac{1}{\alpha} \cdot \left(\frac{1}{M} \sum_{m=0}^{M-1} 4^{N_m} \right)} \leq (L/M) \cdot \sigma^2, \quad (2.64)$$

where $\sigma^2 = \alpha \cdot \left(\frac{1}{4} \right)^{N_{Ave}}$.

2.2.4 Simulations

In this section, we consider the multi-channel sampling system of Figure 2-7 with $M = 3$ and $L = 2$. Following a derivation of the mean squared error for this special case, we then consider four cases, each corresponding to a different assumption with respect to the relative timing between the channels and the quantization step size in each channel. In the first case, the quantization step size in each channel is fixed and equal in all channels, and the relative timing between channels is optimized. In the second case, the relative timing between the channels is specified, and the bit allocation is optimized subject to a bit-budget constraint. In the third case, each channel is allocated a different number of bits, and the relative timing between channels is optimized to maximize the SQNR. In the fourth case, we fix the number of bits in channel 0 and channel 1 and analyze the behavior of the optimal relative timing between the channels as the number of bits allocated to channel 2 varies.

To obtain the expression for the minimum mean square error for the case of $M = 3$ and $L = 2$, we first note that

$$A_3 = \begin{bmatrix} \sum_{m=0}^2 1/\sigma_m^2 & \sum_{m=0}^2 e^{-j\omega_m}/\sigma_m^2 \\ \sum_{m=0}^2 e^{j\omega_m}/\sigma_m^2 & \sum_{m=0}^2 1/\sigma_m^2 \end{bmatrix}. \quad (2.65)$$

Assuming without loss of generality that $\tau_0 = 0$ ($\omega_0 = 0$), it then follows from (2.35) and

(2.65) that

$$\sigma_{e_{min}}^2 = tr(A_3^{-1}) = \frac{(\sigma_0^2 \sigma_1^2 + \sigma_0^2 \sigma_2^2 + \sigma_1^2 \sigma_2^2) / 2}{\sigma_0^2 \sin^2(\frac{\omega_1 - \omega_2}{2}) + \sigma_1^2 \sin^2(\frac{\omega_1}{2}) + \sigma_2^2 \sin^2(\frac{\omega_2}{2})}. \quad (2.66)$$

When $\sigma_0^2 = \sigma_1^2 = \sigma_2^2 = \sigma^2$, the minimum mean squared error in (2.66) reduces to

$$\sigma_{e_{min}}^2 = \frac{(3/2)\sigma^2}{\sin^2(\frac{\omega_1 - \omega_2}{2}) + \sin^2(\frac{\omega_1}{2}) + \sin^2(\frac{\omega_2}{2})}. \quad (2.67)$$

Figure 2-10 shows the factor $\gamma = \sigma^2 / \sigma_{e_{min}}^2$ representing the reduction in the average noise power at the output of the reconstruction of Figure 2-4 with $M = 3$, $L = 2$, and $\tau_0 = 0$, for the case of $\sigma_0^2 = \sigma_1^2 = \sigma_2^2 = \sigma^2$. As follows from eq. (2.67) and is indicated in Figure 2-10, the maximum noise reduction is achieved for $\tau_1 = -\tau_2 = \pm(2/3) \cdot T_N$, for which $\sigma_{e_{min}}^2 = (2/3) \cdot \sigma^2$.

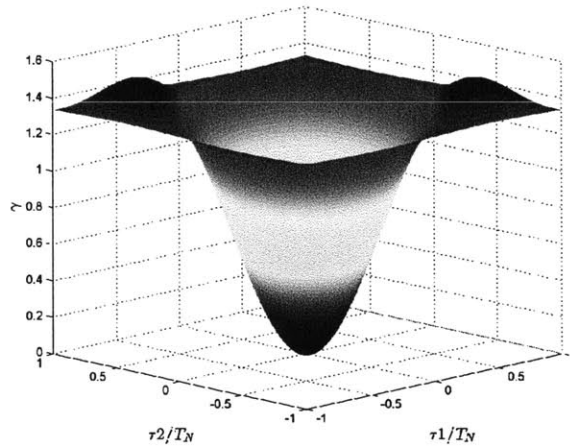


Figure 2-10: The reduction factor γ in the average noise power at the output of the reconstruction of Figure 2-4 achieves its maximum value at $\tau_1 = -\tau_2 = \pm(2/3) \cdot T_N$, i.e., when the multi-channel sampling is equivalent to uniform sampling. Since this curve is based on the additive noise model of the quantization error, which assumes uncorrelated errors, it is less accurate in the vicinity of $\tau_1 = 0$, $\tau_2 = 0$, and $\tau_1 = \tau_2$.

To verify the analysis based on the additive noise model of the quantization error, a simulation of the multi-channel sampling and reconstruction system was obtained in [62], in which actual quantizers were applied to the multi-channel output samples. Figure 2-11 shows the reduction factor γ obtained from simulation for which a 10-bit quantizer is used in each of the channels. Comparing Figure 2-10 which corresponds to the additive noise

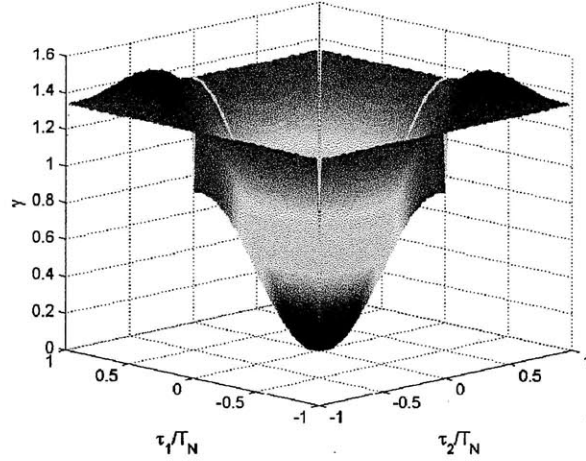


Figure 2-11: The reduction factor γ in the average noise power at the output of the reconstruction system of Figure 2-4 where actual quantizers are applied to the multi-channel output samples with accuracy of 10 bits.

model with Figure 2-11 obtained from simulations, we conclude that the analysis based on the additive noise model is valid except in the vicinity of $\tau_1 = \tau_2$, $\tau_1 = 0$, and $\tau_2 = 0$, where discrepancies occur. Figure 2-11 indicates performance degradation in the vicinity of these lines, which is not predicted with the analysis based on the additive noise model. These discrepancies between the analysis and the simulations occur when the sampling instants of two channels or more fall quite close to each other or exactly on the same grid and the uncorrelated assumption of the additive noise model is no longer reasonable. As analyzed in [62], when the relative timing between adjacent channels is small and the same number of bits is allocated to each of the channels, a positive correlation between the corresponding quantization errors occurs. The positive correlation between the errors results in performance degradation as compared to the performance predicted with the analysis based on the additive noise model.

It follows from eq. (2.45) and as illustrated in the preceding example, for the reconstruction structure suggested in Figure 2-4 and with the quantization step size the same in each channel, the uniform sampling grid achieves the minimum average quantization noise power $(L/M) \cdot \sigma^2$. Any other choice of τ_m for which (2.51) is not satisfied results in a higher average quantization noise power.

We next illustrate with an example that with appropriate design of the quantizer in each

channel we can compensate for the mismatched timing in the channels of Figure 2-7. With 4-bit uniform quantizers in each of the channels, it follows from eq. (2.66) that when the time delays are $\tau_0 = 0$, $\tau_1 = T_N/8$ and $\tau_2 = -(3/4)T_N$, the output average noise power is increased by approximately 20% relative to the case in which $\{\tau_m\}$ are chosen according to (2.1). However, when the quantizer step size is not constrained to be the same in each channel, the reconstruction error variance can be reduced.

Table 2.1 shows the performance gain for different bit allocations as compared to the case in which each channel is allocated 4 bits. The results are sorted from the most to the least preferable where in each choice only 1 bit is shifted from one channel to another, keeping the total number of bits the same.

N_0	N_1	N_2	$(\sigma_{e\min}^2)_{(4,4,4)} / (\sigma_{e\min}^2)_{(N_0,N_1,N_2)}$
3	4	5	1.46
4	3	5	1.36
3	5	4	1.26
5	3	4	1.14
4	5	3	0.41
5	4	3	0.38

Table 2.1: The performance gain for different bit allocations.

In general, we might intuitively expect that since the sampling instants of channel 2 are relatively far from those of the other two channels, it should be allocated more bits in compensation. Also, the relative timing between channel 0 and channel 2 is smaller than the relative timing between channel 2 and channel 1, suggesting allocation of more bits to channel 1 as compared to channel 0. This intuition of bit allocation according to the relative timing between adjacent channels is consistent with the results in Table 2.1 and in particular with the optimal choice shown in Figure 2-12, which suggests allocating 3 bits to channel 0, 4 bits to channel 1, and 5 bits to channel 2. The same results are obtained in [62] in simulating the system using actual quantizers. Once again, the simulations confirm the error analysis based on the additive noise model.

We next fix the number of bits in channel 0 to 3, channel 1 to 4, and channel 2 to 4, and without loss of generality set $\tau_0 = 0$. The values of τ_1 and τ_2 are chosen to minimize the output average noise power. Note that when $\tau_1 = -\tau_2 = \pm(2/3)T_N$, the multi-channel

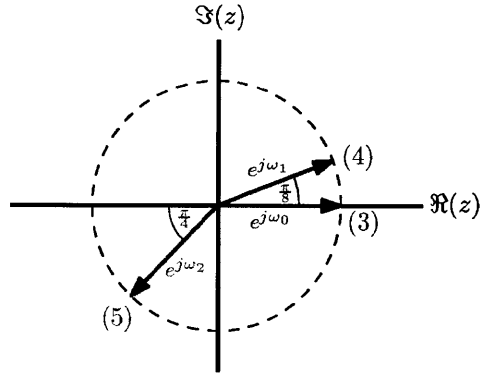


Figure 2-12: Each vector represents a channel whose time delay τ_m is determined by the vector's phase ω_m according to the transformation $\omega_m = 2\pi\tau_m/(LT_N)$, which maps the region $\tau_m \in [-T_N, T_N]$ into the region $\omega_m \in [-\pi, \pi]$. The numbers associated with each of the vectors are the optimal bit allocations for the case of $\tau_0 = 0$, $\tau_1 = T_N/8$, and $\tau_2 = -3T_N/4$.

sampling is equivalent to uniform sampling. More generally, the minimum in (2.66) occurs when τ_1 and τ_2 are chosen according to (2.46). Specifically,

$$64 + 256e^{j\omega_1} + 256e^{j\omega_2} = 0, \quad (2.68)$$

for which $\omega_1 = -\omega_2 = \pm 0.54\pi$ (corresponding to $\tau_1 = -\tau_2 = \pm 0.54T_N$) is a solution, as Figure 2-13 illustrates. Consistent with the intuition expressed earlier, since channels 1 and

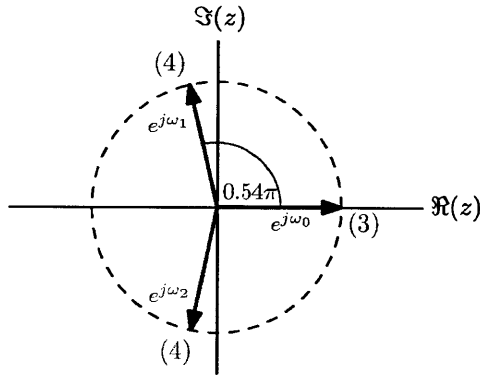


Figure 2-13: With bit allocation $N_0 = 3$, $N_1 = 4$, and $N_2 = 4$, the optimal choice of time delays is $\tau_1 = -\tau_2 = \pm 0.54T_N$, for which the multi-channel sampling system is equivalent to recurrent nonuniform sampling.

2 are both allocated 4 bits and channel 0 is allocated only 3 bits, the optimal choice of τ_1 and τ_2 is such that the relative timing between channel 1 and channel 0, which is equal to

the relative timing between channel 0 and channel 2, is much smaller than that between channel 2 and channel 1, compensating for the low accuracy in channel 0. If channel 0 were allocated 4 bits as the other two channels are, the optimal choice of the time delays would have been $\tau_1 = -\tau_2 = \pm(2/3)T_N$, corresponding to uniform sampling; however, since channel 0 is allocated fewer bits than the other two channels, the sampling instants of the other two channels are getting closer to that of channel 0 in compensation. Since this choice of time delays provides the solution to (2.46), the output average noise power σ_e^2 achieves the lower bound in (2.45).

Figure 2-14 shows the relative gain with respect to output average noise power for all values of τ_1 and τ_2 in the range $[-T_N, T_N]$, as compared to the case of uniform sampling. As indicated, an improvement of 12.5% relative to the uniform sampling case is achieved for the optimal choice $\tau_1 = -\tau_2 = \pm 0.54T_N$.

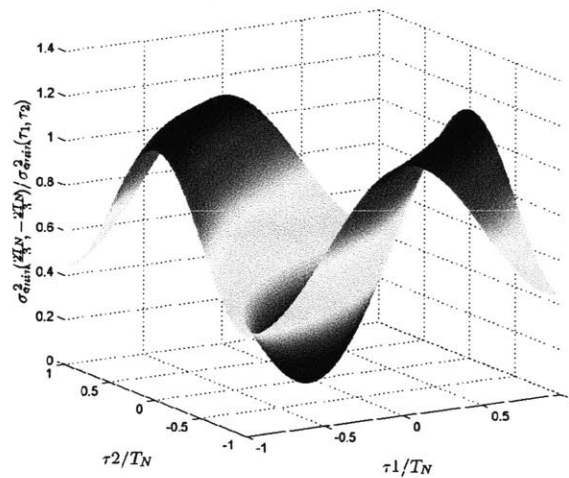


Figure 2-14: The relative performance compared to uniform sampling as a function of τ_1 and τ_2 when $\tau_0 = 0$, $N_0 = 3$, $N_1 = 4$, and $N_2 = 4$. Since this curve is based on the additive noise model of the quantization error, which assumes uncorrelated errors, it is less accurate in the vicinity of $\tau_1 = 0$, $\tau_2 = 0$, and $\tau_1 = \tau_2$.

In the fourth case, we allocate 10 bits to channel 0 and 10 bits to channel 1. The number of bits allocated to channel 2 varies between 9 and 11. For each of these cases, we optimize the time delays to minimize the mean square error given in (2.66). This optimization results in the configurations illustrated in Figure 2-15(a). As indicated in this figure, the relative timing between channel 0 and channel 2 increases as channel 2 is allocated more bits. In the

same time, the relative timing between channel 1 and channel 0 decreases, in compensation.

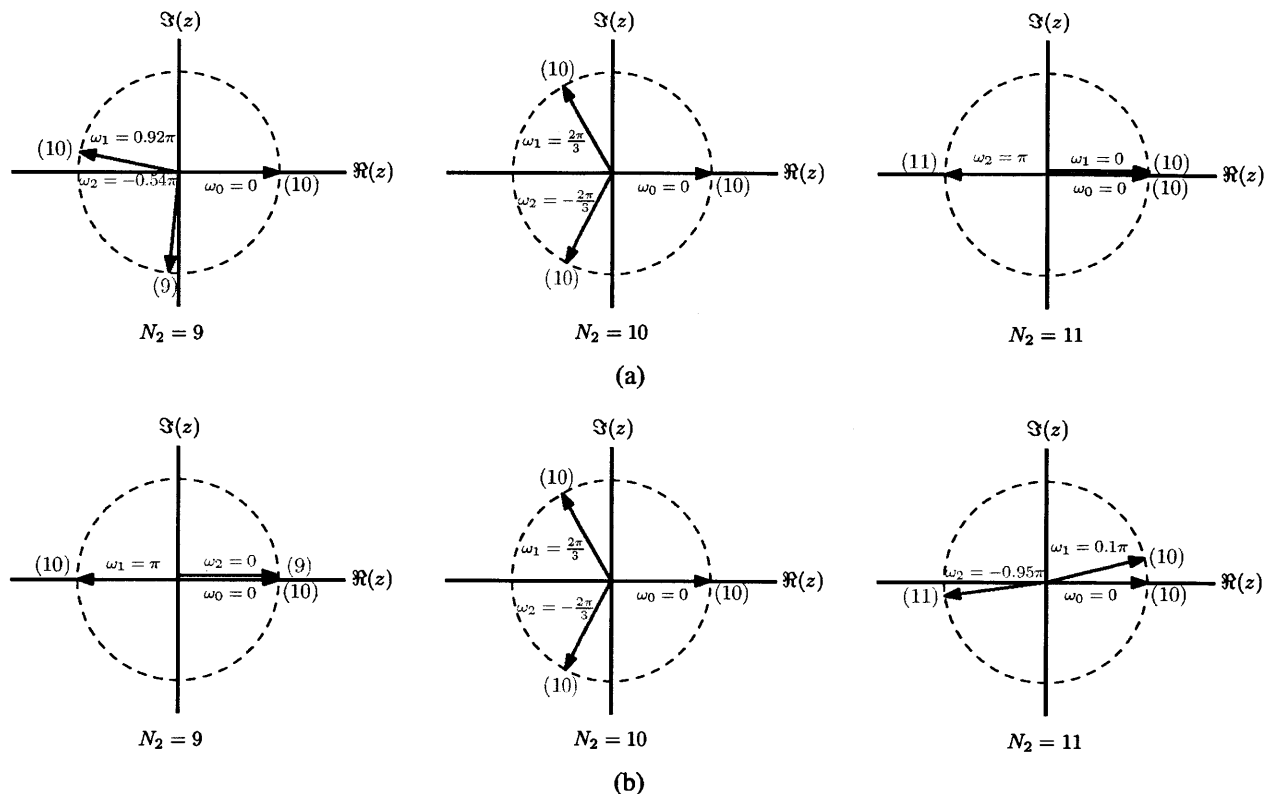


Figure 2-15: Optimal time delays for different choices of N_2 (a) based on the additive noise model, (b) based on simulations with actual quantizers.

As Figure 2-15(b) illustrates, when $N_2 = 10$ the optimal time delays resulting from simulations with actual quantizers, obtained in [62], are consistent with the optimal time delays derived from the analysis based on the additive noise model. However, for $N_2 = 9$ or $N_2 = 11$, the optimal configurations from the simulations are different than those based on the additive noise model. Specifically, for optimal performance, the simulation with $N_2 = 11$ suggests separating channel 0 from channel 1. In addition, due to symmetry, the simulation also suggests setting the time delay of channel 2 to space its sampling instants equidistant from the sampling instants of the other two channels. This nonzero gap between channel 0 and channel 1 is intuitively reasonable since positive correlation between the quantization errors in adjacent channels occurs when the channels are allocated the same number of bits and their relative timing is getting small. As mentioned earlier, this positive correlation results in degradation in performance. For the case of $N_2 = 9$, optimal performance based on simulations is achieved when both a) the sampling instants of chan-

nel 0 are maximally separated from those of channel 1, i.e., the relative timing between the channels is T_N , and b) the time delay of channel 2 is chosen equal to that of either channel 0 or channel 1. This optimal configuration is significantly different from the one based on the analysis with the additive noise model. This discrepancy occurs due to the occurrence of negative correlation between quantization errors of adjacent channels with different bit allocation as their relative timing approaches 0. The negative correlation between the quantization errors together with the optimal reconstruction filters which were designed under the assumption of uncorrelated quantization errors, results in an overall improvement in performance, which is not predicted by the additive noise model.

In summary, we have illustrated that with nonuniform spacing of the time delays, for which the interleaved multi-channel outputs correspond to recurrent nonuniform sampling, equal quantization step size in each channel is not optimal. Allowing different levels of accuracy in the quantizers in the different channels achieves a reduction in the noise variance. Alternatively, when the quantization step size in each of the channels is fixed and varies among channels, choosing the relative timing between adjacent channels to be the same is not optimal, and lower average noise power is achieved with nonuniform spacing of the time delays.

2.3 Differential Uniform Quantization

In this section, differential uniform quantization [20, 24, 40, 68] which is based on the notion of quantizing a prediction error signal rather than the signal itself is incorporated into the multi-channel sampling system of Figure 2-7. By exploiting redundancies in the correlated input signal and representing it in terms of prediction error samples, an increased SQNR can be achieved for a given bit rate or equivalently, a reduction of bit rate for a given SQNR. It is shown that replacing uniform quantization with differential uniform quantization in the multi-channel system of Figure 2-7 results in a higher performance gain when the channel offsets are nonuniformly spaced. It is also shown that with differential quantization, uniform sampling is not necessarily optimal even when using the same number of bits in the quantizers of the different channels.

Uniform quantization can be applied to deterministic signals and does not require the use of a stochastic model, but can also be applied to stochastic signals. The analysis of differential uniform quantization specifically requires stochastic modeling. We therefore assume in this section that $x(t)$ is a realization of a zero-mean stationary Gaussian random process whose autocorrelation function is $R_{xx}(\tau)$, its power spectrum $S_{xx}(\Omega) = 0$ for $|\Omega| \geq \Omega_c$, and its variance is denoted by σ_x^2 . The basic differential quantization system we consider is shown in Figure 2-16 where $\hat{x}[n] = \sum_{j=1}^N h_j \tilde{x}[n-j]$ is a linear predictor of $x[n]$ based on the quantized values $\tilde{x}[n]$.

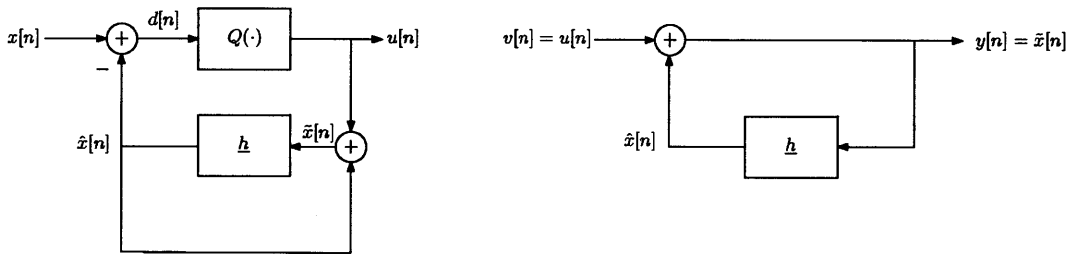


Figure 2-16: Block diagram of differential quantization: coder and decoder.

An important property of the "closed-loop" structure in Figure 2-16 is that quantization error does not accumulate, i.e., with error free transmission of $u[n]$, the reconstruction error $r[n] = y[n] - x[n]$ is equal to the quantization error $q[n] = u[n] - d[n]$. With optimal prediction and adequately fine quantization, modeling the quantization error as an uncorrelated random process is well justified. Also, in the case of fine quantization, $\hat{x}[n]$ can be well approximated as

$$\hat{x}[n] = \sum_{j=1}^N h_j \tilde{x}[n-j] = \sum_{j=1}^N h_j x[n-j] + \sum_{j=1}^N h_j q[n-j] \approx \sum_{j=1}^N h_j x[n-j], \quad (2.69)$$

and the quantization error feedback is therefore not considered [40]. The optimal predictor coefficients $\{h_j\}_{j=1}^N$ are then chosen to minimize the mean square prediction error based on previous unquantized samples, i.e., $E \left\{ \left(x[n] - \sum_{j=1}^N h_j x[n-j] \right)^2 \right\}$.

Note that when the relative timing between adjacent channels in the system of Figure 2-7 are not equal, the optimal choice for the predictor coefficients will in general be different for each of the outputs of the multi-channel sampling system, resulting in a periodic lin-

ear time-varying FIR system and a wide-sense cyclo-stationary prediction error sequence. Consequently, both the quantization error $q[n]$ and the reconstruction error $r[n]$ will be wide-sense cyclo-stationary uncorrelated sequences, and the noise analysis of section 2.2 will remain valid.

To relate the quantization error variance σ_q^2 to the quantizer input signal variance σ_i^2 , we define as in [40] the quantizer performance factor, i.e.,

$$\epsilon_q^2 = \sigma_q^2 / \sigma_i^2, \quad (2.70)$$

which depends on the type of quantizer used, the number of quantization levels, and the pdf of the quantizer input. With differential uniform quantization incorporated into the multi-channel system of Figure 2-7, the variance of the reconstruction error for each of the channels outputs is given by

$$\sigma_r^2[m] = \sigma_q^2[m] = \epsilon_q^2[m]^{(D)} \cdot \sigma_d^2[m] \quad m = 0, 1, \dots, M-1, \quad (2.71)$$

where $\sigma_d^2[m]$ and $\epsilon_q^2[m]^{(D)}$ are the variance of the prediction error and the quantizer performance factor corresponding to channel m .

As follows from (2.70) and (2.71), replacing uniform quantization by differential uniform quantization results in a reduction in reconstruction error in each channel by a factor of

$$\frac{\epsilon_q^2[m] \cdot \sigma_x^2}{\epsilon_q^2[m]^{(D)} \cdot \sigma_d^2[m]} = (\epsilon_q^2[m] / \epsilon_q^2[m]^{(D)}) \cdot (\sigma_x^2 / \sigma_d^2[m]) \quad m = 0, 1, \dots, M-1. \quad (2.72)$$

The ratio $\epsilon_q^2[m] / \epsilon_q^2[m]^{(D)}$ is in general not equal to unity. However, it tends to be close to unity in several cases one of which is the case of Gaussian sources [40] for which the prediction error is also Gaussian and we therefore consider only the performance gain due to the linear predictor. With that assumption and when the same type of quantizer with the same number of levels is used for all channels, it follows from eqs. (2.35), (2.70) and (2.71) that when replacing uniform quantization with differential uniform quantization, the

overall improvement in SQNR at the output of the reconstruction system of Figure 2-4 is

$$\frac{\sigma_{e \min}^2}{\sigma_{e \min}^{2(D)}} = \frac{\text{tr} \left(\left(\sum_{m=0}^{M-1} (\underline{v}_m \cdot \underline{v}_m^H) / \sigma_x^2 \right)^{-1} \right)}{\text{tr} \left(\left(\sum_{m=0}^{M-1} (\underline{v}_m \cdot \underline{v}_m^H) / \sigma_d^2[m] \right)^{-1} \right)}, \quad (2.73)$$

with \underline{v}_m as defined in (2.27).

To illustrate, we consider again the case of $M = 3$ and $L = 2$, where the time delays are now fixed to $\tau_0 = 0$, $\tau_1 = 0.9T_N$, and $\tau_2 = 1.1T_N$. The output samples are quantized according to the system of Figure 2-16 where a first-order predictor is used, and 4 bits uniform quantization is applied to the prediction error samples, satisfying the assumption of fine quantization. Assuming $\tau_0 < \tau_1 < \tau_2$, the optimum value of $h_1[m]$ and its corresponding minimum prediction variance are

$$h_1[m] = \frac{R_{xx}(\tau_{m+1} - \tau_m)}{R_{xx}(0)}, \quad \sigma_d^2[m] = (1 - h_1^2[m]) \sigma_x^2 \quad m = 0, 1, 2, \quad (2.74)$$

where $\tau_3 = \tau_0 + T > \tau_2$.

As follows from eq. (2.35), with uniform quantization and with $\tau_0 = 0$, $\tau_1 = 0.9T_N$, and $\tau_2 = 1.1T_N$ for which the interleaved multi-channel outputs corresponds to recurrent nonuniform samples, there is a degradation in performance by approximately 10% relative to the case of uniform sampling. However, as illustrated in Table 2.2, eq. (2.73) implies that when replacing uniform quantization with differential uniform quantization a higher performance gain in SQNR is achieved in this case as compared to that achieved with uniform sampling. It is also indicated that the relative improvement in SQNR due to differential uniform quantization in uniform and recurrent nonuniform sampling is dependent on the power spectrum of the input signal. Specifically, when the signal's energy is mostly concentrated at high frequencies, the improvement achieved with differential uniform quantization applied in recurrent nonuniform sampling is much more significant than that achieved in uniform sampling.

To summarize, with the same number of bits in each channel, and with uniform quantization, uniform sampling is optimal. When differential uniform quantization is incorporated in the multi-channel sampling system, nonuniform spacing of the channel offsets can

$R_{xx}(\tau) \leftrightarrow S_{xx}(\Omega)$	$(\tau_0 = 0, \tau_1 = \frac{2}{3}T_N, \tau_2 = \frac{4}{3}T_N)$	$(\tau_0 = 0, \tau_1 = 0.9T_N, \tau_2 = 1.1T_N)$
$\text{sinc}^2(\frac{\tau}{2T_N}) \leftrightarrow \begin{array}{c} \uparrow \tau_n \\ \text{---} \\ \downarrow \tau_n \end{array}$	$\sigma_d^2[0] = \sigma_d^2[1] = \sigma_d^2[2] = 0.53$ $\sigma_{e_{min}}^2 / \sigma_{e_{min}}^{2(D)} = 1.88$	$\sigma_d^2[0] = \sigma_d^2[1] = 0.76$ $\sigma_d^2[2] = 0.064, \sigma_{e_{min}}^2 / \sigma_{e_{min}}^{2(D)} = 1.9$
$\text{sinc}(\frac{\tau}{T_N}) \leftrightarrow \begin{array}{c} \uparrow \tau_n \\ \text{---} \\ \downarrow \tau_n \end{array}$	$\sigma_d^2[0] = \sigma_d^2[1] = \sigma_d^2[2] = 0.83$ $\sigma_{e_{min}}^2 / \sigma_{e_{min}}^{2(D)} = 1.21$	$\sigma_d^2[0] = \sigma_d^2[1] = 0.99$ $\sigma_d^2[2] = 0.12, \sigma_{e_{min}}^2 / \sigma_{e_{min}}^{2(D)} = 1.41$
$2\text{sinc}(\frac{\tau}{T_N}) - \text{sinc}^2(\frac{\tau}{2T_N}) \leftrightarrow \begin{array}{c} \uparrow \tau_n \\ \text{---} \\ \downarrow \tau_n \end{array}$	$\sigma_d^2[0] = \sigma_d^2[1] = \sigma_d^2[2] = 0.98$ $\sigma_{e_{min}}^2 / \sigma_{e_{min}}^{2(D)} = 1.02$	$\sigma_d^2[0] = \sigma_d^2[1] = 0.93$ $\sigma_d^2[2] = 0.18, \sigma_{e_{min}}^2 / \sigma_{e_{min}}^{2(D)} = 1.43$

Table 2.2: Examples of overall improvement in SQNR when replacing uniform quantization with differential uniform quantization

result in a higher SQNR.

MMSE RECONSTRUCTION IN MULTI-CHANNEL NONUNIFORM SAMPLING

In Chapter 2 we considered the environment of interleaved multi-channel measurements and the design of optimal reconstruction filters from multi-channel measurements. We designed the reconstruction filters to minimize the averaged noise power at the output of the reconstruction system due to quantization error, under the constraints for perfect reconstruction in the absence of quantization error. In this chapter, we relax the constraints for perfect reconstruction and take an alternative approach to the design of the reconstruction filters, for which the mean squared reconstruction error is reduced.

3.1 Reconstruction Error

We consider the multi-channel sampling and quantization system shown in Figure 2-7, whose input $x(t)$ is now treated as a realization of a bandlimited wide-sense stationary stochastic process. We assume that the random process $x(t)$ is zero-mean, with its autocorrelation function denoted as $R_{xx}(\tau)$, and that its power spectrum $S_{xx}(\Omega)$ vanishes outside the region $|\Omega| < \Omega_c = \pi/T_N$.

Similar to the analysis in Chapter 2, we use the additive noise model for the quantization

error and represent the output samples of the multi-channel system as

$$\tilde{x}_m[n] = x_m[n] + q_m[n], \quad m = 0, 1, \dots, M-1, \quad (3.1)$$

where $x_m[n] = x(nT - \tau_m)$ are uniform samples of $x(t)$ at a rate $1/T = 1/(LT_N)$, and $q_m[n]$ is assumed to be a white-noise random process, uniformly distributed over the range $[-\Delta_m, \Delta_m]$, where Δ_m is the step-size level of the quantizer in the m -th channel. The model also assumes that the sequences $q_m[n]$ are uncorrelated among themselves and uncorrelated with samples of $x(t)$.

For the reconstruction of the Nyquist-rate samples of $x(t)$ from the multi-channel measurements $\tilde{x}_m[n]$, we consider the same structure used in Chapter 2, which is shown in Figure 2-4. The signal $\hat{x}[n]$ at the output of the reconstruction system can be represented as

$$\hat{x}[n] = \sum_{m=0}^{M-1} \sum_{k=-\infty}^{\infty} \tilde{x}_m[k] g_m[n - kL], \quad (3.2)$$

where $g_m[n]$ denotes the impulse response corresponding to the frequency response $G_m(e^{j\omega})$.

Denoting $e[n] = \hat{x}[n] - x[n]$ as the reconstruction error, we obtain

$$e[n] = \left(\sum_{m=0}^{M-1} \sum_{k=-\infty}^{\infty} x_m[k] g_m[n - kL] - x[n] \right) + \sum_{m=0}^{M-1} \sum_{k=-\infty}^{\infty} q_m[k] g_m[n - kL], \quad (3.3)$$

which is a zero-mean random process whose autocorrelation function $R_{ee}[n, n-l]$ is

$$R_{ee}[n, n-l] = R_{e_x e_x}[n, n-l] + R_{e_q e_q}[n, n-l], \quad (3.4)$$

where

$$R_{e_x e_x}[n, n-l] = E \left\{ \left(\sum_{m_1=0}^{M-1} \sum_{k_1=-\infty}^{\infty} x_{m_1}[k_1] g_{m_1}[n - k_1 L] - x[n] \right) \cdot \left(\sum_{m_2=0}^{M-1} \sum_{k_2=-\infty}^{\infty} x_{m_2}[k_2] g_{m_2}[n-l - k_2 L] - x[n-l] \right) \right\} \quad (3.5)$$

and

$$R_{e_q e_q}[n, n-l] = E \left\{ \sum_{m_1=0}^{M-1} \sum_{k_1=-\infty}^{\infty} q_{m_1}[k_1] g_{m_1}[n-k_1 L] \sum_{m_2=0}^{M-1} \sum_{k_2=-\infty}^{\infty} q_{m_2}[k_2] g_{m_2}[n-l-k_2 L] \right\}. \quad (3.6)$$

We denote by σ_e^2 the time and ensemble average of the noise power, i.e.,

$$\sigma_e^2 = \frac{1}{L} \sum_{n=0}^{L-1} R_{ee}[n, n] = \frac{1}{2\pi} \int_{-\pi}^{\pi} S_{ee}(e^{j\omega}) d\omega, \quad (3.7)$$

where $S_{ee}(e^{j\omega})$ is treated as the power spectrum of the random process $e[n]$ as if it were stationary. We show in Appendix B that

$$\begin{aligned} S_{ee}(e^{j\omega}) &= \sum_{k=-(L-1)}^{L-1} \frac{1}{T_N} S_{xx} \left(\frac{\omega - \frac{2\pi}{L}k}{T_N} \right) \left| \frac{1}{L} \sum_{m=0}^{M-1} G_m(e^{j\omega}) e^{-j(\omega - \frac{2\pi}{L}k)\tau_m/T_N} - \delta[k] \right|^2 \\ &+ \sum_{m=0}^{M-1} (\sigma_m^2/L) \cdot |G_m(e^{j\omega})|^2. \end{aligned} \quad (3.8)$$

Note that in the absence of error due to quantization, i.e., when $\sigma_m^2 = 0, \forall m$, and independent of the signal's characteristics, zero mean-squared reconstruction error is achieved in the system of Figure 2-4 when

$$\begin{aligned} \sum_{m=0}^{M-1} G_m(e^{j\omega}) e^{-j(\omega - \frac{2\pi}{L}k)\tau_m/T_N} &= L\delta[k], \quad \omega \in \Delta\omega_i, \\ k &= -i, -i+1, \dots, L-1-i, \quad i = 0, 1, \dots, L-1. \end{aligned} \quad (3.9)$$

These conditions in (3.9) are consistent with the constraints imposed in (2.8) with the deterministic model for perfect reconstruction in the absence of quantization error. Note that using the optimal reconstruction filters that were obtained in Chapter 2 and which satisfy the constraints for perfect reconstruction, makes the first term in (3.8) vanish. Note also that in the design of the reconstruction filters, the remaining degrees of freedom were used to minimize the output average noise power due to quantization error, which is identical to the second term in (3.8). Therefore, by not restricting the filters $G_m(e^{j\omega})$ to satisfy the

constraints in (3.9), and instead utilizing all degrees of freedom in the filters' design to minimize the overall mean-squared error, we can achieve lower mean-squared reconstruction error. As the next section shows, this reduction in the mean-squared reconstruction error comes at the expense of requiring more information about the input signal $x(t)$.

3.2 Optimal Reconstruction Filters

This section considers the design of the reconstruction filters $G_m(e^{j\omega})$ in the multi-channel reconstruction system of Figure 2-4. The optimal filters $G_m(e^{j\omega})$ are chosen to minimize the mean-squared reconstruction error in (3.7). These filters can be obtained by differentiating $S_{ee}(e^{j\omega})$ in (3.8) with respect to $G_m^R(e^{j\omega}) = \Re\{G_m(e^{j\omega})\}$ and $G_m^I(e^{j\omega}) = \Im\{G_m(e^{j\omega})\}$, as shown in Appendix C. Alternatively, as we next show, the filters can be achieved by expanding (3.8) as a quadratic form of $G_m(e^{j\omega})$. Specifically, it follows from (3.8) that

$$\begin{aligned}
S_{ee}(e^{j\omega}) &= \frac{1}{L} \left\{ \sum_{m_1=0}^{M-1} G_{m_1}(e^{j\omega}) e^{-j\omega\tau_{m_1}/T_N} \sum_{m_2=0}^{M-1} G_{m_2}^*(e^{j\omega}) e^{j\omega\tau_{m_2}/T_N} \right. \\
&\quad \cdot \left(\frac{1}{L} \sum_{k=-(L-1)}^{L-1} \frac{1}{T_N} S_{xx} \left(\frac{\omega - \frac{2\pi}{L}k}{T_N} \right) e^{j\frac{2\pi}{L} \left(\frac{\tau_{m_1} - \tau_{m_2}}{T_N} \right) k} + \sigma_m^2 \delta[m_1 - m_2] \right) \\
&\quad - \frac{1}{T_N} S_{xx} \left(\frac{\omega}{T_N} \right) \left(\sum_{m=0}^{M-1} G_m(e^{j\omega}) e^{-j\omega\tau_m/T_N} \right) \\
&\quad \left. - \frac{1}{T_N} S_{xx} \left(\frac{\omega}{T_N} \right) \left(\sum_{m=0}^{M-1} G_m(e^{j\omega}) e^{-j\omega\tau_m/T_N} \right)^* \right\} + \frac{1}{T_N} S_{xx} \left(\frac{\omega}{T_N} \right). \quad (3.10)
\end{aligned}$$

To simplify, we introduce the following notation:

$$\tilde{\mathbf{G}} = [G_0(e^{j\omega}) \cdot e^{-j\omega\tau_0/T_N}, \dots, G_{M-1}(e^{j\omega}) \cdot e^{-j\omega\tau_{M-1}/T_N}]^T, \quad (3.11a)$$

$$\mathbf{\Sigma} = \text{diagonal}[\sigma_0^2, \sigma_1^2, \dots, \sigma_{M-1}^2], \quad (3.11b)$$

and

$$\begin{aligned}
S_{m,l}^{(i)} &= \frac{1}{L} \sum_{k=-(L-1)}^{L-1} \left(\frac{1}{T_N} S_{xx} \left(\frac{\omega - \frac{2\pi}{L}k}{T_N} \right) \right) e^{j\frac{2\pi}{L}(\frac{\tau_m - \tau_l}{T_N})k} \\
&= \frac{1}{L} \sum_{k=-i}^{L-1-i} S_{xx} \left(e^{j(\omega - \frac{2\pi}{L}k)} \right) e^{j\frac{2\pi}{L}(\frac{\tau_m - \tau_l}{T_N})k}, \quad \omega \in \Delta\omega_i \quad i = 0, 1, \dots, L-1 \\
&\quad m = 0, 1, \dots, M-1, \quad l = 0, 1, \dots, M-1,
\end{aligned} \tag{3.11c}$$

which are the elements of an $M \times L$ Hermitian matrix $S^{(i)}$. An alternative representation of $S^{(i)}$ is

$$S^{(i)} = \tilde{V}^{(i)} S_D^{(i)} (\tilde{V}^{(i)})^H, \quad \omega \in \Delta\omega_i, \quad i = 0, 1, \dots, L-1, \tag{3.12}$$

where $S_D^{(i)}$ is a diagonal matrix whose elements on the main diagonal are $\left\{ S_{xx} \left(e^{j(\omega - \frac{2\pi}{L}l)} \right) \right\}_{l=-i}^{L-1-i}$, and $\tilde{V}^{(i)} = (1/\sqrt{L}) \cdot V^{(i)}$ where $V^{(i)}$ is an $M \times L$ matrix whose elements are

$$V_{m,l}^{(i)} = e^{j\frac{2\pi}{L}(\tau_m/T_N)(l-i)}, \quad m = 0, 1, \dots, M-1, \quad l = 0, 1, \dots, L-1. \tag{3.13}$$

Using the notations defined in (3.11), $S_{ee}(e^{j\omega})$ in (3.10) can be written as

$$\begin{aligned}
S_{ee}(e^{j\omega}) &= \frac{1}{L} \left(\tilde{\mathbf{G}}^H (S^{(i)} + \Sigma) \tilde{\mathbf{G}} - S_{xx}(e^{j\omega}) (\mathbf{1}^T \tilde{\mathbf{G}}) - S_{xx}(e^{j\omega}) (\tilde{\mathbf{G}}^H \cdot \mathbf{1}) \right) + S_{xx}(e^{j\omega}), \\
&\quad \omega \in \Delta\omega_i, \quad i = 0, 1, \dots, L-1,
\end{aligned} \tag{3.14}$$

or equivalently as

$$\begin{aligned}
S_{ee}(e^{j\omega}) &= \frac{1}{L} \left| (S^{(i)} + \Sigma)^{1/2} \tilde{\mathbf{G}} - S_{xx}(e^{j\omega}) (S^{(i)} + \Sigma)^{-1/2} \cdot \mathbf{1} \right|^2 \\
&\quad + S_{xx}(e^{j\omega}) \left(1 - S_{xx}(e^{j\omega}) \cdot \frac{\mathbf{1}^T (S^{(i)} + \Sigma)^{-1} \mathbf{1}}{L} \right), \\
&\quad \omega \in \Delta\omega_i, \quad i = 0, 1, \dots, L-1,
\end{aligned} \tag{3.15}$$

provided that the inverse involved exists, where for the case $M > L$ it is true only if $\sigma_m^2 \neq$

0 $\forall m$. It then follows from (3.15) that the choice of $\tilde{\underline{G}}$ that minimizes $S_{ee}(e^{j\omega})$ is

$$\tilde{\underline{G}}^{opt} = S_{xx}(e^{j\omega})(S^{(i)} + \Sigma)^{-1} \cdot \underline{1}, \quad \omega \in \Delta\omega_i, \quad i = 0, 1, \dots, L-1, \quad (3.16)$$

for which the first term in (3.15) is vanished, and $S_{ee}(e^{j\omega})$ becomes

$$S_{ee}^{min}(e^{j\omega}) = S_{xx}(e^{j\omega}) \left(1 - S_{xx}(e^{j\omega}) \cdot \frac{\underline{1}^T (S^{(i)} + \Sigma)^{-1} \underline{1}}{L} \right), \quad \omega \in \Delta\omega_i, \quad i = 0, 1, \dots, L-1. \quad (3.17)$$

3.2.1 Optimal Reconstruction for the Case of Uniform Sampling

We now consider the special case of $M = L$ where $\tau_m = mT_N$, i.e., the case of uniform sampling at the Nyquist rate. When in addition $\sigma_m^2 = \sigma^2 \quad \forall m$, eq. (3.16) reduces to

$$\tilde{\underline{G}}^{opt} = S_{xx}(e^{j\omega}) \left(\tilde{V}^{(i)} S_D^{(i)} (\tilde{V}^{(i)})^H + \sigma^2 I \right)^{-1} \cdot \underline{1}, \quad \omega \in \Delta\omega_i, \quad i = 0, 1, \dots, L-1. \quad (3.18)$$

Noting that $\tilde{V}^{(i)}$ in this case is a unitary matrix, i.e., $(\tilde{V}^{(i)})^H \tilde{V}^{(i)} = \tilde{V}^{(i)} (\tilde{V}^{(i)})^H = I$, it follows that

$$\begin{aligned} \tilde{\underline{G}}^{opt} &= S_{xx}(e^{j\omega}) \left(\tilde{V}^{(i)} (S_D^{(i)} + \sigma^2 I) (\tilde{V}^{(i)})^H \right)^{-1} \cdot \underline{1} \\ &= S_{xx}(e^{j\omega}) \tilde{V}^{(i)} (S_D^{(i)} + \sigma^2 I)^{-1} (\tilde{V}^{(i)})^H \cdot \underline{1}, \quad \omega \in \Delta\omega_i, \quad i = 0, 1, \dots, L-1. \end{aligned} \quad (3.19)$$

Using the identity

$$\left((\tilde{V}^{(i)})^H \cdot \underline{1} \right)_m = \frac{1}{\sqrt{L}} \left(\sum_{l=0}^{L-1} e^{-j\frac{2\pi}{L} l(m-i)} \right) = \sqrt{L} \cdot \delta[m-i], \quad m = 0, 1, \dots, L-1, \quad (3.20)$$

eq. (3.19) reduces to

$$\tilde{\underline{G}}^{opt} = \frac{S_{xx}(e^{j\omega})}{S_{xx}(e^{j\omega}) + \sigma^2} \cdot \underline{1}, \quad (3.21)$$

which is equivalent to

$$G_m^{opt}(e^{j\omega}) = \frac{S_{xx}(e^{j\omega})}{S_{xx}(e^{j\omega}) + \sigma^2} \cdot e^{j\omega m}, \quad m = 0, 1, \dots, L-1. \quad (3.22)$$

Similarly, it can be shown that

$$\begin{aligned} S_{ee}^{min}(e^{j\omega}) &= S_{xx}(e^{j\omega}) \left(1 - S_{xx}(e^{j\omega}) \cdot \frac{\underline{\mathbf{1}}^T \tilde{\mathbf{V}}^{(i)} (S_D^{(i)} + \sigma^2 \mathbf{I})^{-1} (\tilde{\mathbf{V}}^{(i)})^H \underline{\mathbf{1}}}{L} \right) \\ &= S_{xx}(e^{j\omega}) \left(1 - \frac{S_{xx}(e^{j\omega})}{S_{xx}(e^{j\omega}) + \sigma^2} \right) = \frac{S_{xx}(e^{j\omega}) \cdot \sigma^2}{S_{xx}(e^{j\omega}) + \sigma^2}. \end{aligned} \quad (3.23)$$

As expected, for the case of uniform sampling at the Nyquist rate and where the quantizers in the different channels are the same, the optimal reconstruction filters $G_m^{opt}(e^{j\omega})$ in (3.22) suggest that optimal reconstruction is achieved with interleaving of the multi-channel samples $\tilde{x}_m[n]$ followed by Wiener filtering, as illustrated in Figure 3-1.

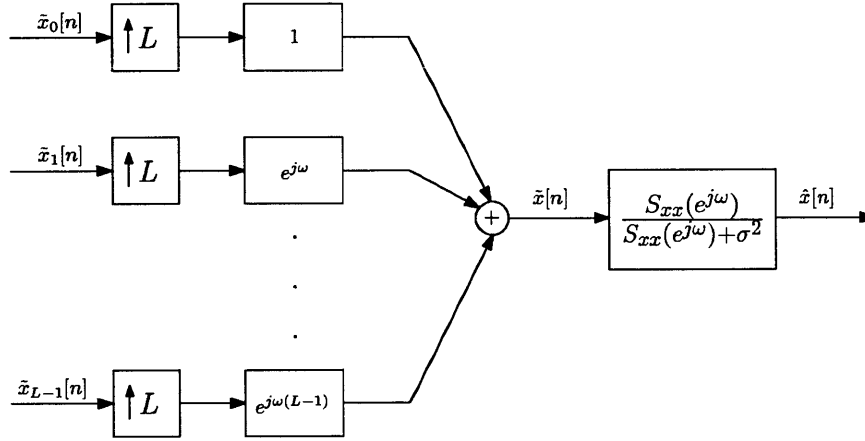


Figure 3-1: Optimal reconstruction is equivalent to interleaving of the multi-channel samples followed by Wiener filtering.

3.3 Illustrative Examples & Simulations

This section discusses and illustrates with examples the design of the quantizers and of the relative timing between the channels in the multi-channel system of Figure 2-7. It considers two cases. The first case illustrates the multi-channel sampling system with two channels,

i.e., $M = 2$, where the sampling rate in each channel is $1/T = 1/(2T_N)$, resulting in an overall sampling rate that is equal to the Nyquist rate of the input signal. The second case illustrates the multi-channel sampling system with $M = 3$ and $L = 2$, corresponding to an oversampling ratio of $M/L = 3/2$. In both cases we develop the optimal reconstruction filters and the corresponding minimum mean-squared reconstruction error.

For the first case, the multi-channel sampling system of Figure 2-7 is considered, where $M = L = 2$, and without loss of generality the time delay $\tau_0 = 0$. We assume that the quantizer step size is the same in both channels, corresponding to $\sigma_0^2 = \sigma_1^2 = \sigma^2$. The matrix $S^{(0)}$ in (3.12) then becomes

$$\begin{aligned} S^{(0)} &= \frac{1}{2} \cdot \begin{bmatrix} 1 & 1 \\ 1 & e^{j\omega_1} \end{bmatrix} \cdot \begin{bmatrix} S_{xx}(e^{j\omega}) & 0 \\ 0 & S_{xx}(e^{j(\omega-\pi)}) \end{bmatrix} \cdot \begin{bmatrix} 1 & 1 \\ 1 & e^{-j\omega_1} \end{bmatrix} \\ &= \frac{1}{2} \begin{bmatrix} S_{xx}(e^{j\omega}) + S_{xx}(e^{j(\omega-\pi)}) & S_{xx}(e^{j\omega}) + e^{-j\omega_1} S_{xx}(e^{j(\omega-\pi)}) \\ S_{xx}(e^{j\omega}) + e^{j\omega_1} S_{xx}(e^{j(\omega-\pi)}) & S_{xx}(e^{j\omega}) + S_{xx}(e^{j(\omega-\pi)}) \end{bmatrix}, \quad \omega \in [0, \pi], \end{aligned} \quad (3.24)$$

where $\omega_1 = \pi \cdot (\tau_1/T_N)$. Substituting (3.24) into (3.16) and into (3.17), we obtain for the optimal reconstruction filters

$$\begin{aligned} \tilde{G}^{opt}(e^{j\omega}) &= \frac{S_{xx}(e^{j\omega}) \cdot \left(\begin{bmatrix} \sigma^2 \\ \sigma^2 \end{bmatrix} + S_{xx}(e^{j(\omega-\pi)}) \cdot \begin{bmatrix} (1 - e^{-j\omega_1})/2 \\ (1 - e^{j\omega_1})/2 \end{bmatrix} \right)}{(S_{xx}(e^{j\omega}) + \sigma^2) \cdot (S_{xx}(e^{j(\omega-\pi)}) + \sigma^2) - S_{xx}(e^{j\omega}) S_{xx}(e^{j(\omega-\pi)}) \cos^2(\frac{\omega_1}{2})}, \\ &\quad \omega \in [0, \pi], \end{aligned} \quad (3.25)$$

and for the minimum achievable $S_{ee}(e^{j\omega})$

$$S_{ee}^{min}(e^{j\omega}) = \frac{\sigma^2 S_{xx}(e^{j\omega}) \cdot (S_{xx}(e^{j(\omega-\pi)}) + \sigma^2)}{(S_{xx}(e^{j\omega}) + \sigma^2) \cdot (S_{xx}(e^{j(\omega-\pi)}) + \sigma^2) - S_{xx}(e^{j\omega}) S_{xx}(e^{j(\omega-\pi)}) \cos^2(\frac{\omega_1}{2})}. \quad (3.26)$$

It is clear from eq. (3.26) that the choice of ω_1 that minimizes the mean squared reconstruction error is $\omega_1 = \pi$, which corresponds to $\tau_1 = T_N$, i.e., uniform sampling. This observation is consistent with the conclusions obtained with the deterministic model in which the re-

construction filters were constrained. Specifically, when the quantizer step size is the same for all channels, an optimal choice of the relative timing between the channels is such that the multi-channel sampling is equivalent to uniform sampling. For this optimal choice of τ_1 , the reconstruction filters become

$$\underline{\tilde{G}}^{opt}(e^{j\omega}) = \frac{S_{xx}(e^{j\omega}) \cdot (\sigma^2 + S_{xx}(e^{j(\omega-\pi)}))}{(S_{xx}(e^{j\omega}) + \sigma^2) \cdot (S_{xx}(e^{j(\omega-\pi)}) + \sigma^2)} \cdot \underline{\mathbf{1}} = \frac{S_{xx}(e^{j\omega})}{(S_{xx}(e^{j\omega}) + \sigma^2)} \cdot \underline{\mathbf{1}}, \quad (3.27)$$

and the minimum achievable $S_{ee}(e^{j\omega})$ reduces to

$$S_{ee}^{min}(e^{j\omega}) = \frac{\sigma^2 S_{xx}(e^{j\omega}) \cdot (S_{xx}(e^{j(\omega-\pi)}) + \sigma^2)}{(S_{xx}(e^{j\omega}) + \sigma^2) \cdot (S_{xx}(e^{j(\omega-\pi)}) + \sigma^2)} = \frac{S_{xx}(e^{j\omega}) \cdot \sigma^2}{(S_{xx}(e^{j\omega}) + \sigma^2)}. \quad (3.28)$$

For the second case, we consider the multi-channel sampling system where $M = 3$, $L = 2$, and $\tau_0 = 0$. The matrix $S^{(0)}$ in this case gets the form

$$S^{(0)} = \frac{1}{2} \begin{bmatrix} 1 & 1 \\ 1 & e^{j\omega_1} \\ 1 & e^{j\omega_2} \end{bmatrix} \cdot \begin{bmatrix} S_{xx}(e^{j\omega}) & 0 \\ 0 & S_{xx}(e^{j(\omega-\pi)}) \end{bmatrix} \cdot \begin{bmatrix} 1 & 1 & 1 \\ 1 & e^{-j\omega_1} & e^{-j\omega_2} \end{bmatrix} =$$

$$\begin{bmatrix} (S_{xx}(e^{j\omega}) + S_{xx}(e^{j(\omega-\pi)}))/2 & (S_{xx}(e^{j\omega}) + S_{xx}(e^{j(\omega-\pi)})e^{-j\omega_1})/2 & (S_{xx}(e^{j\omega}) + S_{xx}(e^{j(\omega-\pi)})e^{-j\omega_2})/2 \\ (S_{xx}(e^{j\omega}) + S_{xx}(e^{j(\omega-\pi)})e^{j\omega_1})/2 & (S_{xx}(e^{j\omega}) + S_{xx}(e^{j(\omega-\pi)}))/2 & (S_{xx}(e^{j\omega}) + S_{xx}(e^{j(\omega-\pi)})e^{j(\omega_1-\omega_2)})/2 \\ (S_{xx}(e^{j\omega}) + S_{xx}(e^{j(\omega-\pi)})e^{j\omega_2})/2 & (S_{xx}(e^{j\omega}) + S_{xx}(e^{j(\omega-\pi)})e^{j(\omega_2-\omega_1)})/2 & (S_{xx}(e^{j\omega}) + S_{xx}(e^{j(\omega-\pi)}))/2 \end{bmatrix},$$

$\omega \in [0, \pi]$. (3.29)

Consequently,

$$\underline{\mathbf{1}}^T \cdot (S^{(0)} + \Sigma)^{-1} \cdot \underline{\mathbf{1}} = \frac{2S_{xx}(e^{j(\omega-\pi)}) \cdot (\sigma_0^2 \sin^2(\frac{\omega_1-\omega_2}{2}) + \sigma_1^2 \sin^2(\frac{\omega_2}{2}) + \sigma_2^2 \sin^2(\frac{\omega_1}{2}))}{\det(S^{(0)} + \Sigma)}$$

$$+ \frac{\sigma_0^2 \sigma_1^2 + \sigma_0^2 \sigma_2^2 + \sigma_1^2 \sigma_2^2}{\det(S^{(0)} + \Sigma)}, \quad \omega \in [0, \pi] \quad (3.30)$$

where

$$\begin{aligned} \det(S^{(0)} + \Sigma) &= S_{xx}(e^{j\omega}) \cdot S_{xx}(e^{j(\omega-\pi)}) \cdot \left(\sigma_0^2 \sin^2 \left(\frac{\omega_1 - \omega_2}{2} \right) + \sigma_1^2 \sin^2 \left(\frac{\omega_2}{2} \right) + \sigma_2^2 \sin^2 \left(\frac{\omega_1}{2} \right) \right) \\ &+ \frac{(S_{xx}(e^{j\omega}) + S_{xx}(e^{j(\omega-\pi)}))}{2} \cdot (\sigma_0^2 \sigma_1^2 + \sigma_0^2 \sigma_2^2 + \sigma_1^2 \sigma_2^2) + \sigma_0^2 \sigma_1^2 \sigma_2^2, \quad \omega \in [0, \pi]. \end{aligned} \quad (3.31)$$

It then follows from (3.16) and (3.17) that

$$\begin{aligned} \tilde{G}_0(e^{j\omega}) &= \frac{S_{xx}(e^{j\omega}) \cdot [S_{xx}(e^{j(\omega-\pi)}) \cdot (\sigma_1^2 \left(\frac{1-e^{-j\omega_2}}{2} \right) + \sigma_2^2 \left(\frac{1-e^{-j\omega_1}}{2} \right)) + \sigma_1^2 \sigma_2^2]}{\det(S^{(0)} + \Sigma)} \\ \tilde{G}_1(e^{j\omega}) &= \frac{S_{xx}(e^{j\omega}) \cdot [S_{xx}(e^{j(\omega-\pi)}) \cdot (\sigma_0^2 \left(\frac{1-e^{j(\omega_1-\omega_2)}}{2} \right) + \sigma_2^2 \left(\frac{1-e^{j\omega_1}}{2} \right)) + \sigma_0^2 \sigma_2^2]}{\det(S^{(0)} + \Sigma)} \\ \tilde{G}_2(e^{j\omega}) &= \frac{S_{xx}(e^{j\omega}) \cdot [S_{xx}(e^{j(\omega-\pi)}) \cdot (\sigma_0^2 \left(\frac{1-e^{j(\omega_2-\omega_1)}}{2} \right) + \sigma_2^2 \left(\frac{1-e^{j\omega_2}}{2} \right)) + \sigma_0^2 \sigma_1^2]}{\det(S^{(0)} + \Sigma)} \\ \omega &\in [0, \pi], \end{aligned} \quad (3.32)$$

and that

$$S_{ee}^{min}(e^{j\omega}) = \frac{S_{xx}(e^{j\omega}) \left(S_{xx}(e^{j(\omega-\pi)}) \cdot (\sigma_0^2 \sigma_1^2 + \sigma_0^2 \sigma_2^2 + \sigma_1^2 \sigma_2^2) / 2 + \sigma_0^2 \sigma_1^2 \sigma_2^2 \right)}{\det(S^{(0)} + \Sigma)}. \quad (3.33)$$

Thus, the optimal choice of ω_1 and ω_2 that achieves the lowest possible $S_{ee}^{min}(e^{j\omega})$ is also the one that maximizes $\det(S^{(0)} + \Sigma)$. Since $S_{xx}(e^{j\omega})$ is non-negative, the optimization reduces to maximizing the function $d(\omega_1, \omega_2)$ introduced in (3.34) with respect to ω_1 and ω_2 .

$$d(\omega_1, \omega_2) = \sigma_0^2 \sin^2 \left(\frac{\omega_1 - \omega_2}{2} \right) + \sigma_1^2 \sin^2 \left(\frac{\omega_2}{2} \right) + \sigma_2^2 \sin^2 \left(\frac{\omega_1}{2} \right). \quad (3.34)$$

Differentiating (3.34) with respect to ω_1 and ω_2 , we obtain

$$\frac{1}{2} (\sigma_2^2 \cdot \sin(\omega_1) + \sigma_0^2 \cdot \sin(\omega_1 - \omega_2)) = 0 \quad (3.35a)$$

$$\frac{1}{2} (\sigma_1^2 \cdot \sin(\omega_2) - \sigma_0^2 \cdot \sin(\omega_1 - \omega_2)) = 0. \quad (3.35b)$$

Note that eqs. (3.35a) and (3.35b) are equivalent to the equations in (2.46a) which set the conditions to achieve the lower bound on the mean squared reconstruction error, i.e., to achieve equality in (2.45).

When the quantizer step size is the same in all channels, i.e., when $\sigma_0^2 = \sigma_1^2 = \sigma_2^2 = \sigma^2$, eqs. (3.35) are solved for $\omega_1 = -\omega_2 = \pm 2\pi/3$, corresponding to $\tau_1 = -\tau_2 = \pm 2/3T_N$, i.e., uniform sampling. In that case, the optimal reconstruction filters are

$$\tilde{G}_m(e^{j\omega}) = \frac{2}{3} \frac{S_{xx}(e^{j\omega})}{S_{xx}(e^{j\omega}) + \frac{2}{3}\sigma^2}, \quad (3.36)$$

with which the multi-channel reconstruction is equivalent to interleaving the multi-channel output samples followed by sampling rate conversion and Wiener filtering, as illustrated in Figure 3-2.

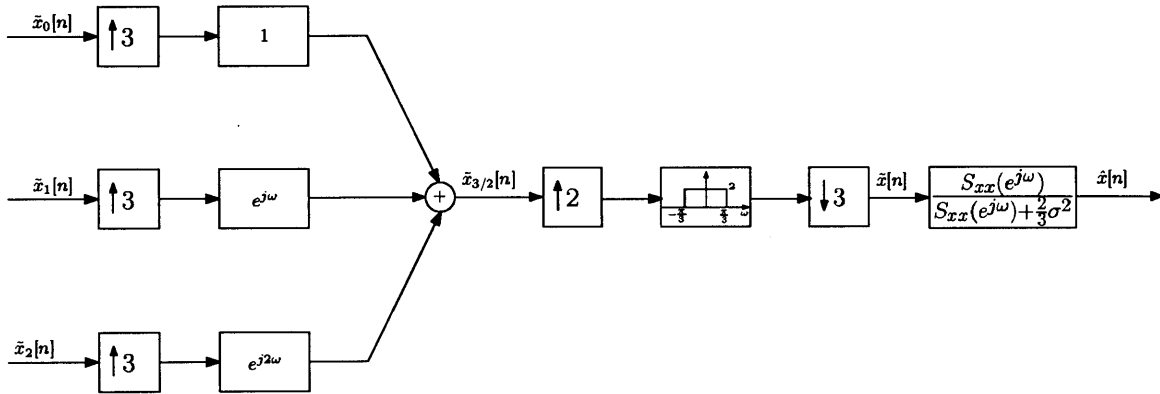


Figure 3-2: Interleaving followed by sampling rate converter and Wiener filtering.

Correspondingly,

$$S_{ee}^{min}(e^{j\omega}) = \frac{\sigma^2 \cdot S_{xx}(e^{j\omega})}{\frac{3}{2}S_{xx}(e^{j\omega}) + \sigma^2} \leq \frac{\sigma^2 \cdot S_{xx}(e^{j\omega})}{S_{xx}(e^{j\omega}) + \sigma^2}, \quad (3.37)$$

where the right side of the inequality is achieved with uniform sampling at the Nyquist rate.

Note also that by writing $S_{ee}^{min}(e^{j\omega})$ from (3.37) as

$$S_{ee}^{min}(e^{j\omega}) = \frac{1}{\frac{2}{3}\sigma^2 + \frac{1}{S_{xx}(e^{j\omega})}}, \quad (3.38)$$

we conclude that $S_{ee}^{min}(e^{j\omega}) \leq \frac{2}{3}\sigma^2$, from which it follows that $\sigma_e^{2min} \leq \frac{2}{3}\sigma^2$. In other words, the minimum mean squared reconstruction error achieved with this approach is lower than $\frac{2}{3}\sigma^2$, corresponding to the minimum mean squared reconstruction error achieved with the constrained reconstruction filters.

However, when the quantizer step size is not the same for all channels, the choice of $\tau_1 = -\tau_2 = \pm 2/3T_N$, which corresponds to uniform sampling, is no longer optimal, and better performance can be achieved with a different choice of the time delays τ_1 and τ_2 , for which the multi-channel sampling is equivalent to recurrent nonuniform sampling. Figure 3-3 illustrates the relative gain of $d(\omega_1, \omega_2)$ over the case of uniform sampling when 3 bits are allocated to channel 0, 4 bits to channel 1, and 4 bits to channel 2. As illustrated, the optimal time delays are $\tau_1/T_N = -\tau_2/T_N = \pm 0.54$, which are identical to those obtained in (2.68) where the filters are constrained, and correspond to recurrent nonuniform sampling.

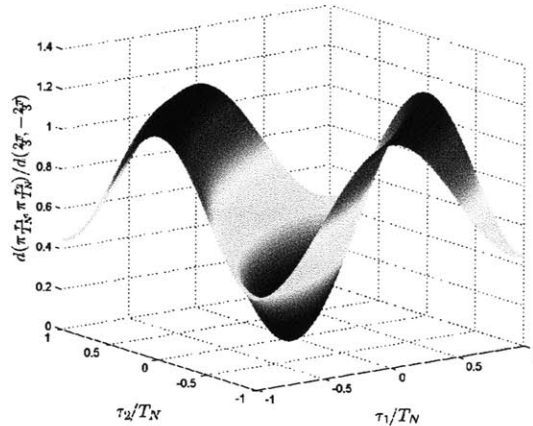


Figure 3-3: The relative gain of $d(\omega_1, \omega_2)$ as compared to the case of uniform sampling when $N_0 = 3, N_1 = 4, N_2 = 4$.

SINC INTERPOLATION OF NONUNIFORM SAMPLES

It is well known that a bandlimited signal can be uniquely recovered from nonuniformly spaced samples under certain conditions on the nonuniform grid and provided that the average sampling rate meets or exceeds the Nyquist rate. However, reconstruction of the continuous-time signal from nonuniform samples is typically more difficult to implement than from uniform samples. Motivated by the fact that sinc interpolation results in perfect reconstruction for uniform sampling, we develop a class of approximate reconstruction methods from nonuniform samples based on the use of time-invariant lowpass filtering, i.e., sinc interpolation. The methods discussed consist of four cases incorporated in a single framework.

4.1 Introduction

Discrete-time signals can arise in many ways, but they most commonly occur as representations of sampled continuous-time signals. The most common form of sampling used in the context of discrete-time processing of continuous-time signals is uniform sampling corresponding to samples of continuous-time signals obtained at equally spaced time intervals. Under certain conditions, specified by the Nyquist-Shannon sampling theorem, the original signal can be reconstructed from this set of equally-spaced samples. The reconstruction is done through sinc interpolation¹ corresponding to the impulse response of a

¹Throughout the thesis we refer to convolution of an impulse train of samples with the function $h(t) = \text{sinc}(\frac{\pi}{T}t)$ as sinc interpolation and use the historical unnormalized definition of the sinc function,

linear time-invariant ideal lowpass filter.

In a variety of contexts, nonuniform sampling naturally arises or is preferable to uniform sampling. For example, some biomedical devices utilize low-power sensors that use self-timed circuits, thus removing the need for power-intensive clock buffers and clock distribution. However, these self-timed circuits tend to introduce nonuniformity in the sampling clock [1]. Nonuniform sampling also often arises in time-interleaved analog-to-digital converters, where a signal is passed through multiple parallel channels, each uniformly sampling the signal at the same rate. The output samples of the channels are then multiplexed to obtain a full discrete-time representation of the signal. For the case in which the clock phases of these channels are asynchronous, interleaving samples from each channel leads to recurrent nonuniform sampling [100]. Recurrent nonuniform sampling also often arises in sensor networks in which each sensor uniformly samples the environment asynchronously and transmits to a main base station, where the samples are interleaved.

In many cases nonuniform sampling is deliberate and advantageous. In the spatial domain, non-uniformity of the spacing of the array elements in an antenna or acoustic sensor array is often part of the array design as a trade off between the length of the array and the number of elements. In ray traced computer graphics, it has been shown that nonuniform sampling yields aliasing that is less conspicuous to the observer [65].

Exact reconstruction of a bandlimited continuous-time signal from nonuniform samples is based on Lagrange interpolation. For the case of uniform sampling, Lagrange interpolation reduces to sinc interpolation and can be approximated with well designed low pass filtering. When the sampling grid is not uniform, Lagrange interpolation is more difficult as discussed in section 4.2. In this chapter we consider sinc interpolation of nonuniform samples as a way to approximately reconstruct the continuous-time signal. A class of approximate reconstruction methods is proposed in which each method corresponds to a different assumption with respect to the knowledge of the exact sampling times and of the probability distribution of their deviation from a uniform sampling grid.

i.e., $\text{sinc}(x) \triangleq \frac{\sin(x)}{x}$

4.2 Reconstruction of Bandlimited Signals from Nonuniform Samples

A variety of approaches to reconstruction of signals from nonuniform samples have been previously proposed and discussed. In a classic paper on nonuniform sampling of bandlimited signals [100], Yen introduced several reconstruction theorems to address the cases of a finite number of nonuniform samples on an otherwise uniform grid, a single gap in uniform sampling and recurrent nonuniform sampling. Other reconstruction approaches, specific to recurrent nonuniform sampling have also been proposed [71], [43], [61], [23], [82]. In the work of Yao and Thomas [98], the Lagrange interpolation functions were applied to the reconstruction of bandlimited signals from nonuniform samples. It is shown there that a finite-energy signal $x(t)$ bandlimited to $\pm\pi/T_N$ can be reconstructed from its nonuniform samples $x(t_n)$ using Lagrange interpolation when the sampling instants t_n do not deviate by more than $T_N/4$ from a uniform grid with spacing of T_N . Specifically, if

$$|t_n - nT_N| \leq d < T_N/4, \quad \forall n \in \mathbb{Z}, \quad (4.1)$$

then

$$x(t) = \sum_{n=-\infty}^{\infty} x(t_n) l_n(t), \quad (4.2a)$$

where

$$l_n(t) = \frac{G(t)}{G'(t_n)(t - t_n)}, \quad (4.2b)$$

$$G(t) = (t - t_0) \prod_{\substack{k=-\infty \\ k \neq 0}}^{\infty} \left(1 - \frac{t}{t_k}\right), \quad (4.2c)$$

and $G'(t) \triangleq \frac{dG(t)}{dt}$. Interpolation using eqs. (4.2) is referred to as Lagrange interpolation. This theorem is based on a theorem proved by Levinson [53] which states that the functions $\{L_n(\Omega)\}$, defined as the Fourier transform of $\{l_n(t)\}$, are bandlimited and form a sequence biorthogonal to $\{e^{j\Omega t_n}\}$ over $[-\frac{\pi}{T_N}, \frac{\pi}{T_N}]$ given that the condition of eq. (4.1) is satisfied.

Specifically,

$$L_n(\Omega) = \int_{-\infty}^{\infty} l_n(t) e^{-j\Omega t} dt = 0, \quad |\Omega| > \frac{\pi}{T_N}, \quad (4.3)$$

and

$$\frac{1}{2\pi} \int_{-\frac{\pi}{T_N}}^{\frac{\pi}{T_N}} L_n(\Omega) e^{j\Omega t_k} d\Omega = l_n(t_k) = \delta[n - k]. \quad (4.4)$$

Eq. (4.4) utilizes the interpolation condition of the Lagrange kernel which ensures that the property of consistent resampling is upheld, i.e., that sampling the reconstructed signal on the nonuniform grid $\{t_n\}$ yields the original samples $\{x(t_n)\}$. Note that expressing $L_n(\Omega)$ as the Fourier transform of $l_n(t)$ in (4.4) results in biorthogonality of the sequences $\{l_n(t)\}$ and $\{\text{sinc}(\pi/T_N(t - t_n))\}$, i.e.,

$$\int_{-\infty}^{\infty} l_n(t) \text{sinc}(\pi/T_N(t - t_k))/T_N dt = \delta[n - k], \quad (4.5)$$

from which the expansion in (4.2) for bandlimited signals is clearly followed.

The difficulty of exact reconstruction of bandlimited signals from nonuniform samples through Lagrange interpolation is partly due to the fact that the interpolating functions at different sampling times do not have the same form except in special cases. Also, each interpolating function depends on all sampling instants. The complexity of the implementation motivates the need for simpler approximate approaches to reconstruction and a variety of methods has previously been proposed. One practical approach to recovering a signal from its nonuniform samples has been the use of nonuniform splines [10]. Iterative reconstruction methods for nonuniform sampling which are computationally demanding and have potential issues of convergence have also been previously proposed [25], [26], [30]. In a different approach, time-warping methods were applied by Papoulis in [70] to reconstruct bandlimited signals from jittered samples. In [17] and [103], time-warping was used for reconstruction from samples of signals with time-varying frequency content. A method of designing FIR filters in such a way that the effect of input clock jitter is diminished is discussed in [84]. In [60] several approaches are suggested and analyzed for approximate

reconstruction from jittered samples. Mean-square comparison of various interpolators is done in [52] for the case of uniform sampling, uniform sampling with skips, and Poisson sampling. A modification of the conventional Lagrange interpolator is proposed in [77] which allows approximating a bandlimited signal from its nonuniform samples with high accuracy. A comprehensive review of literature concerning other techniques in nonuniform sampling can be found in [33] and [58].

4.3 Sinc Interpolation of Nonuniform Samples

With uniform sampling, i.e., when $t_n = nT$, $G(t)$ of eq. (4.2c) reduces to

$$G(t) = \frac{\sin(\frac{\pi}{T}t)}{\frac{\pi}{T}}, \quad (4.6)$$

and Lagrange interpolation reduces to sinc interpolation. In this section we restrict $l_n(t)$ in eq. (4.2a) to be of the form $l_n(t) = (T/T_N)\text{sinc}(\pi/T_N \cdot (t - \tilde{t}_n))$ corresponding to sinc interpolation. Note that since the kernel used in this framework is time-invariant, the exact sampling instants are not needed in designing the reconstruction filter. This is in contrast to Lagrange interpolation in which this knowledge is required in forming the interpolating functions since these functions do not have the same form at each sampling instant and each interpolating function depends on all sampling instants, i.e., it is not a time-invariant convolution. It will be assumed throughout this section that the average sampling rate meets or exceeds the Nyquist rate, or equivalently that $T \leq T_N$ where T denotes the nominal sampling interval.

We consider and analyze four cases incorporated in a single framework where the choice for the values \tilde{t}_n differs for each of the methods discussed below. In the first case, it is assumed that both the exact sampling instants and the probability distribution of their deviation from a uniform sampling grid are known. As we will see in section 4.3.6, even with the knowledge of the exact sampling instants, it can sometimes be beneficial to place the samples on a grid other than the actual nonuniform grid corresponding to the sampling instants. In determining this grid we utilize the probability distribution of the deviation of

the sampling instants from a uniform sampling grid. In the second case, sinc interpolation is applied to the samples placed on a uniform grid with spacing corresponding to the average or nominal spacing of the nonuniform sampling grid. In that approximation it is not necessary to know the exact sampling instants since they are not used. This may occur in situations where the samples are stored in memory and their exact timing information is lost. The third case consists of applying sinc interpolation to the samples located at the actual nonuniform sampling times. This method requires knowledge of the nonuniform grid. However, as opposed to Lagrange interpolation where the sampling instants are needed in advance to generate the interpolating functions, the sinc interpolation function requires only knowledge of the nominal sample spacing. In the fourth case, it is assumed that the exact sampling times are not known but that the probability distribution of their deviation from a uniform sampling grid is known.

4.3.1 Mathematical Formulation

To have a common framework that incorporates these four cases, we denote by $x[n]$ a sequence of nonuniform samples of $x(t)$, i.e.,

$$x[n] = x(t_n) \quad (4.7)$$

where $\{t_n\}$ represent a nonuniform grid which we model as a perturbation of a uniform grid with spacing T , i.e.,

$$t_n = nT + \xi_n. \quad (4.8)$$

For analysis purposes, we consider $x(t)$ to be a continuous-time zero-mean wide-sense stationary random process with autocorrelation function $R_{xx}(\tau)$ and power spectral density (PSD) $S_{xx}(\Omega)$ which is zero for $|\Omega| \geq \Omega_c = \pi/T_N$. ξ_n is characterized as an i.i.d. sequence of zero-mean random variables independent of $x(t)$ with probability density function (pdf) $f_\xi(\xi)$ and characteristic function $\Phi_\xi(\Omega) = \int_{-\infty}^{\infty} f_\xi(\xi') e^{j\Omega\xi'} d\xi'$.

For the reconstruction of $x(t)$ from its nonuniform samples $x[n]$, we apply sinc interpolation to the samples placed on a second nonuniform grid $\tilde{t}_n = nT + \zeta_n$ that in general is

not restricted to the nonuniform grid on which the samples were originally acquired, i.e., ζ_n and ξ_n are not necessarily equal. The reconstruction takes the form

$$\hat{x}(t) = \sum_{n=-\infty}^{\infty} (T/T_N) \cdot x(t_n) \cdot h(t - \tilde{t}_n), \quad (4.9)$$

with $h(t) = \text{sinc}(\frac{\pi}{T_N}t)$ as illustrated in Figure 4-1, where $\frac{\pi}{T_N}$ is the highest frequency in $x(t)$.

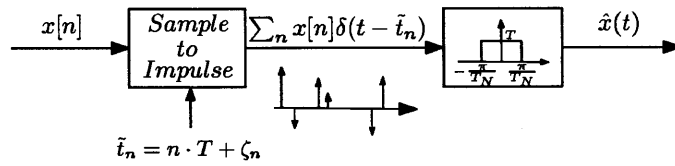


Figure 4-1: Reconstruction using sinc interpolation.

The four cases outlined above are incorporated into this general framework as follows: For the first case, we characterize ζ_n as another i.i.d sequence of random variables independent of $x(t)$ and for which ζ_n is independent of ξ_k when $n \neq k$. This case will be referred to as Randomized Sinc Interpolation (RSI) and is the most general case we consider, since the other three cases can be treated as special cases of it. In the second case, we assume that only the average spacing of the nonuniform grid is known rather than the exact location of the sampling times. This corresponds to choosing $\zeta_n = 0$ and applying sinc interpolation to the samples placed on a uniform grid. We refer to this case as Uniform Sinc Interpolation (USI). The third case referred to as Nonuniform Sinc Interpolation (NSI) corresponds to choosing $\zeta_n = \xi_n$, i.e., the reconstruction is carried out on the nonuniform grid corresponding to the sampling instants. In the fourth case, we assume that the deviations ξ_n of the sampling instants from a uniform grid are not known but their probability distribution is known. Therefore, ζ_n is characterized as an i.i.d sequence of random variables independent of $x(t)$ and for which ζ_n is independent of ξ_k for all n, k . This case will be referred to as Independent Sinc Interpolation (ISI). Table 4.1 summarizes these four cases.

Table 4.1: Sinc Interpolation Reconstruction Methods

<p>Randomized Sinc Interpolation (RSI) Sinc interpolation is applied to the samples placed on a grid determined by both the exact sampling instants and the pdf of their deviation from a uniform sampling grid</p>	<p>Nonuniform Sinc Interpolation (NSI) Sinc interpolation is applied to the samples placed on the nonuniform grid corresponding to the sampling instants</p>
<p>Independent Sinc Interpolation (ISI) Sinc interpolation is applied to the samples located on a grid independent of the actual nonuniform grid</p>	<p>Uniform Sinc Interpolation (USI) Sinc interpolation is applied to the samples placed on a uniform grid</p>

4.3.2 Randomized Sinc Interpolation

Appendix D shows an equivalence with respect to second-order statistics² between the nonuniform sampling discussed above when followed by Randomized Sinc Interpolation and the system in Figure 4-2.

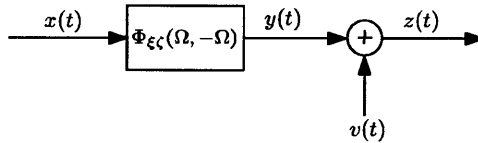


Figure 4-2: A second-order statistics model for nonuniform sampling followed by Randomized Sinc Interpolation for the case where $T \leq T_N$.

The frequency response of the LTI system in Figure 4-2 is the joint characteristic function $\Phi_{\xi\zeta}(\Omega_1, \Omega_2)$ of ξ_n and ζ_n , defined as the Fourier transform of their joint pdf $f_{\xi\zeta}(\xi, \zeta)$. In the same figure, $v(t)$ is zero-mean additive colored noise, uncorrelated with $x(t)$, with PSD as follows:

$$S_{vv}(\Omega) = \begin{cases} \frac{T}{2\pi} \int_{-\Omega_c}^{\Omega_c} S_{xx}(\Omega') (1 - |\Phi_{\xi\zeta}(\Omega', -\Omega)|^2) d\Omega' & |\Omega| < \Omega_c \\ 0 & |\Omega| \geq \Omega_c \end{cases} \quad (4.10)$$

Thus, with respect to second-order statistics, $\hat{x}(t)$ can equivalently be represented by the signal $z(t)$ in Figure 4-2.

²Throughout the thesis we use the terminology of equivalence between two systems with respect to second-order statistics to mean that for the same input, the output means, auto-correlation functions, and cross-correlation functions are identical.

We denote $e^R(t) = \hat{x}(t) - x(t)$ as the error between $x(t)$ and its approximation $\hat{x}(t)$ obtained by RSI. Then, as shown in Appendix D, the corresponding mean square error (MSE) is given by

$$\sigma_{e^R}^2 = \frac{1}{2\pi} \int_{-\Omega_c}^{\Omega_c} S_{xx}(\Omega) \cdot Q(\Omega) d\Omega, \quad (4.11)$$

where

$$Q(\Omega) = |1 - \Phi_{\xi\xi}(\Omega, -\Omega)|^2 + \frac{1}{r} \cdot \int_{-\Omega_c}^{\Omega_c} \frac{1 - |\Phi_{\xi\xi}(\Omega, -\Omega_1)|^2}{2\Omega_c} d\Omega_1, \quad (4.12)$$

and $r = T_N/T \geq 1$ denotes the oversampling ratio.

4.3.3 Uniform Sinc Interpolation

In the case where neither the sampling instants nor their distribution is known, we set the perturbations ζ_n in the reconstruction of Figure 4-1 to zero. This results in

$$\hat{x}(t) = \sum_{n=-\infty}^{\infty} (T/T_N) \cdot x(t_n) \cdot h(t - nT), \quad (4.13)$$

which corresponds to treating the nonuniform samples as being on a uniform grid and reconstructing $x(t)$ with sinc interpolation of these samples as though the sampling was uniform, corresponding to USI. Note that when USI is used for reconstruction, the signal $x(t)$ in the equivalent system of Figure 4-2 is in effect pre-filtered by the characteristic function $\Phi_{\xi}(\Omega)$ of ξ_n , and the additive uncorrelated noise $v(t)$ is white. Since $|\Phi_{\xi}(\Omega)| \leq \Phi_{\xi}(\Omega)|_{\Omega=0} = 1$, the characteristic function has in general the behavior of a lowpass filter when viewed as a frequency response of an LTI system³.

The error between $x(t)$ and its approximation $\hat{x}(t)$ obtained by USI is denoted by $e^U(t)$ and the corresponding MSE follows directly from (4.11) by replacing $\Phi_{\xi\xi}(\Omega_1, \Omega_2)$ with

³Note that when ξ_n is symmetrically distributed on $(-T/2, T/2)$, the characteristic function $\Phi_{\xi}(\Omega)$ is real and symmetric. In addition, in the region $\Omega \in (-\pi/T, \pi/T)$ $\Phi_{\xi}(\Omega)$ is non-negative, concave and bounded from below by $\cos(\Omega T/2)$, as elaborated in Appendix E. Its radius of curvature at $\Omega = 0$ is also shown to be inversely proportional to the variance σ_{ξ}^2 of ξ_n .

$\Phi_\xi(\Omega_1)$, i.e.,

$$\sigma_{eU}^2 = \frac{1}{2\pi} \int_{-\Omega_c}^{\Omega_c} S_{xx}(\Omega) \cdot \left\{ |1 - \Phi_\xi(\Omega)|^2 + \frac{1}{r} \cdot (1 - |\Phi_\xi(\Omega)|^2) \right\} d\Omega. \quad (4.14)$$

For the case of no oversampling, i.e., when the oversampling factor $r = 1$, the MSE in eq. (4.14) reduces to

$$\begin{aligned} \sigma_{eU}^2 &= 2 \cdot \frac{1}{2\pi} \int_{-\Omega_c}^{\Omega_c} S_{xx}(\Omega) \cdot (1 - \Re(\Phi_\xi(\Omega))) d\Omega \\ &= 2 \cdot \left(R_{xx}(0) - \frac{1}{2\pi} \int_{-\Omega_c}^{\Omega_c} S_{xx}(\Omega) \cdot \Re(\Phi_\xi(\Omega)) d\Omega \right) \\ &= 2 \cdot \left(R_{xx}(0) - \int_{-\infty}^{\infty} R_{xx}(\tau) \cdot f_\xi^{(\text{even})}(\tau) d\tau \right), \end{aligned} \quad (4.15)$$

where $f_\xi^{(\text{even})}(\tau) = (f_\xi(\tau) + f_\xi(-\tau))/2$ is the even part of $f_\xi(\tau)$. When in addition, ξ_n is symmetrically distributed on $(-T_N/2, T_N/2)$, the following inequalities on the mean square reconstruction error follow by utilizing the properties of $R_{xx}(\tau)$ and $\Phi_\xi(\Omega)$ given in Appendix E,

$$1 - \min(\rho_{xx}(\xi_0), \Phi_\xi(\Omega_0)) \leq \frac{\sigma_{eU}^2}{2R_{xx}(0)} \leq 1 - \max(\rho_{xx}(T_N/2), \Phi_\xi(\pi/T_N)), \quad (4.16)$$

where $\rho_{xx}(\tau) = R_{xx}(\tau)/R_{xx}(0)$, $\xi_0 = E(|\xi|)$ and $\Omega_0 = \int_{-\Omega_c}^{\Omega_c} |\Omega| \cdot \frac{S_{xx}(\Omega)}{\int_{-\Omega_c}^{\Omega_c} S_{xx}(\Omega') d\Omega'} d\Omega$. The fact that $R_{xx}(\tau)$ is monotonically decreasing in $(0, T_N/2)$ and $\Phi_\xi(\Omega)$ is monotonically decreasing in $(0, \pi/T_N)$ leads to

$$\int_{-T_N/2}^{T_N/2} R_{xx}(\tau) f_\xi(\tau) d\tau \geq R_{xx}(T_N/2) \int_{-T_N/2}^{T_N/2} f_\xi(\tau) d\tau = R_{xx}(T_N/2), \quad (4.17)$$

$$\frac{1}{2\pi} \int_{-\Omega_c}^{\Omega_c} S_{xx}(\Omega) \cdot \Phi_\xi(\Omega) d\Omega \geq \frac{1}{2\pi} \int_{-\Omega_c}^{\Omega_c} S_{xx}(\Omega) d\Omega \cdot \Phi_\xi(\pi/T_N) = R_{xx}(0) \cdot \Phi_\xi(\pi/T_N), \quad (4.18)$$

from which the upper bound in (4.16) clearly follows. To obtain the lower bound in (4.16)

we use the concavity of $R_{xx}(\tau)$ and $\Phi_\xi(\Omega)$ in the appropriate regions. Specifically,

$$\begin{aligned} \int_{-T_N/2}^{T_N/2} R_{xx}(\tau) f_\xi(\tau) d\tau &= \int_0^{T_N/2} R_{xx}(\tau) \cdot 2f_\xi(\tau) d\tau \leq R_{xx} \left(\int_0^{T_N/2} \tau \cdot 2f_\xi(\tau) d\tau \right) = \\ R_{xx} \left(\int_0^{T_N/2} \tau \cdot (f_\xi(\tau) + f_\xi(-\tau)) d\tau \right) &= R_{xx}(E(|\xi|)), \end{aligned} \quad (4.19)$$

and

$$\begin{aligned} \frac{1}{2\pi} \int_{-\Omega_c}^{\Omega_c} S_{xx}(\Omega) \cdot \Phi_\xi(\Omega) d\Omega &= R_{xx}(0) \cdot \frac{1}{2\pi} \int_{-\Omega_c}^{\Omega_c} \frac{S_{xx}(\Omega)}{\frac{1}{2\pi} \int_{-\Omega_c}^{\Omega_c} S_{xx}(\Omega') d\Omega'} \cdot \Phi_\xi(\Omega) d\Omega = \\ R_{xx}(0) \cdot \int_0^{\Omega_c} \frac{2S_{xx}(\Omega)}{\int_{-\Omega_c}^{\Omega_c} S_{xx}(\Omega') d\Omega'} \cdot \Phi_\xi(\Omega) d\Omega &\leq R_{xx}(0) \cdot \Phi_\xi \left(\int_0^{\Omega_c} \Omega \cdot \frac{2S_{xx}(\Omega)}{\int_{-\Omega_c}^{\Omega_c} S_{xx}(\Omega') d\Omega'} d\Omega \right) = \\ R_{xx}(0) \cdot \Phi_\xi \left(\int_{-\Omega_c}^{\Omega_c} |\Omega| \cdot \frac{S_{xx}(\Omega)}{\int_{-\Omega_c}^{\Omega_c} S_{xx}(\Omega') d\Omega'} d\Omega \right). \end{aligned} \quad (4.20)$$

Note that the inequality in (4.19) suggests that when $E(|\xi|) = \xi_0 < T_N/2$ is fixed, minimum mean square reconstruction error of USI is achieved when ξ_n takes the values $\pm \xi_0$ with equal probabilities, i.e., when $\Phi_\xi(\Omega) = \cos(\xi_0 \Omega)$. Alternatively, when $\int_{-\Omega_c}^{\Omega_c} |\Omega| \cdot \frac{S_{xx}(\Omega)}{\int_{-\Omega_c}^{\Omega_c} S_{xx}(\Omega') d\Omega'} d\Omega = \Omega_0 < \pi/T_N$ is fixed, it follows from (4.20) that minimum mean square reconstruction error of USI is achieved when $\rho_{xx}(\tau) = \cos(\Omega_0 \tau)$. The lower bound in (4.16) together with the fact that when a lower bound is achieved it is the greatest lower bound results in the following upper bounds on $\rho_{xx}(\tau)$ and $\Phi_\xi(\Omega)$,

$$\begin{aligned} \rho_{xx}(\tau) &\leq \cos(\Omega_0 \tau) \quad |\tau| < T_N/2, \\ \Phi_\xi(\Omega) &\leq \cos(\xi_0 \Omega) \quad |\Omega| < \pi/T_N. \end{aligned} \quad (4.21)$$

We would expect the performance of USI to be inversely proportional to the signal's bandwidth B_x , as defined in (4.31). This is intuitively reasonable since with slow variations of the signal, the uniform samples $x(nT_N)$ are accurately approximated by the nonuniform samples $x(t_n)$. The upper bound on σ_{eU}^2 seems to agree with this intuition since it decreases as $R_{xx}(T_N/2)$ increases, and $R_{xx}(T_N/2)$ is expected to increase as the radius of curvature of $R_{xx}(\tau)$ at $\tau = 0$ increases or equivalently as the bandwidth B_x of $x(t)$ decreases.

4.3.4 Nonuniform Sinc Interpolation

When the sampling instants t_n are known, we can alternatively set the reconstruction perturbations ζ_n to be equal to the sampling perturbations ξ_n so that the impulses in Figure 4-1 are located on the correct grid. This is another special case of eq. (4.9) for which the reconstruction takes the form

$$\hat{x}(t) = \sum_{n=-\infty}^{\infty} (T/T_N) \cdot x(t_n) \cdot h(t - t_n). \quad (4.22)$$

Note that for this approximation, referred to as Nonuniform Sinc Interpolation, the distribution of the perturbations is not needed. The corresponding MSE of the reconstruction error $e^N(t)$ follows directly from eq. (4.11) by replacing $\Phi_{\xi\zeta}(\Omega_1, \Omega_2)$ with $\Phi_{\xi}(\Omega_1 - \Omega_2)$, i.e.,

$$\begin{aligned} \sigma_{e^N}^2 &= \frac{1}{r} \cdot \left(R_{xx}(0) - \frac{1}{2\Omega_c} \int_{-\Omega_c}^{\Omega_c} (S_{xx}(\Omega) * |\Phi_{\xi}(\Omega)|^2) d\Omega \right) \\ &= \frac{1}{r} \cdot \frac{1}{2\pi} \int_{-\Omega_c}^{\Omega_c} S_{xx}(\Omega) \cdot \left(\int_{\Omega-\Omega_c}^{\Omega+\Omega_c} \frac{1 - |\Phi_{\xi}(\Omega')|^2}{2\Omega_c} d\Omega' \right) d\Omega. \end{aligned} \quad (4.23)$$

4.3.5 Independent Sinc Interpolation

When the exact sampling times are not known but the probability distribution $f_{\xi}(\xi)$ of their deviation from a uniform sampling grid is known, and choosing ζ_n in the reconstruction of Figure 4-1 to be independent of ξ_k for all n, k , we obtain

$$\begin{aligned} \sigma_{e^I}^2 &= \frac{1}{2\pi} \int_{-\Omega_c}^{\Omega_c} S_{xx}(\Omega) \cdot |1 - \Phi_{\xi}(\Omega) \Phi_{\zeta}(-\Omega)|^2 d\Omega + \\ &+ \frac{1}{r} \cdot \frac{1}{2\pi} \int_{-\Omega_c}^{\Omega_c} S_{xx}(\Omega) \cdot \left(1 - |\Phi_{\xi}(\Omega)|^2 \cdot \frac{1}{2\Omega_c} \int_{-\Omega_c}^{\Omega_c} |\Phi_{\zeta}(\Omega_1)|^2 d\Omega_1 \right) d\Omega. \end{aligned} \quad (4.24)$$

As with any characteristic function, $|\Phi_{\zeta}(\Omega)| \leq 1$ for all Ω . Consequently, the second term in eq. (4.24) is minimized when $\Phi_{\zeta}(\Omega) = 1$, corresponding to $\zeta_n = 0$, i.e., Uniform Sinc Interpolation. In minimizing the first term in eq. (4.24) we restrict $f_{\xi}(\xi)$ to be symmetric. Furthermore, the deviation from the uniform grid is restricted to be less than $T/2$, i.e., $f_{\xi}(\xi) = 0$ for $|\xi| \geq T/2$. From this it follows that the Fourier transform of $f_{\xi}(\xi)$, i.e.,

$\Phi_\xi(\Omega)$ is guaranteed to be real and non-negative for $|\Omega| \leq \pi/T$ (see Appendix E). Since the average sampling rate is at or above the Nyquist rate, i.e., $\frac{\pi}{T} \geq \Omega_c$, $\Phi_\xi(\Omega)$ will always be real and non-negative in the interval of integration for the first term in eq. (4.24). Consequently, to minimize that term we again choose $\Phi_\zeta(\Omega) = 1$, corresponding to Uniform Sinc Interpolation.

In summary, when the probability density function of ξ_n is symmetric and has bounded support, Uniform Sinc Interpolation is an optimal reconstruction within this framework. More generally, the optimal choice for $f_\zeta(\zeta)$ may not correspond to Uniform Sinc Interpolation and lower MSE may be achieved with $\Phi_\zeta(\Omega) = e^{-j\zeta_0\Omega}$ corresponding to $\zeta_n = -\zeta_0$, i.e., Uniform Sinc Interpolation with an offset of the uniform grid. The offset ζ_0 can be optimized to minimize σ_e^2 in (4.24). Specifically,

$$\begin{aligned}
\zeta_0^{opt} &= \arg \min_{\zeta_0} \Re \left\{ \frac{1}{2\pi} \int_{-\Omega_c}^{\Omega_c} S_{xx}(\Omega) \cdot \left| 1 - \Phi_\xi(\Omega) e^{j\zeta_0\Omega} \right|^2 d\Omega \right. \\
&\quad \left. + \frac{1}{r} \cdot \frac{1}{2\pi} \int_{-\Omega_c}^{\Omega_c} S_{xx}(\Omega) \cdot (1 - |\Phi_\xi(\Omega)|^2) d\Omega \right\} \\
&= \arg \max_{\zeta_0} \Re \left\{ \frac{1}{2\pi} \int_{-\Omega_c}^{\Omega_c} S_{xx}(\Omega) \Phi_\xi(\Omega) e^{j\zeta_0\Omega} d\Omega \right\}, \tag{4.25}
\end{aligned}$$

or equivalently,

$$\begin{aligned}
\zeta_0^{opt} &= \arg \max_{\zeta_0} R_{xx}(\tau) * f_\xi(\tau) \Big|_{\tau=\zeta_0} \\
&= \arg \max_{\zeta_0} \int_{-\infty}^{\infty} R_{xx}(\tau - \zeta_0) f_\xi(\tau) d\tau \\
&= \arg \max_{\zeta_0} E_\xi (R_{xx}(\xi - \zeta_0)). \tag{4.26}
\end{aligned}$$

Note that when $f_\xi(\xi)$ is symmetric and the deviation from the uniform grid is less than $T/2$, $\zeta_0^{opt} = 0$ consistent with the observation that the optimal reconstruction in this case does not depend on the specific shape of the pdf and corresponds to Uniform Sinc

Interpolation. This follows by noting that

$$\int_{-T/2}^{T/2} R_{xx}(\tau - \zeta_0) f_{\xi}(\tau) d\tau = \int_0^{T/2} [R_{xx}(\tau - \zeta_0) + R_{xx}(\tau + \zeta_0)] f_{\xi}(\tau) d\tau \leq \int_{-T/2}^{T/2} R_{xx}(\tau) f_{\xi}(\tau) d\tau, \quad (4.27)$$

where we used the symmetry of the pdf $f_{\xi}(\xi)$ and of $R_{xx}(\tau)$, and the property that

$$R_{xx}(\tau) \geq \frac{1}{2} (R_{xx}(\tau - \zeta_0) + R_{xx}(\tau + \zeta_0)) \quad \forall |\tau| < T/2, \zeta_0, \quad (4.28)$$

which is shown to be true in Appendix E for the autocorrelation function of a bandlimited signal.

4.3.6 RSI - Minimum Mean Square Reconstruction Error

As eq. (4.11) shows, the performance of RSI depends on the power spectrum $S_{xx}(\Omega)$ of the continuous-time signal $x(t)$ as well as on the joint characteristic function $\Phi_{\xi\zeta}(\Omega_1, \Omega_2)$ of the perturbations, which can be designed to reduce the MSE. In order to formulate the optimal reconstruction within the framework of RSI, i.e., to design ζ_n in the reconstruction method of Figure 4-1 to achieve minimum MSE, eq. (4.11) should be optimized with respect to $\Phi_{\xi\zeta}(\Omega_1, \Omega_2)$ subject to the constraint $\Phi_{\xi\zeta}(\Omega, 0) = \Phi_{\xi}(\Omega)$. This optimization requires in general the knowledge of both the exact sampling instants and the probability distribution of their deviation from a uniform sampling grid. As we will next see, even though the exact sampling instants are known, the optimal reconstruction may not correspond to NSI, i.e., the optimal grid on which the samples are placed in reconstruction prior to sinc interpolation may possibly be different than the actual nonuniform sampling grid.

In minimizing the MSE we consider two cases. The first is the case of small, zero-mean perturbations from a uniform grid, for which in the region $|\Omega_1| < \Omega_c$ and $|\Omega_2| < \Omega_c$, $\Phi_{\xi\zeta}(\Omega_1, \Omega_2)$ can be approximated well by the second-order Taylor expansion

$$\Phi_{\xi\zeta}(\Omega_1, \Omega_2) \approx 1 - \sigma_{\xi\zeta} \Omega_1 \Omega_2 - \frac{1}{2} \sigma_{\xi}^2 \Omega_1^2 - \frac{1}{2} \sigma_{\zeta}^2 \Omega_2^2, \quad (4.29)$$

with the corresponding standard deviations σ_ξ and σ_ζ of ξ_n and ζ_n assumed to be small enough relative to T so that (4.29) holds. Substituting (4.29) into (4.11) for the case $r = 1$ yields

$$\sigma_{eR}^2 \approx R_{xx}(0) \cdot \left(\sigma_\xi^2 \cdot B_x + 1/3 \cdot \sigma_\zeta^2 \cdot \Omega_c^2 \right), \quad (4.30)$$

where B_x is a measure of the signal's bandwidth defined as

$$B_x = \int_{-\Omega_c}^{\Omega_c} \Omega^2 \cdot \left(\frac{S_{xx}(\Omega)}{\int_{-\Omega_c}^{\Omega_c} S_{xx}(\Omega') d\Omega'} \right) d\Omega. \quad (4.31)$$

From (4.30) we see that independent of the detailed characteristics of the perturbation or the signal spectrum, as long as the perturbations around the uniform grid are small enough so that (4.29) holds, it is preferable to reconstruct the signal using USI, corresponding to $\zeta_n = 0$. This is despite the fact that USI uses only the nominal rather than actual sampling times.

We next consider the case in which the sampling perturbation errors are uniformly distributed over the range $(-\frac{T}{2}, \frac{T}{2})$. As previously mentioned, the optimal perturbations ζ_n in the reconstruction of Figure 4-1 are chosen to minimize (4.11) with respect to $\Phi_{\xi\zeta}(\Omega_1, \Omega_2)$. One interesting case is when the joint characteristic function $\Phi_{\xi\zeta}(\Omega_1, \Omega_2)$ is characterized by a finite set of parameters, and the optimization of the MSE in (4.11) reduces to optimization over those parameters. Consider as an example the case when ζ_n is a k^{th} -order polynomial of ξ_n whose coefficients are to be designed. For simplicity, we will consider here only the linear case, i.e., $\zeta_n = \beta \xi_n$ with $\beta \in [0, 1]$ for which the case of $\beta = 0$ corresponds to USI and the case of $\beta = 1$ corresponds to NSI. It then follows that the Fourier transform of the joint pdf $f_{\xi\zeta}(\xi, \zeta)$ is

$$\Phi_{\xi\zeta}(\Omega_1, \Omega_2) = \Phi_\xi(\Omega_1 + \beta\Omega_2), \quad (4.32)$$

and $Q(\Omega)$ as defined in (4.12) reduces to

$$Q(\Omega) = |1 - \Phi_\xi((1 - \beta)\Omega)|^2 + \frac{1}{r} \cdot \int_{-\Omega_c}^{\Omega_c} \frac{1 - |\Phi_\xi(\Omega - \beta\Omega_1)|^2}{2\Omega_c} d\Omega_1, \quad (4.33)$$

where $\Phi_\xi(\Omega) = \text{sinc}(\frac{T}{2}\Omega)$.

Figure 4-3 shows $Q(\Omega)$ for different values of β with no oversampling, i.e., when the oversampling factor $r = 1$. As indicated, at low frequencies $Q(\Omega)$ is minimized when β is close to 0, whereas at high frequencies it is minimized when β is close to 1. More generally, the optimal choice of β that minimizes the reconstruction MSE will depend on the specific shape of the power spectrum $S_{xx}(\Omega)$ of the input signal $x(t)$. As Figure 4-3 suggests, it will tend to be small for signals that vary slowly, i.e., when B_x as defined in (4.31) is small. As an illustration, Figure 4-4 demonstrates this behavior of the optimal choice of β as a function of B_x for an example in which $S_{xx}(\Omega)$ is of the form

$$S_{xx}(\Omega) = \begin{cases} \frac{\pi}{d \tan(\Omega_c/d)} \cdot \frac{1}{1+(\Omega/d)^2} & |\Omega| < \Omega_c \\ 0 & |\Omega| \geq \Omega_c \end{cases} \quad (4.34)$$

in which case

$$B_x = \frac{\Omega_c d}{\arctan(\Omega_c/d)} - d^2, \quad (4.35)$$

and

$$\frac{1}{2\pi} \int_{-\Omega_c}^{\Omega_c} S_{xx}(\Omega) d\Omega = 1. \quad (4.36)$$

As indicated, when the bandwidth B_x of the input signal is small, the samples are positioned close to the uniform sampling grid. As B_x is increased, β is increased and as a result the samples are positioned closer to their original locations but still with a tendency towards the uniform grid due to the optimality of USI.

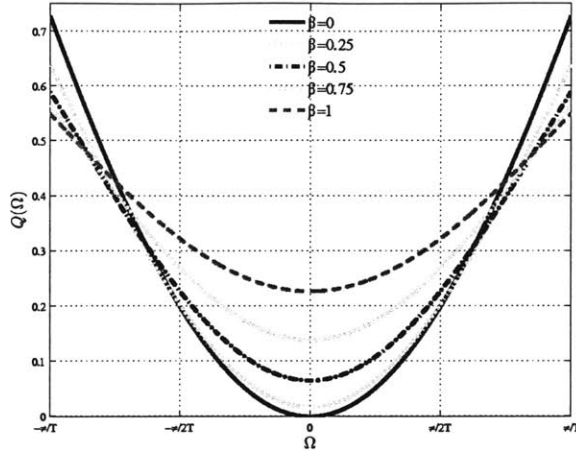


Figure 4-3: $Q(\Omega)$ for the case where $\xi_n \sim u[-T/2, T/2]$ and $T = T_N = 1$.

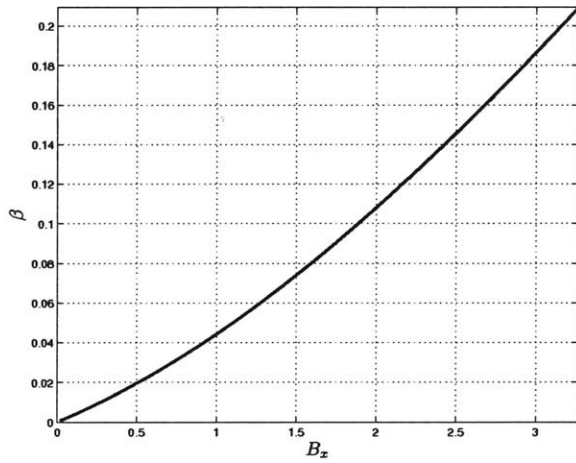


Figure 4-4: The optimal choice of β that minimizes σ_{eR}^2 as a function of B_x for the case where $T = T_N = 1$.

4.3.7 Discussion

While USI uses only the zero-mean assumption of the perturbation error and does not require the knowledge of the exact sampling instants, this knowledge is necessary for NSI. Comparing USI with NSI with respect to mean square reconstruction error, it is in general not possible to claim which of these methods is preferable. Their relative performance is dependent on the power spectrum $S_{xx}(\Omega)$ of the continuous-time signal, the distribution $f_\xi(\xi)$ of the sampling perturbations and the oversampling ratio r . For ISI, not only the mean but the entire probability distribution function of the deviation from a uniform sampling grid is needed in general. Since USI can be viewed as a special case of ISI for which

$f_{\zeta}(\zeta) = \delta(\zeta)$, it might be possible in general to obtain a lower MSE with ISI than with USI. As previously discussed, there are cases in which even though the entire probability distribution of the sampling perturbations is known, the mean square reconstruction error of ISI is minimized when $f_{\zeta}(\zeta) = \delta(\zeta)$, corresponding to USI. USI, NSI and ISI can all be formulated as special cases of RSI, which is more general. With an appropriate choice of $f_{\xi\zeta}(\xi, \zeta)$, it might be possible in general to obtain a lower MSE with RSI than with USI, NSI or ISI.

In the problem formulation, the samples were taken on a nonuniform grid that is a perturbation of a uniform grid, and the objective was to design the grid on which to locate the samples in reconstruction prior to sinc interpolation. Nevertheless, this framework can handle other cases of interest as well. Consider for example the case in which the samples are taken on an accurate uniform grid, but there are timing inaccuracies in the discrete-to-continuous processing. This case can be formed as a special case of the general framework for which $\Phi_{\xi\zeta}(\Omega_1, \Omega_2) = \Phi_{\zeta}(\Omega_2)$.

TIMING ERRORS IN DISCRETE-TIME PROCESSING OF CONTINUOUS-TIME SIGNALS

A major application of discrete-time systems occurs in the processing of continuous-time signals. When timing errors arise in the conversion from continuous to discrete time and from discrete to continuous, discrepancies between the desired continuous-time system and its implementation by a discrete-time system occur. This chapter explores these discrepancies and proposes a method of designing the discrete-time system to compensate for the timing errors.

5.1 Introduction

In an ideal scenario, the system of Figure 5-1, which consists of sampling followed by an LTI discrete-time system and discrete-to-continuous conversion, is equivalent under certain conditions [69], to continuous-time LTI processing of the bandlimited input signal.

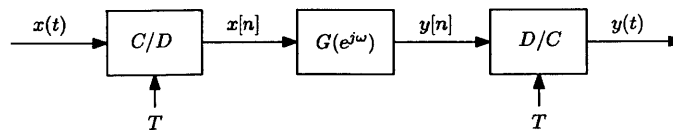


Figure 5-1: Discrete-time processing of continuous-time signals.

In particular, when the input signal $x(t)$ is bandlimited and the sampling interval T satisfies the Nyquist condition, the overall system in Figure 5-1 has an effective frequency

response of the form

$$G_{eff}(\Omega) = \begin{cases} G(e^{j\Omega T}) & |\Omega| < \frac{\pi}{T} \\ 0 & |\Omega| \geq \frac{\pi}{T}. \end{cases} \quad (5.1)$$

Thus, for the system in Figure 5-1 to correspond, in the absence of errors, to a specified continuous-time LTI system whose frequency response is

$$G_{eff}(\Omega) = \begin{cases} G(\Omega) & |\Omega| < \frac{\pi}{T} \\ 0 & |\Omega| \geq \frac{\pi}{T}, \end{cases} \quad (5.2)$$

the frequency response of the discrete-time LTI system should satisfy the following condition:

$$G(e^{j\omega}) = G\left(\frac{\omega}{T}\right), \quad |\omega| < \pi. \quad (5.3)$$

We next discuss the effects of timing errors in the conversion from continuous to discrete time and from discrete to continuous in the system of Figure 5.1 and the design of an optimal discrete-time LTI system $G(e^{j\omega})$, which compensates for these timing errors. The time jitter problem was first considered in 1962 by Balakrishnan [3], who studied the properties of the jittered samples and proposed an explicit solution for optimal (in the mean-square sense) linear operation of these samples. Independently, in 1963 Brown [11] provided optimum interpolation of sampled data when various types of jitter are present. Tarczynski [84] presents a method of designing FIR filters whose input signals are sampled irregularly due to clock jitter. These filters which were designed to diminish the input clock jitter are claimed to perform better than traditional filters, for which the effect of jitter is ignored at the designing stage. Similar to [84], we consider in this chapter the design of a discrete-time system that compensates for the time jitter errors for the more general case in which time jitter occurs both in acquiring the samples and in forming the interpolation.

5.2 The Effects of Timing Errors in Discrete-time Processing of Continuous-time Signals

To analyze the effects of timing errors in discrete-time processing of continuous-time signals, we consider the system of Figure 5-2. The input signal $x(t)$ is assumed to be a realization of a zero-mean wide-sense stationary random process with an autocorrelation function $R_{xx}(\tau)$ and power spectrum $S_{xx}(\Omega) = 0$ for $\Omega \geq \pi/T$. Due to timing imperfections, the sampling instants do not form an exact uniform grid. The sampling grid is modeled as a perturbation of a uniform grid with spacing T , i.e.,

$$t_n = nT + \xi_n, \quad (5.4)$$

where ξ_n is characterized as an i.i.d sequence of zero-mean random variables, independent of $x(t)$ with pdf $f_\xi(\xi)$ and characteristic function $\Phi_\xi(\Omega)$. The sequence $y[n]$ is obtained from processing $x[n] = x(t_n)$ with a discrete-time LTI system whose frequency response is $G(e^{j\omega})$. The grid on which the samples are placed prior to sinc interpolation in the conversion from discrete to continuous is modeled as another perturbation of a uniform grid with spacing T , i.e.,

$$\tilde{t}_n = nT + \zeta_n, \quad (5.5)$$

where ζ_n is an i.i.d sequence of random variables independent of $x(t)$ and of ξ_k for all n, k .

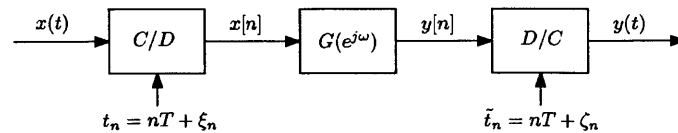


Figure 5-2: Time jitter in discrete-time processing of continuous-time signals.

With respect to second-order statistics, the system of Figure 5-2 is shown in Appendix F to be equivalent to the continuous-time system of Figure 5-3. In this system, the signals $x(t)$, $v_\xi(t)$, $v_\zeta(t)$, and $v_{\xi\zeta}(t)$ are zero-mean, uncorrelated, wide-sense stationary random processes. $v_\xi(t)$ is a white-noise process whose power spectrum $S_{v_\xi v_\xi} = \frac{T}{2\pi} \int_{-\pi/T}^{\pi/T} S_{xx}(\Omega') (1 -$

$|\Phi_\xi(\Omega')|^2 d\Omega'$. The power spectrums of $v_\zeta(t)$ and $v_{\xi\zeta}(t)$ are

$$S_{v_\zeta v_\zeta}(\Omega) = \begin{cases} (1 - |\Phi_\zeta(-\Omega)|^2) \frac{T}{2\pi} \int_{-\pi/T}^{\pi/T} S_{xx}(\Omega') |\Phi_\xi(\Omega')|^2 |G(e^{j\Omega'T})|^2 d\Omega' & |\Omega| < \frac{\pi}{T} \\ 0 & |\Omega| \geq \frac{\pi}{T}, \end{cases} \quad (5.6)$$

and

$$S_{v_{\xi\zeta} v_{\xi\zeta}}(\Omega) = \begin{cases} (1 - |\Phi_\zeta(-\Omega)|^2) \cdot \frac{T}{2\pi} \int_{-\pi/T}^{\pi/T} S_{xx}(\Omega') (1 - |\Phi_\xi(\Omega')|^2) d\Omega' \cdot \frac{1}{2\pi} \int_{-\pi}^{\pi} |G(e^{j\omega})|^2 d\omega & |\Omega| < \frac{\pi}{T} \\ 0 & |\Omega| \geq \frac{\pi}{T}, \end{cases} \quad (5.7)$$

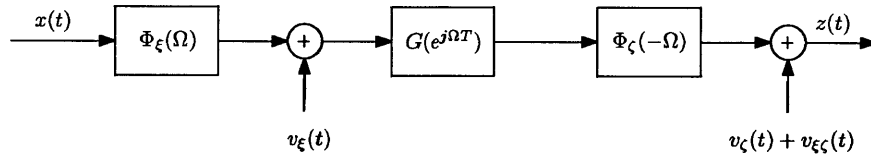


Figure 5-3: A second-order statistics model for the system of Figure 5-2.

To show the equivalence between the systems, we first show that the cross-spectrum between the output $y(t)$ of the system in Figure 5-2 and its input is

$$S_{yx}(\Omega) = \begin{cases} S_{xx}(\Omega) \Phi_\xi(\Omega) \Phi_\zeta(-\Omega) G(e^{j\Omega T}) & |\Omega| < \frac{\pi}{T} \\ 0 & |\Omega| \geq \frac{\pi}{T}, \end{cases} \quad (5.8)$$

and the power spectrum of $y(t)$ is

$$S_{yy}(\Omega) = \begin{cases} (S_{xx}(\Omega) \cdot |\Phi_\xi(\Omega)|^2 + S_{v_\xi v_\xi}) |\Phi_\zeta(-\Omega)|^2 |G(e^{j\Omega T})|^2 + S_{v_\zeta v_\zeta}(\Omega) + S_{v_{\xi\zeta} v_{\xi\zeta}}(\Omega) & |\Omega| < \frac{\pi}{T} \\ 0 & |\Omega| \geq \frac{\pi}{T} \end{cases} \quad (5.9)$$

We then note that the power spectrum $S_{zz}(\Omega)$ of the output $z(t)$ in the system of Figure 5-3 is identical to $S_{yy}(\Omega)$ in (5.9) and the cross-spectrum $S_{zx}(\Omega)$ is identical to $S_{yx}(\Omega)$ in (5.8). Thus, as a result of the timing errors in sampling and in reconstruction, the signal $x(t)$ in the equivalent system of Figure 5-3 is filtered by the LTI system whose frequency response is $\Phi_\xi(\Omega) \Phi_\zeta(-\Omega)$, and additive zero-mean uncorrelated noise components occur.

For comparison purposes, we denote $e(t) = y(t) - x(t) * g(t)$ as the error between the output of processing $x(t)$ with a continuous-time LTI system whose impulse response is $g(t)$ and the output $y(t)$ of the system in Figure 5-2 to an input $x(t)$. It then follows from eqs. (5.8) and (5.9) that the power spectrum $S_{ee}(\Omega)$ of $e(t)$ is

$$\begin{aligned}
S_{ee}(\Omega) &= S_{yy}(\Omega) - S_{yx}(\Omega)G^*(\Omega) - S_{xy}(\Omega)G(\Omega) + S_{xx}(\Omega)|G(\Omega)|^2 \\
&= S_{xx}(\Omega) \cdot \left(|\Phi_\xi(\Omega)|^2 |\Phi_\zeta(-\Omega)|^2 |G(e^{j\Omega T})|^2 - \Phi_\xi(\Omega)\Phi_\zeta(-\Omega)G(e^{j\Omega T})G^*(\Omega) \right. \\
&\quad \left. - \Phi_\xi^*(\Omega)\Phi_\zeta^*(-\Omega)G^*(e^{j\Omega T})G(\Omega) + |G(\Omega)|^2 \right) \\
&\quad + |G(e^{j\Omega T})|^2 |\Phi_\zeta(-\Omega)|^2 \cdot \frac{T}{2\pi} \int_{-\pi/T}^{\pi/T} S_{xx}(\Omega') (1 - |\Phi_\xi(\Omega')|^2) d\Omega' \\
&\quad + (1 - |\Phi_\zeta(-\Omega)|^2) \cdot \frac{T}{2\pi} \int_{-\pi/T}^{\pi/T} S_{xx}(\Omega') (1 - |\Phi_\xi(\Omega')|^2) d\Omega' \cdot \frac{1}{2\pi} \int_{-\pi}^{\pi} |G(e^{j\omega})|^2 d\omega \\
&\quad + (1 - |\Phi_\zeta(-\Omega)|^2) \cdot \frac{T}{2\pi} \int_{-\pi/T}^{\pi/T} S_{xx}(\Omega') |\Phi_\xi(\Omega')|^2 |G(e^{j\Omega' T})|^2 d\Omega' \quad |\Omega| < \frac{\pi}{T}.
\end{aligned} \tag{5.10}$$

As expected, in the absence of timing errors, i.e., when $\xi_n = 0$ and $\zeta_n = 0$, the choice of $G(e^{j\omega})$ as in (5.3) results in zero mean-squared error. More generally, the power spectrum $S_{ee}(\Omega)$ of eq. (5.11) for the case in which $G(e^{j\omega})$ is specified in (5.3) becomes

$$\begin{aligned}
S_{ee}(\Omega) &= S_{xx}(\Omega) \cdot |G(\Omega)|^2 \cdot |1 - \Phi_\xi(\Omega)\Phi_\zeta(-\Omega)|^2 \\
&\quad + |G(\Omega)|^2 |\Phi_\zeta(-\Omega)|^2 \cdot \frac{T}{2\pi} \int_{-\pi/T}^{\pi/T} S_{xx}(\Omega') (1 - |\Phi_\xi(\Omega')|^2) d\Omega' \\
&\quad + (1 - |\Phi_\zeta(-\Omega)|^2) \cdot \frac{T}{2\pi} \int_{-\pi/T}^{\pi/T} S_{xx}(\Omega') (1 - |\Phi_\xi(\Omega')|^2) d\Omega' \cdot \frac{T}{2\pi} \int_{-\pi/T}^{\pi/T} |G(\Omega')|^2 d\Omega' \\
&\quad + (1 - |\Phi_\zeta(-\Omega)|^2) \cdot \frac{T}{2\pi} \int_{-\pi/T}^{\pi/T} S_{xx}(\Omega') |\Phi_\xi(\Omega')|^2 |G(\Omega')|^2 d\Omega', \quad |\Omega| < \frac{\pi}{T}. \tag{5.11}
\end{aligned}$$

With ideal uniform sampling, i.e., when $\xi_n = 0$, the second-order statistics modeling of Figure 5-3 reduces to that shown in Figure 5-4, and the power-spectrum $S_{ee}(\Omega)$ in eq. (5.11) reduces to

$$\begin{aligned}
S_{ee}(\Omega) &= S_{xx}(\Omega) \cdot |G(\Omega)|^2 \cdot |1 - \Phi_\zeta(-\Omega)|^2 \\
&\quad + (1 - |\Phi_\zeta(-\Omega)|^2) \cdot \frac{T}{2\pi} \int_{-\pi/T}^{\pi/T} S_{xx}(\Omega') |G(\Omega')|^2 d\Omega', \quad |\Omega| < \frac{\pi}{T}. \tag{5.12}
\end{aligned}$$

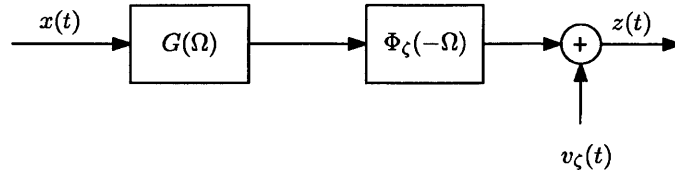


Figure 5-4: A second-order statistics model for the system of Figure 5-2 with $G(e^{j\omega}) = G(\frac{\omega}{T})$, $|\omega| < \pi$ and where $\xi_n = 0$.

Alternatively, if there are no timing errors in reconstruction, i.e., $\zeta_n = 0$, the second-order statistics modeling of Figure 5-3 reduces to that shown in Figure 5-5, and

$$S_{ee}(\Omega) = S_{xx}(\Omega) \cdot |G(\Omega)|^2 \cdot |1 - \Phi_{\xi}(\Omega)|^2 + |G(\Omega)|^2 \cdot \frac{T}{2\pi} \int_{-\pi/T}^{\pi/T} S_{xx}(\Omega') (1 - |\Phi_{\xi}(\Omega')|^2) d\Omega', \quad |\Omega| < \frac{\pi}{T}. \quad (5.13)$$

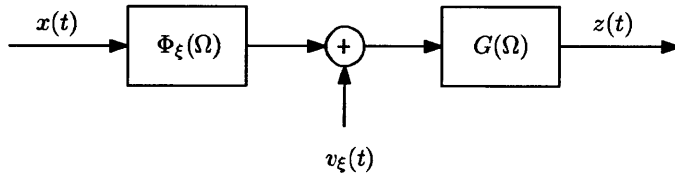


Figure 5-5: A second-order statistics model for the system of Figure 5-2 with $G(e^{j\omega}) = G(\frac{\omega}{T})$, $|\omega| < \pi$ and where $\zeta_n = 0$.

With respect to second-order statistics, the effect of timing errors is similar in both cases, i.e., lowpass filtering of $x(t)$ and the occurrence of additive uncorrelated noise. Figure 5-4 and eq. (5.12) suggest that with ideal uniform sampling, the effect of the additive uncorrelated noise due to timing errors in reconstruction is more significant at high frequencies. This severity in high frequencies contrasts with the case of ideal reconstruction, in which the additive uncorrelated noise component due to perturbations in sampling is shaped according to the frequency response $G(\Omega)$ of the desired system, as Figure 5-5 and eq. (5.13) show.

The next section discusses the design of the discrete-time system $G(e^{j\omega})$ to compensate for the timing errors in the implementation of the continuous-time system.

5.3 Jitter Compensation

The previous section discusses the effects of timing errors on the overall system of Figure 5-1. Specifically, we show that the system of Figure 5-2 with $G(e^{j\omega}) = G(\frac{\omega}{T})$, $|\omega| < \pi/T$ is no longer equivalent to the desired continuous-time system represented by $G_{eff}(\Omega)$ in (5.2). In this section, we design the discrete-time system $G(e^{j\omega})$ to mitigate the effects of the timing errors by reducing the mean-squared error between the output of the desired continuous-time system and the output of its implementation by a discrete-time system.

Optimizing $S_{ee}(\Omega)$ in (5.11) with respect to $G(e^{j\Omega T})$ is analytically difficult. However, since the mean-squared error can be expressed as an integral of a quadratic form of $G(e^{j\Omega T})$, the optimization becomes much easier. Specifically, integrating $S_{ee}(\Omega)$ in (5.11), we obtain the following mean-squared error

$$\begin{aligned} \sigma_e^2 &= \frac{1}{2\pi} \int_{-\pi/T}^{\pi/T} A(\Omega) \cdot |G(e^{j\Omega T})|^2 - G(e^{j\Omega T}) \cdot S_{xx}(\Omega) \Phi_{\xi}(\Omega) \Phi_{\zeta}(-\Omega) G^*(\Omega) \\ &\quad - G^*(e^{j\Omega T}) \cdot S_{xx}(\Omega) \Phi_{\xi}^*(\Omega) \Phi_{\zeta}^*(-\Omega) G(\Omega) + S_{xx}(\Omega) |G(\Omega)|^2 d\Omega, \end{aligned} \quad (5.14)$$

where

$$\begin{aligned} A(\Omega) &= S_{xx}(\Omega) \cdot |\Phi_{\xi}(\Omega)|^2 |\Phi_{\zeta}(-\Omega)|^2 + |\Phi_{\zeta}(-\Omega)|^2 \frac{T}{2\pi} \int_{-\pi/T}^{\pi/T} S_{xx}(\Omega') (1 - |\Phi_{\xi}(\Omega')|^2) d\Omega' \\ &\quad + \frac{T}{2\pi} \int_{-\pi/T}^{\pi/T} S_{xx}(\Omega') (1 - |\Phi_{\xi}(\Omega')|^2) d\Omega' \cdot \frac{T}{2\pi} \int_{-\pi/T}^{\pi/T} (1 - |\Phi_{\zeta}(-\Omega')|^2) d\Omega' \\ &\quad + S_{xx}(\Omega) |\Phi_{\xi}(\Omega)|^2 \cdot \frac{T}{2\pi} \int_{-\pi/T}^{\pi/T} (1 - |\Phi_{\zeta}(-\Omega')|^2) d\Omega', \quad |\Omega| < \frac{\pi}{T}. \end{aligned} \quad (5.15)$$

Then, the optimal filter $G(e^{j\Omega T})$ that minimizes the mean-squared error σ_e^2 is obtained by differentiating the integrand in (5.14) with respect to $G(e^{j\Omega T})$, which results in

$$G_{opt}(e^{j\Omega T}) = \frac{\Phi_{\xi}^*(\Omega) \Phi_{\zeta}(\Omega) S_{xx}(\Omega)}{A(\Omega)} \cdot G(\Omega), \quad |\Omega| < \frac{\pi}{T}. \quad (5.16)$$

Substituting $G_{opt}(e^{j\Omega T})$ from (5.16) into (5.14), the minimum mean-squared error (MMSE)

is obtained

$$\sigma_{e \min}^2 = \frac{1}{2\pi} \int_{-\pi/T}^{\pi/T} S_{xx}(\Omega) |G(\Omega)|^2 \left(1 - \frac{S_{xx}(\Omega) |\Phi_{\xi}(\Omega)|^2 |\Phi_{\zeta}(-\Omega)|^2}{A(\Omega)} \right) d\Omega. \quad (5.17)$$

When $\xi_n = 0$, the optimal filter $G_{opt}(e^{j\Omega T})$ reduces to

$$G_{opt}(e^{j\Omega T}) = \frac{\Phi_{\zeta}(\Omega)}{|\Phi_{\zeta}(-\Omega)|^2 + \frac{T}{2\pi} \int_{-\pi/T}^{\pi/T} (1 - |\Phi_{\zeta}(-\Omega')|^2) d\Omega'} \cdot G(\Omega), \quad |\Omega| < \frac{\pi}{T}, \quad (5.18)$$

and its corresponding MMSE is

$$\sigma_{e \min}^2 = \frac{1}{2\pi} \int_{-\pi/T}^{\pi/T} S_{xx}(\Omega) |G(\Omega)|^2 \left(\frac{\frac{T}{2\pi} \int_{-\pi/T}^{\pi/T} (1 - |\Phi_{\zeta}(-\Omega')|^2) d\Omega'}{|\Phi_{\zeta}(-\Omega)|^2 + \frac{T}{2\pi} \int_{-\pi/T}^{\pi/T} (1 - |\Phi_{\zeta}(-\Omega')|^2) d\Omega'} \right) d\Omega. \quad (5.19)$$

Interestingly, when $\xi_n = 0$, the characteristics of the input signal $x(t)$ are not needed in the design of the optimal discrete-time filter $G(e^{j\omega})$. Alternatively, when $\zeta_n = 0$, $G_{opt}(e^{j\Omega T})$ reduces to

$$G_{opt}(e^{j\Omega T}) = \frac{\Phi_{\xi}^*(\Omega) S_{xx}(\Omega)}{S_{xx}(\Omega) \cdot |\Phi_{\xi}(\Omega)|^2 + \frac{T}{2\pi} \int_{-\pi/T}^{\pi/T} S_{xx}(\Omega') (1 - |\Phi_{\xi}(\Omega')|^2) d\Omega'} \cdot G(\Omega), \quad |\Omega| < \frac{\pi}{T}, \quad (5.20)$$

and the corresponding MMSE is

$$\sigma_{e \min}^2 = \frac{1}{2\pi} \int_{-\pi/T}^{\pi/T} S_{xx}(\Omega) |G(\Omega)|^2 \left(\frac{\frac{T}{2\pi} \int_{-\pi/T}^{\pi/T} S_{xx}(\Omega') (1 - |\Phi_{\xi}(\Omega')|^2) d\Omega'}{S_{xx}(\Omega) \cdot |\Phi_{\xi}(\Omega)|^2 + \frac{T}{2\pi} \int_{-\pi/T}^{\pi/T} S_{xx}(\Omega') (1 - |\Phi_{\xi}(\Omega')|^2) d\Omega'} \right) d\Omega. \quad (5.21)$$

When both $\xi_n = 0$ and $\zeta_n = 0$, it follows that

$$G_{opt}(e^{j\Omega T}) = G(\Omega), \quad |\Omega| < \frac{\pi}{T}, \quad (5.22)$$

and $\sigma_{e \min}^2 = 0$.

SUB-NYQUIST SAMPLING - ALIASING MITIGATION

The Nyquist-Shannon sampling theorem provides a sufficient condition for perfect reconstruction of a bandlimited signal from its equally spaced samples. When the Nyquist condition is not satisfied, frequency components of the original signal that are higher than half the sampling rate are then folded into lower frequencies resulting in aliasing. The common approach to avoid aliasing in sampling is pre-filtering of the continuous-time signal, prior to sampling, with an LTI low-pass filter, whose cut-off frequency is lower than half the sampling rate. This processing is referred to as anti-aliasing. For certain applications such as ray-traced computer graphics, anti-aliasing filters are either not possible or not preferable to implement, and non-uniform sampling is used as an effective technique to mitigate the impact of aliasing. By appropriate design of the non-uniform sampling grid and of the reconstruction method, we show in this chapter that aliasing can be traded off with uncorrelated noise, which may be preferable in some circumstances.

6.1 Introduction

In Chapter 4 we considered the case where the sampling interval T is less or equal to the Nyquist interval T_N for which, under certain conditions, perfect reconstruction of a continuous-time bandlimited signal from its nonuniform samples is possible using Lagrange interpolation. When $T > T_N$ perfect reconstruction is in general not possible. However, the biorthogonality condition in (4.4) guarantees that whether or not $T \leq T_N$, the

output of the system in Figure 6-1 with $l_n(t)$ as given by eq. (4.2b) corresponds to the least squares approximation of $x(t)$. In other words, when the sampling instants $\{t_n\}$ satisfy the condition

$$|t_n - nT| \leq d < T/4 \quad \forall n \in \mathbb{Z}, \quad (6.1)$$

the use of an anti-aliasing LTI filter with cut-off frequency of half the average sampling rate, followed by nonuniform sampling and Lagrange interpolation results in an orthogonal projection from the space of finite energy signals to the subspace of finite energy bandlimited signals.

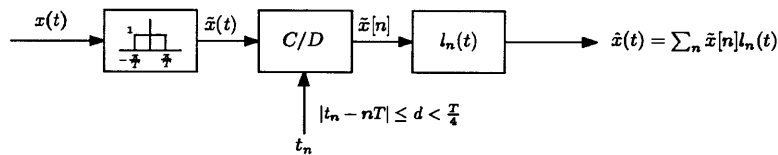


Figure 6-1: Anti-aliasing followed by nonuniform sampling and Lagrange interpolation.

In certain applications, such as ray-traced computer graphics, it is either not possible or not preferable to implement anti-aliasing filtering. With uniform sampling and when the Nyquist condition is not satisfied, frequency components of the original signal that are higher than half the sampling rate are then folded into lower frequencies resulting in aliasing. More generally, when the sampling grid is nonuniform and satisfies the condition of eq. (6.1), the approximation resulting from Lagrange interpolation can be viewed in general as an oblique projection from the space of finite energy signals into the space of finite energy bandlimited signals. This follows from noting that the composition of sampling at times $\{t_n\}$ and reconstruction using the kernel $l_n(t)$ as given by eq. (4.2b) is a linear operator $f(\cdot)$. Since the Lagrange kernel is bandlimited, applying the operator $f(\cdot)$ to $x(t)$ yields a bandlimited signal $\hat{x}(t) = f(x(t))$. Since Lagrange interpolation results in perfect reconstruction from nonuniform samples of bandlimited signals, $f(\hat{x}(t)) = f(x(t))$, i.e., $f(\cdot)$ is a projection. Consequently, aliasing with uniform or nonuniform sampling is a projection from the space of out of band signals into the space of bandlimited signals [88]. The projection representing aliasing with nonuniform sampling is in general an oblique rather than orthogonal projection.

Nonuniform sampling can offer an advantage over uniform sampling when the nominal sampling rate is less than the Nyquist rate, i.e., for undersampled signals. It has previously been suggested by several authors [18, 65, 80] that nonuniform sampling can be utilized to mitigate the impact of aliasing. In certain applications, particularly perceptual ones, the distortion resulting from nonuniform sampling is often preferable to aliasing artifacts. For example, a form of randomized sampling is used in the computer graphics community to anti-alias ray-traced images. In this chapter, we consider the framework developed in Chapter 4 for reconstruction from nonuniform samples for the case where $T > T_N$, i.e., sub-Nyquist sampling, and discuss the second-order statistics characteristics and the aliasing behavior of these methods.

6.2 Sinc Interpolation of sub-Nyquist Samples

In this section, we consider the reconstruction methods developed in Chapter 4 for the case of sub-Nyquist sampling, i.e., $T > T_N$. Specifically, we consider the reconstruction system of Figure 6-2, where the cut-off frequency of the ideal low-pass filter is $\frac{\pi}{T}$ and the choice of ζ_n differs for each of the reconstruction methods.

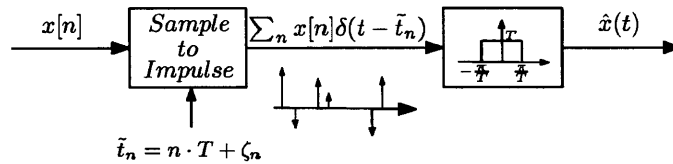


Figure 6-2: Reconstruction from nonuniform samples for the case $T > T_N$ using sinc interpolation.

6.2.1 Randomized Sinc Interpolation

Applying Randomized Sinc Interpolation to the nonuniform samples $\{x(t_n)\}$ as shown in Figure 6-2, results in $\hat{x}(t)$ whose power spectrum and cross-correlation with $x(t)$ are shown

in Appendix G to be

$$\begin{aligned}
S_{\hat{x}\hat{x}}(\Omega) &= \sum_{n=-\infty}^{\infty} S_{xx} \left(\Omega - \frac{2\pi}{T}n \right) \left| \Phi_{\xi\xi} \left(\Omega - \frac{2\pi}{T}n, -\Omega \right) \right|^2 \\
&+ \frac{T}{2\pi} \int_{-\Omega_c}^{\Omega_c} S_{xx}(\Omega') \left(1 - \left| \Phi_{\xi\xi}(\Omega', -\Omega) \right|^2 \right) d\Omega' \quad |\Omega| < \frac{\pi}{T}, \quad (6.2)
\end{aligned}$$

and

$$\begin{aligned}
R_{\hat{x}\hat{x}}(t, t - \tau) &= \frac{1}{2\pi} \int_{-\pi/T}^{\pi/T} \sum_{n=-\infty}^{\infty} \left(S_{xx} \left(\Omega - \frac{2\pi}{T}n \right) \Phi_{\xi\xi} \left(\Omega - \frac{2\pi}{T}n, -\Omega \right) e^{j\frac{2\pi}{T}n(t-\tau)} \right) e^{j\Omega\tau} d\Omega \\
&= \int_{-\infty}^{\infty} R_{xx}(t_1) \cdot \sum_{n=-\infty}^{\infty} \left[f_{\xi\xi}(t_1 + t - nT - \tau, \zeta) * \text{sinc}\left(\frac{\pi}{T}\zeta\right) \right] \Big|_{\zeta=t-nT} dt_1. \quad (6.3)
\end{aligned}$$

Once again, the perturbations in sampling and reconstruction can be designed to shape the power spectrum of the reconstructed signal through the joint characteristic function $\Phi_{\xi\xi}(\Omega_1, \Omega_2)$. Notice that in the case of $T = T_N$, eqs. (6.2) and (6.3) coincide with the output power spectrum and the input-output cross-correlation of the system in Figure 4-2.

6.2.2 Uniform Sinc Interpolation

In the case of Uniform Sinc Interpolation, sinc interpolation is applied to the samples placed on a uniform grid with spacing corresponding to the average spacing of the nonuniform sampling grid. With respect to second-order statistics, nonuniform sampling followed by USI is equivalent to the system of Figure 6-3 where $v^U(t)$ is zero-mean additive white noise, uncorrelated with $x(t)$. For the system of Figure 6-3 it is straight forward to show that

$$\begin{aligned}
S_{z^U z^U}(\Omega) &= \sum_{n=-\infty}^{\infty} S_{xx} \left(\Omega - \frac{2\pi}{T}n \right) \cdot \left| \Phi_{\xi} \left(\Omega - \frac{2\pi}{T}n \right) \right|^2 \\
&+ \underbrace{\frac{T}{2\pi} \int_{-\Omega_c}^{\Omega_c} S_{xx}(\Omega') \cdot \left(1 - \left| \Phi_{\xi}(\Omega') \right|^2 \right) d\Omega'}_{T^2 S_{v^U v^U}(\Omega)} \quad |\Omega| < \frac{\pi}{T}, \quad (6.4)
\end{aligned}$$

and that

$$R_{z^U x}(t, t - \tau) = \frac{1}{2\pi} \int_{-\pi/T}^{\pi/T} \left(\sum_{n=-\infty}^{\infty} S_{xx} \left(\Omega - \frac{2\pi}{T}n \right) \Phi_{\xi} \left(\Omega - \frac{2\pi}{T}n \right) e^{j\frac{2\pi}{T}n(t-\tau)} \right) e^{j\Omega\tau} d\Omega. \quad (6.5)$$

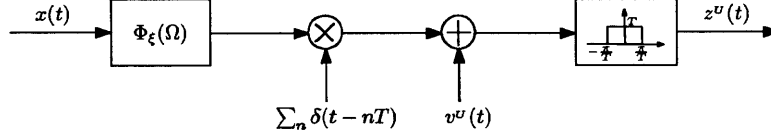


Figure 6-3: A second-order-statistics equivalent of nonuniform sampling followed by Uniform Sinc Interpolation for the case where $T > T_N$.

To show the equivalence, we note that with Uniform Sinc Interpolation, i.e., when $\zeta_n = 0$, $S_{\hat{x}\hat{x}}(\Omega)$ in eq. (6.2) reduces to $S_{z^U z^U}(\Omega)$ in eq. (6.4) and the cross-correlation $R_{\hat{x}\hat{x}}(t, t - \tau)$ in eq. (6.3) reduces to $R_{z^U x}(t, t - \tau)$ in eq. (6.5). The structure of Figure 6-3 suggests that with respect to second-order statistics, nonuniform sampling with stochastic perturbations can be modeled as uniform sampling of the signal pre-filtered by the Fourier transform of the pdf of the sampling perturbation. Correspondingly, the pdf $f_{\xi}(\xi)$ can be designed subject to the constraints on $f_{\xi}(\xi)$ as a probability density function so that the characteristic function $\Phi_{\xi}(\Omega)$ acts as an equivalent anti-aliasing LPF. Of course the stochastic perturbation still manifests itself through the additive white noise source $v^U(t)$ in Figure 6-3. Thus, Figure 6-3 suggests that aliasing can be traded off with uncorrelated white noise by appropriate design of the pdf of the sampling perturbation.

6.2.3 Nonuniform Sinc Interpolation

In the case of Nonuniform Sinc Interpolation, sinc interpolation is applied to the samples located at the actual nonuniform sampling grid. With respect to second-order statistics this is equivalent to the system in Figure 6-4 where $v^N(t)$ is zero-mean additive noise, uncorrelated with $x(t)$.

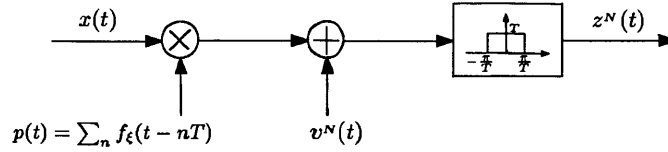


Figure 6-4: A second-order-statistics equivalent of nonuniform sampling followed by Nonuniform Sinc Interpolation for the case where $T > T_N$.

For the system of Figure 6-4 it is straight forward to show that

$$\begin{aligned}
 S_{z^N z^N}(\Omega) &= \sum_{n=-\infty}^{\infty} S_{xx} \left(\Omega - \frac{2\pi}{T}n \right) \cdot \left| \Phi_{\xi} \left(\frac{2\pi}{T}n \right) \right|^2 \\
 &+ \underbrace{\frac{T}{2\pi} \int_{-\Omega_c}^{\Omega_c} S_{xx}(\Omega') \cdot \left(1 - \left| \Phi_{\xi}(\Omega - \Omega') \right|^2 \right) d\Omega'}_{T^2 S_{v^N v^N}(\Omega)} \quad |\Omega| < \frac{\pi}{T}, \quad (6.6)
 \end{aligned}$$

and that

$$R_{z^N x}(t, t - \tau) = \int_{-\infty}^{\infty} R_{xx}(\tau - \tau') p(t - \tau') \text{sinc} \left(\frac{\pi}{T} \tau' \right) d\tau', \quad (6.7)$$

where $p(t) = \sum_{n=-\infty}^{\infty} f_{\xi}(t - nT)$. The equivalence is shown by noting that with Nonuniform Sinc Interpolation, i.e., when $\zeta_n = \xi_n$, $S_{\hat{x}\hat{x}}(\Omega)$ in eq. (6.2) reduces to $S_{z^N z^N}(\Omega)$ in eq. (6.6) and $R_{\hat{x}\hat{x}}(t, t - \tau)$ in eq. (6.3) reduces to $R_{z^N x}(t, t - \tau)$ in eq. (6.7). Figure 6-4 suggests that with respect to second-order statistics, nonuniform sampling followed by NSI is equivalent to modulating the signal with a periodic signal $p(t)$ with period T , obtained from the pdf $f_{\xi}(\xi)$ of the perturbation error and adding uncorrelated noise. In the frequency domain, this corresponds to scaling each replica of the spectrum by $|\Phi_{\xi}(\frac{2\pi}{T}n)|^2$. Correspondingly, the components in (6.6) associated with aliasing can be eliminated by designing the pdf $f_{\xi}(\xi)$ so that $\Phi_{\xi}(\frac{2\pi}{T}n) = 0$ for all $n \neq 0$, which corresponds in the time-domain to $p(t) = c$ where c is a nonzero constant. Of course, similar to USI, the stochastic perturbation still manifests itself through additive uncorrelated noise, as shown in Figure 6-4. However, as opposed to USI where the additive noise is white and the signal is pre-filtered by the characteristic function of the perturbation, the additive noise in NSI is in general not white, its power spectrum is determined by the convolution of $S_{xx}(\Omega)$ with $(1 - |\Phi_{\xi}(\Omega)|^2)$, and the shape of the original signal is preserved in reconstruction.

6.2.4 Independent Sinc Interpolation

With respect to second-order statistics, Independent Sinc Interpolation corresponds to the system of Figure 6-5 where $v^I(t)$ is zero-mean additive noise, uncorrelated with both $v^U(t)$ and $x(t)$,

$$S_{z^I z^I}(\Omega) = \left(\sum_{n=-\infty}^{\infty} S_{xx} \left(\Omega - \frac{2\pi n}{T} \right) \left| \Phi_{\xi} \left(\Omega - \frac{2\pi n}{T} \right) \right|^2 + \underbrace{\frac{T}{2\pi} \int_{-\Omega_c}^{\Omega_c} S_{xx}(\Omega') (1 - |\Phi_{\xi}(\Omega')|^2) d\Omega'}_{T^2 \cdot S_{v^U v^U}(\Omega)} \right) \cdot \underbrace{|\Phi_{\zeta}(-\Omega)|^2 + (1 - |\Phi_{\zeta}(-\Omega)|^2) \cdot \frac{T}{2\pi} \int_{-\Omega_c}^{\Omega_c} S_{xx}(\Omega') d\Omega'}_{T^2 \cdot S_{v^I v^I}(\Omega)} \quad |\Omega| < \frac{\pi}{T} \quad (6.8)$$

and

$$R_{z^I x}(t, t - \tau) = \frac{1}{2\pi} \int_{-\pi/T}^{\pi/T} \left(\sum_{n=-\infty}^{\infty} S_{xx} \left(\Omega - \frac{2\pi n}{T} \right) \Phi_{\xi} \left(\Omega - \frac{2\pi n}{T} \right) e^{j\frac{2\pi}{T} n(t-\tau)} \right) \Phi_{\zeta}(-\Omega) e^{j\Omega \tau} d\Omega. \quad (6.9)$$

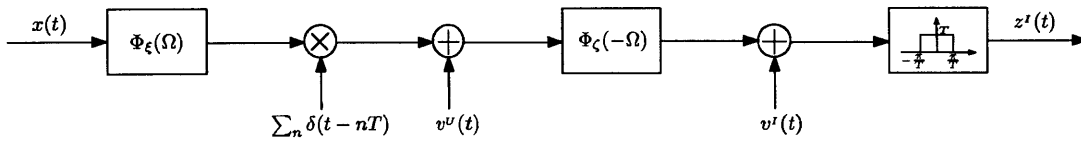


Figure 6-5: A second-order-statistics equivalent of nonuniform sampling followed by Independent Sinc Interpolation for the case where $T > T_N$.

As Figure 6-5 suggests, perturbing the grid on which the samples are placed prior to sinc interpolation has a similar effect to that of the stochastic perturbations in sampling, i.e., the characteristic function of the perturbations acts as a low-pass filter and an uncorrelated noise is added.

6.3 Simulations

In Figure 6-7 we illustrate the different types of artifacts resulting from sub-Nyquist sampling and with each of the reconstruction methods discussed above. We choose the signal $x(t)$ to be the output of an LTI system driven by white noise for which the transfer function $H_c(s)$ has unity gain at $s = 0$, and as shown in Figure 6-6 its poles and zeros locations are $\{0.1\pi e^{j\pi(2k+9)/20}\}_{k=1}^{10}$ and $\{0.1\pi(-0.1 \pm \frac{5}{8}j)\}$, respectively.

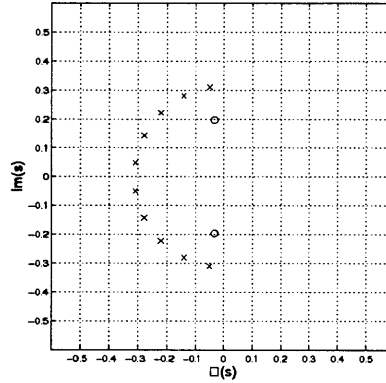


Figure 6-6: Pole-zero diagram of the transfer function $H_c(s)$.

To simulate a discrete-time signal whose power spectrum is consistent with the power spectrum of $x(t)$, we process discrete-time white noise with a discrete-time LTI system whose impulse response $h[n]$ is obtained using the method of impulse invariance, i.e., by sampling the impulse response $h_c(t)$ of the continuous-time system every $T_d = 1$ [sec]. The spacing on this grid is considered to be sufficiently dense so that aliasing is negligible and it accurately represents the impulse response of the continuous-time system. Figure 6-7(a) shows $\hat{S}_{xx}(\Omega)$, the estimated power spectrum of $x(t)$ obtained by applying Welch's method [73] with Hanning window of length 6656 [sec] and with 50% overlap. 500 blocks are averaged to obtain the estimate. This method and parameters are used for all spectral estimates in Figure 6-7.

From the parameters used for generating $x(t)$ and consistent with Figure 6-7(a) we consider the bandwidth of $x(t)$ to be approximately 0.14π [rad/sec] and the corresponding value of T_N to be approximately 7 [sec]. In the remaining simulations in Figure 6-7, the average or nominal spacing is $T = 13$ [sec] $\approx 1.8T_N$, and the power spectrum estimates are shown over the region $[-\frac{\pi}{T}, \frac{\pi}{T}]$ as if an ideal reconstruction filter was applied.

Figure 6-7(b) corresponds to the case of uniform sampling where reconstruction is obtained by applying USI to the samples of $x(t)$. This figure shows the estimated PSD $\hat{S}_{\hat{x}\hat{x}}^U(\Omega)$ of the approximation obtained by simulations vs. the theoretical results of the PSD and its components as follows from eq. (6.4) for the uniform sampling case, i.e., when $\xi_n = 0$. As shown in this figure, aliasing occurs as a result of undersampling and the interference is therefore correlated with the signal. (c), (d) and (e) of Figure 6-7 correspond to reconstruction obtained by applying USI, NSI and ISI respectively to the nonuniform samples of $x(t)$ with $T = 13$ [sec], and the deviation ξ_n from a uniform sampling grid uniformly distributed over $(-T/2, T/2)$. Those figures compare the estimated PSD $\hat{S}_{\hat{x}\hat{x}}^{USI}(\Omega)$, $\hat{S}_{\hat{x}\hat{x}}^{NSI}(\Omega)$ and $\hat{S}_{\hat{x}\hat{x}}^{ISI}(\Omega)$ obtained by simulations with the theoretical results, as follow from eqs. (6.4), (6.6) and (6.8), respectively. As shown in (b)-(e) of Figure 6-7, the theoretical results are consistent with those obtained by simulations.

Consistent with the fact that the characteristic function $\Phi_\xi(\Omega)$ of the sampling perturbations acts as an anti-aliasing filter in the model of Figure 6-3, the aliasing produced in USI as shown in Figure 6-7(c) is reduced relative to that produced with uniform sampling. However, this reduced aliasing is at the expense of an additional additive uncorrelated white noise component. Note that in Figure 6-7(d) there is no aliasing but only uncorrelated noise. This is because the pdf $f_\xi(\xi)$ of the perturbations satisfies the following condition

$$\Phi_\xi\left(\frac{2\pi}{T}n\right) = 0 \quad \forall n \neq 0, \quad (6.10)$$

which ensures no aliasing artifact when applying NSI to the nonuniform samples. Figure (e) corresponds to ISI with ζ_n uniformly distributed over $(-T/2, T/2)$. Comparing this figure with figure (c), we notice that due to the filtering by the characteristic function $\Phi_\zeta(-\Omega)$ of the perturbations ζ_n as shown in Figure 6-5, high frequency components of the signal and its replicas are attenuated in ISI compared to USI, and the additive uncorrelated noise is appropriately shaped. Superimposed on $\hat{S}_{\hat{x}\hat{x}}(\Omega)$ are shown in Figure 6-7(f) the estimated PSD of the various approximations obtained by simulations of the reconstruction methods discussed above. As we can see from these figures, the artifacts resulting in sub-Nyquist sampling differ in each of the reconstruction methods discussed above and can be controlled

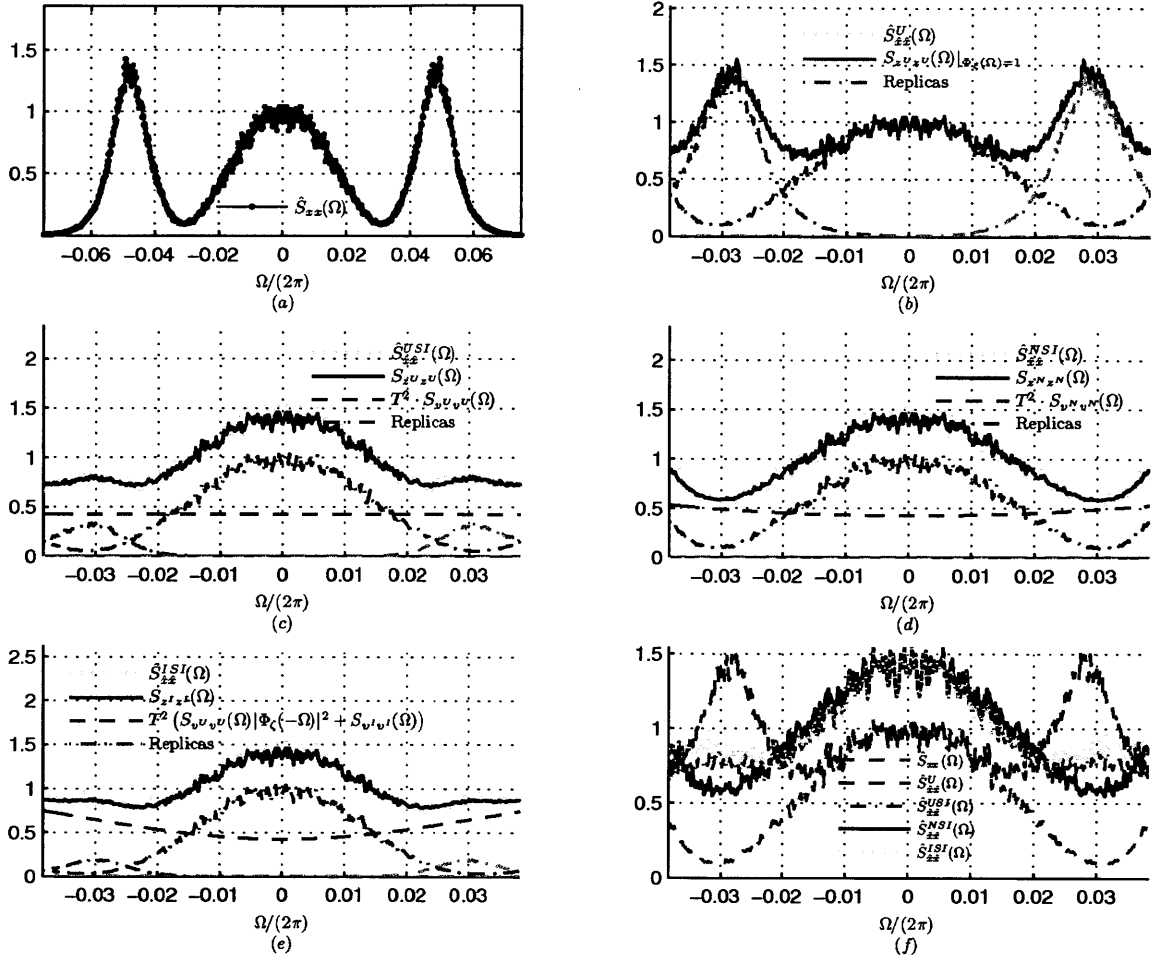


Figure 6-7: Artifacts with sub-Nyquist sampling. (a) The estimated power spectrum of $x(t)$. The estimated power spectrum vs. analytic results in the case of (b) Uniform Sampling, (c) USI applied to nonuniform sampling, (d) NSI applied to nonuniform sampling, and (e) ISI applied to nonuniform sampling. (f) The estimated power spectrum of $x(t)$ and of its approximations.

by designing the perturbations in sampling and in reconstruction to trade off aliasing with uncorrelated noise. The artifacts correspond to uniform sampling are more severe in high frequencies and are correlated with the signal, whereas the artifacts correspond to the reconstruction methods from nonuniform sampling have reduced or no correlation with the signal and are more balanced across frequency.

SUB-NYQUIST SAMPLING & ALIASING

7.1 Introduction

This chapter explores various sampling schemes for which the sampling rate is below the Nyquist rate, but additional information about the signal apart from its bandwidth is exploited. Specifically, in Section 7.2 we consider sampling of non-negative bandlimited signals, in which nonlinearity is incorporated prior to sampling as a way to decrease the signal's bandwidth. When perfect reconstruction is not possible with this approach, the nonlinear processing is viewed as an alternative to anti-aliasing LTI lowpass filtering. Section 7.3 suggests a different approach, referred to as inphase-quadrature anti-aliasing, in which a bandlimited signal is approximated by another bandlimited signal with reduced bandwidth. In Section 7.4 we develop co-sampling which suggests exploiting dependencies between signals in order to reduce their effective total sampling rate.

7.2 Sampling a Non-negative Bandlimited Signal

The Nyquist-Shannon sampling theorem provides a sufficient rate for which perfect reconstruction of a bandlimited signal is possible from its equally spaced samples. If the only information available about a bandlimited signal is its bandwidth, the Nyquist rate is the minimum sampling rate for which perfect reconstruction is possible. With additional information exploited apart from the signal's bandwidth, there is the possibility of reducing the sampling rate below the Nyquist rate and still achieving perfect reconstruction. For example, when a bandlimited signal is processed through a nonlinear system, the informa-

tion about the system can sometimes be exploited to reduce the signal's sampling rate. To illustrate the concept, consider the following example:

$$y(t) = |x(t)|^2 = x(t) \cdot x^*(t), \quad (7.1)$$

where $x(t)$ is bandlimited. Utilizing the fact that the bandwidth of $x(t)$ is half the bandwidth of $y(t)$, we can extract the signal $x(t)$ and sample it at its Nyquist rate, which is half the Nyquist rate of $y(t)$. Provided that $x(t)$ is real, we achieve with this approach a sampling rate reduction by a factor of two. However, obtaining $x(t)$ from $y(t)$ is not a trivial task since the absolute square root of $y(t)$ does not yield in general a bandlimited signal. For example, when $y(t) = \text{sinc}^2(\frac{\pi}{T}t)$, its absolute square root is clearly not bandlimited as it has infinitely many non-differentiable points. Thus, the recovery of the signal's phase becomes crucial for this sampling approach. The bandlimitedness of $x(t)$ can be exploited for this purpose.

Figure 7-1 suggests a system for sampling and reconstruction of the bandlimited signal $y(t)$, in which the relation in (7.1) is utilized. The sampling system consists of bandlimited-square-root processing, whose output is a bandlimited signal $x(t)$ such that $y(t) = |x(t)|^2$, followed by uniform sampling at half the Nyquist rate of $y(t)$. The reconstruction is accomplished by taking the magnitude square of the continuous-time signal obtained from sinc interpolation of the equally-spaced samples of $x(t)$.

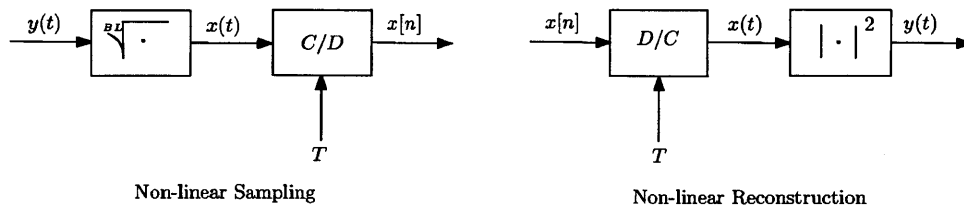


Figure 7-1: A sampling-reconstruction scheme of a non-negative bandlimited signal. The sampling system consists of non-linear pre-processing whose output signal $x(t)$ is bandlimited to $\pm\pi/T$ and satisfies the relation $y(t) = |x(t)|^2$.

7.2.1 Bandlimited Square-roots

Boas and Kak [45] have shown that for a real non-negative function $y(t)$, integrable on $(-\infty, \infty)$, and whose spectrum has no component at or above the frequency $2\pi/T$, there exists a function $x(t)$ whose spectrum $X(\Omega)$ vanishes outside $(-\pi/T, \pi/T)$, and for which

$$Y(\Omega) = \frac{1}{2\pi} \int_{-\pi/T}^{\pi/T} X(\xi)X^*(\xi - \Omega)d\xi. \quad (7.2)$$

This theorem asserts that there exists a bandlimited signal $x(t)$ that satisfies (7.1) and whose bandwidth is half the bandwidth of $y(t)$. The signal $x(t)$ will be referred to as a bandlimited square-root of $y(t)$.

The problem of finding bandlimited square-roots of a real non-negative bandlimited signal is equivalent in the time-domain to the problem of finding the set of all time-limited functions having a specified autocorrelation function, a problem which E. M. Hofstetter considered in [34]. To explore the former problem, we take a similar approach to that introduced in [34]. Specifically, we obtain the analytic continuation of $y(t)$ on the complex plane by transforming the frequency response $Y(\Omega)$ into the complex s -domain, i.e.,

$$y(s) = \frac{1}{2\pi} \int_{-\infty}^{\infty} Y(\Omega) \cdot e^{-s\Omega} d\Omega, \quad (7.3)$$

from which $y(t)$ is obtained along the line $s = -jt$.

According to the Paley-Wiener theorem [8], since $y(t)$ is bandlimited or, equivalently, since the support of $Y(\Omega)$ is finite, $y(s)$ is an entire function of an exponential type, meaning that there is a constant C such that

$$|y(s)| \leq Ce^{\alpha|s|}. \quad (7.4)$$

This fact combined with Hadamard's factorization theorem [86] implies that

$$y(s) = As^n e^{\alpha s} \prod_{k=1}^{\infty} \left(1 - \frac{s}{s_k}\right) e^{s/s_k}, \quad (7.5)$$

i.e., $y(s)$ is completely specified (up to a complex constant) by the location of its zeros.

With (7.2) substituted into (7.3), we obtain

$$y(s) = x(s) \cdot x^*(-s^*), \quad (7.6)$$

from which it follows that the same spectrum $Y(\Omega)$ can correspond to two different signals $x_1(s)$ and $x_2(s)$, provided that

$$x_1(s) \cdot x_1^*(-s^*) = x_2(s) \cdot x_2^*(-s^*). \quad (7.7)$$

Specifically, if $x_1(t)$ is bandlimited and its analytic continuation on the complex plane $x_1(s)$ satisfies (7.6), then any other signal obtained from $x_1(s)$ by replacing its zeros with their negative conjugates will also correspond to a bandlimited signal which satisfies (7.6) [34]. The number of different bandlimited square-roots may be either finite or infinite, depending on the signal $y(t)$.

7.2.1.1 Min-Phase Bandlimited Square-root

As discussed in the previous section, we can replace some or all zeros of one solution of eq. (7.6) with their negative conjugates to obtain other solutions of eq. (7.6). Provided that $y(s)$ has no zeros on the imaginary axis, the solution whose zeros are all located in the left region of the complex plane is of particular interest. This solution, denoted as $x_{min}(s)$, will be referred to as the min-phase bandlimited square-root. Defining the partial energy of $x(t)$ as

$$E_x(\xi) = \frac{1}{2\pi} \int_{-\infty}^{\xi} |X(\Omega)|^2 d\Omega, \quad (7.8)$$

it can be shown that the energy of the min-phase signal is delayed the least of all signals $x(t)$ satisfying eq. (7.1), i.e.,

$$\frac{1}{2\pi} \int_{-\infty}^{\xi} |X_{min}(\Omega)|^2 d\Omega \geq \frac{1}{2\pi} \int_{-\infty}^{\xi} |X(\Omega)|^2 d\Omega, \quad \forall \xi. \quad (7.9)$$

To prove the inequality in (7.9), we first note that since all solutions satisfy the relation

$|x(t)|^2 = y(t)$, they all have the same total energy. Therefore, equality in (7.9) is achieved for $\xi \rightarrow \infty$, i.e.,

$$\frac{1}{2\pi} \int_{-\infty}^{\infty} |X_{min}(\Omega)|^2 d\Omega = \frac{1}{2\pi} \int_{-\infty}^{\infty} |X(\Omega)|^2 d\Omega. \quad (7.10)$$

To prove that (7.9) is true for any other ξ , we follow a similar argument to that presented in [69] for the discrete-time case. Specifically, we assume that s_0 is a zero of $x_{min}(s)$ and represent it as

$$x_{min}(s) = q(s) \cdot (s - s_0), \quad (7.11)$$

where $q(s)$ is another min-phase signal. Processing $x_{min}(s)$ through an all-pass term which moves its zero at $s = s_0$ to its mirror image location, $s = -s_0^*$, we obtain

$$x(s) = x_{min}(s) \cdot \frac{s + s_0^*}{s - s_0} = q(s) \cdot (s + s_0^*), \quad (7.12)$$

which is another solution of (7.6). Denoting $Q(\Omega)$ as the frequency response corresponding to $q(s)$, it follows from (7.11) and (7.12) that the frequency response $X_{min}(\Omega)$ corresponding to $x_{min}(s)$ and the frequency response $X(\Omega)$ corresponding to $x(s)$ can be represented as follows:

$$\begin{aligned} X_{min}(\Omega) &= \frac{dQ(\Omega)}{d\Omega} - s_0 \cdot Q(\Omega), \\ X(\Omega) &= \frac{dQ(\Omega)}{d\Omega} + s_0^* \cdot Q(\Omega), \end{aligned} \quad (7.13)$$

from which it follows that

$$|X_{min}(\Omega)|^2 - |X(\Omega)|^2 = -4\Re(s_0) \cdot \Re\left(Q(\Omega) \cdot \frac{dQ^*(\Omega)}{d\Omega}\right) = -2\Re(s_0) \cdot \frac{d|Q(\Omega)|^2}{d\Omega}. \quad (7.14)$$

Integrating (7.14) with respect to Ω and noting that s_0 lies in the left half plane, we obtain

$$\frac{1}{2\pi} \int_{-\infty}^{\xi} (|X_{min}(\Omega)|^2 - |X(\Omega)|^2) d\Omega = -\frac{\Re(s_0)}{\pi} \cdot |Q(\xi)|^2 \geq 0. \quad (7.15)$$

Rearranging (7.15) completes the proof of (7.9). The minimum delay energy property will be utilized in section 7.2.3.

7.2.1.2 Real Bandlimited Square-roots

If $x(t)$ is real, its Fourier transform is conjugate symmetric and $x(s) = x^*(-s^*)$. It then follows that zeros of $x(s)$ which are not purely imaginary occur in pairs $(s_0, -s_0^*)$ and that

$$y(s) = x^2(s). \quad (7.16)$$

As suggested by eq. (7.16), a necessary condition for the existence of a real bandlimited square root is that all zeros of $y(s)$ will have an even order.

7.2.2 Signals with Real Bandlimited Square-roots

We next discuss some of the characteristics of a real non-negative bandlimited signal $y(t)$ which possess a real bandlimited square-root. Applying the Fourier transform to eq. (7.1), we obtain

$$Y(\Omega) = \frac{1}{2\pi} \int_{-\infty}^{\infty} X(\xi) \cdot X^*(\xi - \Omega) d\xi, \quad (7.17)$$

from which the following inequality clearly follows:

$$|Y(\Omega)| \leq Y(\Omega)|_{\Omega=0}. \quad (7.18)$$

Adding the fact that $x(t)$ is bandlimited to $\pm\pi/T$, it follows from (7.17) that

$$Y(\Omega) = \begin{cases} \frac{1}{2\pi} \int_{-\pi/T+\Omega}^{\pi/T} X(\xi) \cdot X^*(\xi - \Omega) d\xi & 0 \leq \Omega < \frac{2\pi}{T} \\ \frac{1}{2\pi} \int_{-\pi/T}^{\pi/T-\Omega} X(\xi) \cdot X^*(\xi - \Omega) d\xi & -\frac{2\pi}{T} < \Omega < 0 \end{cases}. \quad (7.19)$$

Applying the Cauchy-Schwartz inequality to (7.19) results in the following inequality:

$$|Y(\Omega)|^2 \leq \frac{1}{2\pi} \int_{|\Omega|-\pi/T}^{\pi/T} |X(\xi)|^2 d\xi \cdot \frac{1}{2\pi} \int_{|\Omega|-\pi/T}^{\pi/T} |X^*(-\xi)|^2 d\xi \quad 0 \leq |\Omega| \leq 2\pi/T, \quad (7.20)$$

which reduces to the following inequality when $x(t)$ is real

$$\begin{aligned}
 |Y(\Omega)| &\leq \frac{1}{2\pi} \int_{|\Omega|-\frac{\pi}{T}}^{\frac{\pi}{T}} |X(\xi)|^2 d\xi, \quad 0 \leq |\Omega| < 2\pi/T \\
 &= \begin{cases} \frac{1}{2}Y(\Omega)|_{\Omega=0} + \frac{1}{2\pi} \int_{|\Omega|-\frac{\pi}{T}}^0 |X(\xi)|^2 d\xi, & \forall 0 \leq |\Omega| \leq \frac{\pi}{T}, \\ \frac{1}{2}Y(\Omega)|_{\Omega=0} - \frac{1}{2\pi} \int_0^{|\Omega|-\frac{\pi}{T}} |X(\xi)|^2 d\xi, & \forall \frac{\pi}{T} \leq |\Omega| \leq \frac{2\pi}{T}. \end{cases} \quad (7.21)
 \end{aligned}$$

As implied from (7.21), a necessary but not sufficient condition for a non-negative bandlimited signal to possess a real bandlimited square root is that

$$|Y(\pi/T - |\xi|)| + |Y(\pi/T + |\xi|)| \leq Y(\Omega)|_{\Omega=0} \quad \forall 0 \leq |\xi| \leq \pi/T. \quad (7.22)$$

The inequality in (7.22) suggests alternative upper bounds to those implied by (7.18) on the value of $|Y(\pi/T)|$ and on the area under $|Y(\Omega)|$. Specifically,

$$|Y(\pi/T)| \leq (1/2) \cdot Y(\Omega)|_{\Omega=0}, \quad (7.23a)$$

and

$$\frac{T}{2\pi} \int_0^{2\pi/T} |Y(\Omega)| d\Omega \leq (1/2) \cdot Y(\Omega)|_{\Omega=0}. \quad (7.23b)$$

Figure 7-2 specifies a region that bounds all possible $|Y(\Omega)|$ that satisfy (7.21). Indicated within this region is the triangular-shape frequency response of $y(t) = \text{sinc}^2(\frac{\pi}{T}t)$, which achieves (7.21) with equality. Note that a non-negative real bandlimited signal $y(t)$ whose absolute frequency response $|Y(\Omega)|$ violates the boundaries of this region cannot possess a real bandlimited square-root.

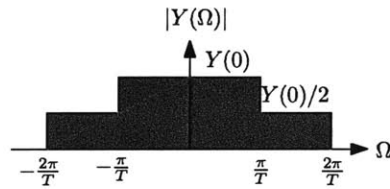


Figure 7-2: The region within which all possible $|Y(\Omega)|$ that satisfy (7.21) lie.

7.2.3 Nonlinear Anti-aliasing

When the Nyquist condition is not satisfied and we wish to avoid aliasing in sampling, additional information about the signal apart from its bandwidth can be exploited to developing alternative pre-processing instead of the traditional LTI anti-aliasing lowpass filter. With these alternative approaches there is the possibility of reducing the approximation error obtained with LTI anti-aliasing. In addition, when the bandlimited signal is non-negative, for example, LTI anti-aliasing may be undesirable as it does not preserve the non-negativity of the signal. We next address various nonlinear approaches for processing a non-negative bandlimited signal prior to sampling it. This processing will be referred to as non-linear anti-aliasing. The general structure of the sampling-reconstruction system that will be considered here is motivated by the system of Figure 7-1.

7.2.3.1 Complex Nonlinear Anti-aliasing

This section considers the system depicted in Figure 7-3, in which the bandlimited signal $y(t)$ is assumed to possess only complex bandlimited square roots. The signal $x(t)$, representing a complex bandlimited square-root of $y(t)$, is processed through an LTI system, whose impulse response, possibly complex, is $h(t)$, to yield the following approximation:

$$\hat{x}(t) = x(t) * h(t). \quad (7.24)$$

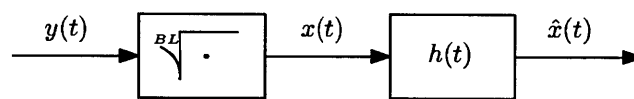


Figure 7-3: Non-linear anti-aliasing.

Approximating the signal $y(t)$ with $\hat{y}(t) = |\hat{x}(t)|^2$ and denoting $e(t) = y(t) - \hat{y}(t)$ as the approximation error, its energy can be represented as follows:

$$\begin{aligned} \int_{-\infty}^{\infty} (y(t) - \hat{y}(t))^2 dt &= \frac{1}{2\pi} \int_{-\frac{2\pi}{T}}^{\frac{2\pi}{T}} |Y(\Omega) - \hat{Y}(\Omega)|^2 d\Omega \\ &= \frac{1}{2\pi} \int_{-\frac{2\pi}{T}}^{\frac{2\pi}{T}} \left| \frac{1}{2\pi} \int_{-\frac{\pi}{T}}^{\frac{\pi}{T}} (X(\xi)X^*(\xi - \Omega) - \hat{X}(\xi)\hat{X}^*(\xi - \Omega)) d\xi \right|^2 d\Omega. \end{aligned} \quad (7.25)$$

Using the Cauchy-Schwartz inequality in (7.26), the following upper bound on the approximation error is obtained

$$\begin{aligned} \int_{-\infty}^{\infty} (y(t) - \hat{y}(t))^2 dt &\leq \frac{1}{T} \cdot \frac{1}{2\pi} \int_{-\frac{2\pi}{T}}^{\frac{2\pi}{T}} \left(\frac{1}{2\pi} \int_{-\frac{\pi}{T}}^{\frac{\pi}{T}} |X(\xi)X^*(\xi - \Omega) - \hat{X}(\xi)\hat{X}^*(\xi - \Omega)|^2 d\xi \right) d\Omega \\ &= \frac{1}{T} (E_X^2 - 2|R_{X\hat{X}}|^2 + E_{\hat{X}}^2), \end{aligned} \quad (7.26)$$

in which

$$\begin{aligned} E_X &= \frac{1}{2\pi} \int_{-\frac{\pi}{T}}^{\frac{\pi}{T}} |X(\Omega)|^2 d\Omega, \\ E_{\hat{X}} &= \frac{1}{2\pi} \int_{-\frac{\pi}{T}}^{\frac{\pi}{T}} |\hat{X}(\Omega)|^2 d\Omega, \end{aligned} \quad (7.27)$$

and

$$R_{X\hat{X}} = \frac{1}{2\pi} \int_{-\frac{\pi}{T}}^{\frac{\pi}{T}} X(\Omega)\hat{X}^*(\Omega) d\Omega. \quad (7.28)$$

We now consider the LTI system in Figure 7-3, whose impulse response is $h(t)$, to have the following frequency response:

$$H(\Omega) = \begin{cases} 1 & -\pi/T \leq \Omega \leq \gamma < \pi/T \\ 0 & \text{otherwise} \end{cases}, \quad (7.29)$$

as depicted in Figure 7-4.

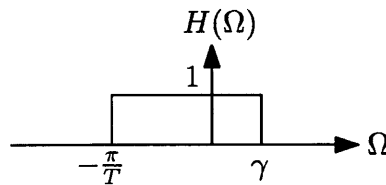


Figure 7-4: The frequency response $H(\Omega)$ of the LTI system in Figure 7-3.

With this choice of $h(t)$, the bandwidth of the approximation $\hat{x}(t)$ is reduced relative to

the bandwidth of $x(t)$, and the upper bound in (7.26) satisfies the following inequalities:

$$\begin{aligned}
\frac{1}{T} (E_{\hat{x}}^2 - 2|R_{X\hat{x}}|^2 + E_X^2) &\geq \frac{1}{T} \left(E_{\hat{x}}^2 - 2E_{\hat{x}} \cdot \frac{1}{2\pi} \int_{-\pi/T}^{\gamma} |X(\Omega)|^2 d\Omega + E_X^2 \right) \\
&\geq \frac{1}{T} \left(E_X^2 - \left| \frac{1}{2\pi} \int_{-\pi/T}^{\gamma} |X(\Omega)|^2 d\Omega \right|^2 \right) \\
&\geq \frac{1}{T} \left(E_X^2 - \left| \frac{1}{2\pi} \int_{-\pi/T}^{\gamma} |X_{min}(\Omega)|^2 d\Omega \right|^2 \right). \quad (7.30)
\end{aligned}$$

The first inequality is obtained from applying the Cauchy-Schwartz inequality on $R_{X\hat{x}}$ in (7.28), i.e.,

$$|R_{X\hat{x}}|^2 \leq \frac{1}{2\pi} \int_{-\pi/T}^{\gamma} |X(\Omega)|^2 d\Omega \cdot \frac{1}{2\pi} \int_{-\pi/T}^{\gamma} |\hat{X}^*(\Omega)|^2 d\Omega, \quad (7.31)$$

where equality is achieved if and only if

$$\hat{X}(\Omega) = X(\Omega), \quad -\pi/T \leq \Omega \leq \gamma. \quad (7.32)$$

The second inequality follows by noting that with respect to $E_{\hat{x}}$ we have a quadratic form whose minimum occurs at $E_{\hat{x}} = \frac{1}{2\pi} \int_{-\pi/T}^{\gamma} |X(\Omega)|^2 d\Omega$. The last inequality exploits the minimum energy delay property of the min-phase solution $x_{min}(s)$, as discussed in section 7.2.1.1, while taking into account the fact that the energy E_X is the same for all signals satisfying (7.1).

Thus, it follows from (7.26) together with (7.30) that the upper bound on the error in approximating $y(t)$ with $\hat{y}(t) = |\hat{x}(t)|^2$ is minimized when

$$\hat{X}(\Omega) = \hat{X}_{min}(\Omega) = X_{min}(\Omega) \cdot H(\Omega) = \begin{cases} X_{min}(\Omega) & -\pi/T \leq \Omega \leq \gamma \\ 0 & \text{otherwise} \end{cases}. \quad (7.33)$$

In this case,

$$\int_{-\infty}^{\infty} (y(t) - |\hat{x}_{min}(t)|)^2 dt \leq \frac{1}{T} \cdot \left(E_X^2 - \left| \frac{1}{2\pi} \int_{-\pi/T}^{\gamma} |X_{min}(\Omega)|^2 d\Omega \right|^2 \right). \quad (7.34)$$

In this approach, we first extract the min-phase bandlimited square-root $x_{min}(t)$ of $y(t)$, and then process it through the LTI system whose impulse response is $h(t)$. Though the min-phase solution can be obtained from spectral decomposition of $y(s)$, an alternative approach can be taken, in which we utilize the facts that for min-phase signals, the continuous-time phase $\arg(x_{min}(t))$ is related to $\log|x_{min}(t)|$ by the Hilbert transform and that the magnitude $|x_{min}(t)|$ is the absolute square root of $y(t)$.

As a simple illustration of the nonlinear anti-aliasing approach, we consider the signal used in [34]

$$y(t) = \frac{\sinh^2(a\Omega_x)}{\pi^2(a^2 + t^2)}, \quad (7.35)$$

whose frequency response is zero outside the support $(-2\Omega_x, 2\Omega_x)$, and

$$Y(\Omega) = \begin{cases} \frac{\sinh(a(2\Omega_x - \Omega))}{2\pi a} & 0 \leq \Omega < 2\Omega_x \\ \frac{\sinh(a(2\Omega_x + \Omega))}{2\pi a} & -2\Omega_x < \Omega < 0. \end{cases} \quad (7.36)$$

Transforming $Y(\Omega)$ into the complex s -domain using (7.6), we obtain

$$\begin{aligned} y(s) &= \frac{1}{2\pi^2} \cdot \frac{\cosh(2s\Omega_x) - \cosh(2a\Omega_x)}{(s-a)(s+a)} \\ &= \frac{\sinh((s-a)\Omega_x)}{\pi(s-a)} \cdot \frac{\sinh((s+a)\Omega_x)}{\pi(s+a)}, \end{aligned} \quad (7.37)$$

from which it follows that the zeros of $y(s)$ are located at

$$s = \pm a + j\frac{\pi}{\Omega_x}k, \quad k = \pm 1, \pm 2, \dots \quad (7.38)$$

Since the zeros of $y(s)$ do not have an even order, $y(t)$ does not possess a real bandlimited square root. Instead, there are infinitely many complex solutions. One of particular interest is the min-phase solution

$$x_{min}(s) = \frac{\sinh((s-a)\Omega_x)}{\pi(s-a)}, \quad (7.39)$$

whose zeros are all located in the left half plane, i.e.,

$$z_k = a + j(\pi/\Omega_x)k, \quad k = \pm 1, \pm 2, \dots \quad (7.40)$$

and its corresponding frequency response is

$$X_{min}(\Omega) = \begin{cases} e^{a\Omega} & |\Omega| < \Omega_x \\ 0 & |\Omega| \geq \Omega_x \end{cases} \quad (7.41)$$

Other solutions may be obtained by replacing zeros of $x_{min}(s)$ with their negative conjugates. Specifically, applying the all-pass system

$$\begin{aligned} H(s) &= \frac{s + (a - j\pi/\Omega_x)}{s - (a + j\pi/\Omega_x)} \cdot \frac{s + (a + j\pi/\Omega_x)}{s - (a - j\pi/\Omega_x)} \\ &= \frac{(s+a)^2 + (\pi/\Omega_x)^2}{(s-a)^2 + (\pi/\Omega_x)^2} \\ &= 1 + 4a \frac{s-a}{(s-a)^2 + (\pi/\Omega_x)^2} + \frac{4a^2}{\pi/\Omega_x} \cdot \frac{\pi/\Omega_x}{(s-a)^2 + (\pi/\Omega_x)^2} \end{aligned} \quad (7.42)$$

to $x_{min}(s)$ will replace its zeros located at $a \pm j\pi/\Omega_x$ with their negative conjugates $-(a \pm j\pi/\Omega_x)$. In the frequency domain, this processing corresponds to convolving $X_{min}(\Omega)$ with

$$H(\Omega) = 2\pi \cdot \left[\delta(\Omega) + 4ae^{a\Omega} \cdot \left(\cos(\pi\Omega/\Omega_x) + \frac{a\Omega_x}{\pi} \sin(\pi\Omega/\Omega_x) \right) u(\Omega) \right], \quad (7.43)$$

which yields

$$\begin{aligned} X_1(\Omega) &= \frac{1}{2\pi} X_{min}(\Omega) * H(\Omega) \\ &= \begin{cases} e^{a\Omega} \left(1 + \frac{4a}{\pi/\Omega_x} \cdot \left(\frac{a\Omega_x}{\pi} + \frac{a\Omega_x}{\pi} \cdot \cos(\pi\Omega/\Omega_x) - \sin(\pi\Omega/\Omega_x) \right) \right), & |\Omega| < \Omega_x \\ 0, & |\Omega| \geq \Omega_x \end{cases} \end{aligned} \quad (7.44)$$

Replacing the even index zeros of $x_{min}(s)$ with their negative conjugates will obtain

another solution, $x_2(s)$, whose frequency response is

$$X_2(\Omega) = \begin{cases} e^{a(\Omega+\Omega_x)} & -\Omega_x \geq \Omega < 0 \\ e^{a(\Omega-\Omega_x)} & 0 \leq \Omega < \Omega_x. \end{cases} \quad (7.45)$$

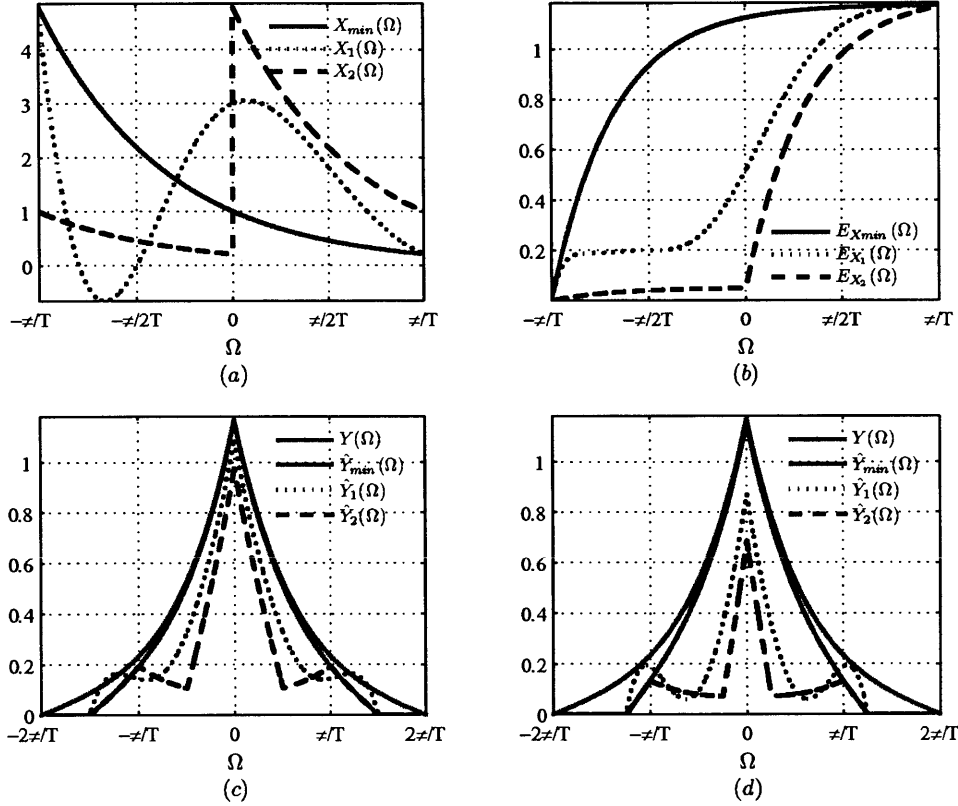


Figure 7-5: Complex anti-aliasing applied to $y(t)$ from (7.35) where $a = -\pi/2$ and $\Omega_x = \pi/T$. (a) The spectrums of the complex bandlimited square roots. (b) The partial energies of the complex bandlimited square roots. (c) The frequency responses of $y(t)$ and of its approximations $\hat{y}(t) = |\hat{x}(t)|^2$ where the cut-off frequency of $H(\Omega)$ is $\gamma = \pi/(2T)$. (d) The frequency responses of $y(t)$ and of its approximations $\hat{y}(t) = |\hat{x}(t)|^2$ where the cut-off frequency of $H(\Omega)$ is $\gamma = \pi/(4T)$.

Figure (a) of 7-5 shows the spectrums $X_{min}(\Omega)$, $X_1(\Omega)$ and $X_2(\Omega)$, as indicated in (7.41), (7.44) and (7.45) for the case of $a = -\pi/2$ and $\Omega_x = \pi/T$. In Figure (b) the partial energies of these signals are shown and the minimum energy delay property is illustrated, i.e., the energy of the min-phase signal is shown to be delayed the least of the other two signals considered. (c) and (d) of Figure 7-5 show the spectrum $Y(\Omega)$ of the given signal $y(t)$ along with the spectrums of its approximations obtained from the system of Figure 7-3 for

different bandlimited square roots, i.e., $\hat{y}_{min}(t) = |\hat{x}_{min}(t)|^2$, $\hat{y}_1(t) = |\hat{x}_1(t)|^2$, and $\hat{y}_2(t) = |\hat{x}_2(t)|^2$. The cut-off frequency γ of $H(\Omega)$ used in the approximations of Figure (c) is $\pi/(2T)$ and in the approximation of Figure (d) is $\pi/(4T)$. In both cases, the approximation of $y(t)$ obtained with the min-phase bandlimited square-root yields the lowest error.

This approach suggests a constructive procedure for obtaining a non-negative approximation of $y(t)$ whose bandwidth is reduced. In addition, the choice $x(t) = x_{min}(t)$ minimizes, among all bandlimited square-roots, the error in approximating $x(t)$ with $\hat{x}(t) = x(t) * h(t)$, where $h(t)$ is the impulse response whose frequency response is specified in (7.29). Note, however, that minimizing the error in approximating $x(t)$ with $\hat{x}(t) = x(t) * h(t)$ does not necessarily imply that the error in approximating $y(t)$ with $\hat{y}(t) = |\hat{x}(t)|^2$ is the minimum possible for that bandwidth constraint. In fact, a lower error may be achieved with LTI anti-aliasing filter at the expense of not preserving the non-negativity property of the signal.

The complex bandlimited square-root signal can be a base for a variety of other approximate non-negative representations of $y(t)$ with a reduced bandwidth. The signal $y(t)$ can be still approximated with $|\hat{x}(t)|^2$; however, we may consider other ways for approximating $x(t)$. For example,

$$\hat{x}(t) = \Re\{x(t)\} * h_1(t) + j\Im\{x(t)\} * h_2(t), \quad (7.46)$$

where $h_1(t)$ and $h_2(t)$ are LTI selective filters that determine the total bandwidth of the approximate representation. Special cases of this choice are the real part $x_R(t) = \Re\{x(t)\}$ or the imaginary part $x_i(t) = \Im\{x(t)\}$ of the complex bandlimited square root $x(t)$. Note that since with this choice of $\hat{x}(t)$, the actual bandwidth of $\hat{y}(t)$ may be larger than its effective bandwidth, this approximation may produce a lower error than that produced with the appropriate LTI anti-aliasing lowpass filtering.

7.2.3.2 Bandlimited Square-root as a Nonlinear Least-squares Problem

If a real bandlimited square root does not exist, a real bandlimited signal $\hat{x}(t)$ can be obtained whose square is closest, in the least square sense, to the non-negative bandlimited

signal $y(t)$. Specifically, we formulate the following nonlinear least-squares problem,

$$y(t) \approx \hat{x}^2(t), \quad (7.47)$$

and solve for $\hat{x}(t)$. To restrict the solution to be bandlimited, we represent $\hat{x}(t)$ in (7.47) as the sinc interpolation of its Nyquist rate samples $\hat{x}[n] = \hat{x}(nT)$. We then choose these samples to minimize the least-squares error, i.e.,

$$\min_{\hat{x}[n]} \int_{-\infty}^{\infty} \left[y(t) - \left(\sum_{n=-\infty}^{\infty} \hat{x}[n] \cdot h(t - nT) \right)^2 \right]^2 dt, \quad (7.48)$$

where $h(t) = \text{sinc}(\frac{\pi}{T}t)$. Rather than solving the nonlinear optimization in (7.48), we will linearize it and solve instead a linear least squares problem [6]. Linearization of $\hat{x}^2(t) = (\sum_{n=-\infty}^{\infty} \hat{x}[n]h(t - nT))^2$ around $\hat{x}[n] = x_*[n]$ will obtain

$$\hat{x}^2(t) \approx \left(\sum_{k=-\infty}^{\infty} x_*[k]h(t - kT) \right)^2 + 2 \left(\sum_{k=-\infty}^{\infty} x_*[k]h(t - kT) \right) \cdot \sum_{n=-\infty}^{\infty} h(t - nT)(\hat{x}[n] - x_*[n]). \quad (7.49)$$

Denoting by $y_*(t) = (x_*(t))^2 = (\sum_{k=-\infty}^{\infty} x_*[k]h(t - kT))^2$ and by $z_*(t) = (y(t) + y_*(t))/2$, the solution to the non-linear least squares problem in (7.47) can be approximated by the solution to the following linear least-squares problem

$$z_*(t) \approx x_*(t) \cdot \sum_{n=-\infty}^{\infty} x[n]h(t - nT). \quad (7.50)$$

Iteratively solving the linear least-squares problem in (7.50), we obtain

$$\frac{1}{2\pi} \int_{-\frac{\pi}{T}}^{\frac{\pi}{T}} X^{(l+1)}(\xi) \cdot Y^{(l)}(\Omega - \xi) d\xi = \frac{1}{2\pi} \int_{-\frac{\pi}{T}}^{\frac{\pi}{T}} X^{(l)}(\xi) \cdot Z^{(l)}(\Omega - \xi) d\xi \quad \forall |\Omega| \leq \frac{\pi}{T}, \quad (7.51)$$

where $X^{(l)}(\Omega)$, $Y^{(l)}(\Omega)$ and $Z^{(l)}(\Omega)$ are the frequency responses of $x^{(l)}(t)$, $y^{(l)}(t)$ and $z^{(l)}(t)$, respectively, and where the superscripts indicate the iteration number. Note that as suggested by eq. (7.51), the nonlinear deconvolution of the original problem is replaced with

an iterative set of linear deconvolutions.

7.2.4 Generalization

Given two bandlimited signals $x_1(t)$ and $x_2(t)$ whose bandwidths are W_1 and W_2 , the bandwidth W of the signal $y(t)$ obtained from multiplying $x_1(t)$ with $x_2(t)$ can in general be equal, greater or lower than the sum of their bandwidths. Each of these cases is illustrated in the examples of Figures (7-6), (7-7) and (7-8).

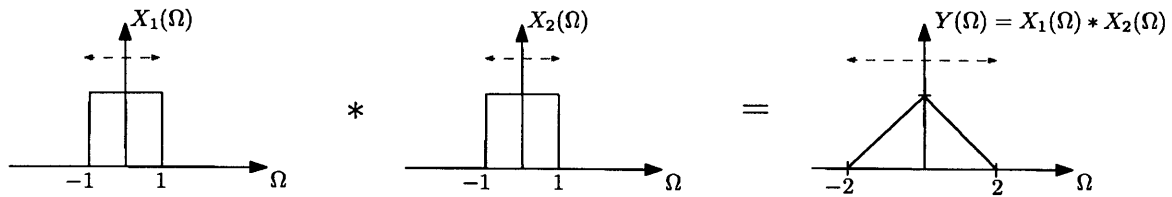


Figure 7-6: An example for which the bandwidth of $y(t)$ is equal to the sum of the bandwidths of $x_1(t)$ and $x_2(t)$.

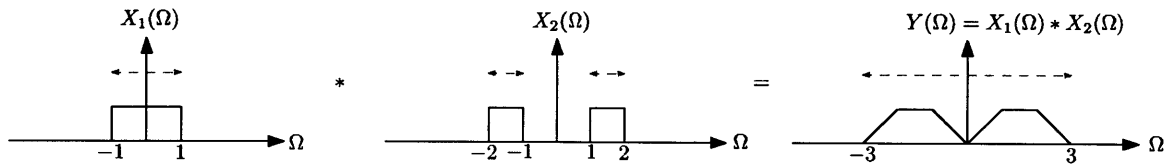


Figure 7-7: An example for which the bandwidth of $y(t)$ is greater than the sum of the bandwidths of $x_1(t)$ and $x_2(t)$.

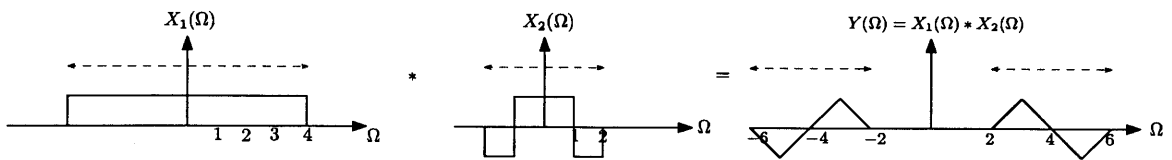


Figure 7-8: An example for which the bandwidth of $y(t)$ is less than the sum of the bandwidths of $x_1(t)$ and $x_2(t)$.

This observation may suggest approximating a bandlimited signal as a multiplication of two or more signals whose total bandwidth is lower than the bandwidth of the original signal. This is a further generalization of the notion of nonlinear anti-aliasing to a broader class of signals, not just non-negative bandlimited signals, which offers a way to optimize the trade off between the sampling rate and the approximation error.

7.3 Inphase and Quadrature Anti-aliasing

A straightforward generalization of anti-aliasing low pass filtering is multi-channel anti-aliasing. In this case, the continuous-time signal is first decomposed in the frequency domain into sub-bands. Each sub-band is then processed according to its frequency content through a frequency selective filter, and the outputs are finally composed to obtain the reduced bandwidth approximation. As a special case, the selective filters can be replaced by multipliers with zero or one depending on the energy of the corresponding sub-band component and the desired bandwidth with which we wish to approximate the signal. The resulting approximation is associated with an error which is proportional to the total energy of the sub-band components that were filtered out. Clearly, the more sub-bands we include in the approximation, the higher its bandwidth is and the lower its corresponding error is.

In this section we introduce a different orthogonal decomposition, which suggests an alternative anti-aliasing method referred to as inphase-quadrature (IQ) anti-aliasing. With this method there is the possibility of reducing the approximation error as compared to the error associated with LTI anti-aliasing filtering. Section 7.3.1 introduces the inphase-quadrature decomposition. In section 7.3.2, we propose an anti-aliasing approach that utilizes the IQ decomposition and discuss its relation to recurrent nonuniform sampling.

7.3.1 Inphase and Quadrature Decomposition

Consider a bandlimited signal $y(t)$ whose frequency response $Y(\Omega)$ contains no component at or above the frequency Ω_c . Defining the inphase and quadrature components of $y(t)$ as

$$i_y(t) = \left(\sqrt{2}/2\right) \cdot \cos(\Omega_c t/2) \cdot y(t) + \left(\sqrt{2}/2\right) \cdot \sin(\Omega_c t/2) \cdot \tilde{y}(t), \quad (7.52a)$$

and

$$q_y(t) = \left(\sqrt{2}/2\right) \cdot \sin(\Omega_c t/2) \cdot y(t) - \left(\sqrt{2}/2\right) \cdot \cos(\Omega_c t/2) \cdot \tilde{y}(t), \quad (7.52b)$$

where $\tilde{y}(t) = 1/\pi \int_{-\infty}^{\infty} y(\tau)/(t - \tau)d\tau$ is the Hilbert transform of $y(t)$, we can decompose $y(t)$ as

$$y(t) = \underbrace{\sqrt{2} \cdot \cos(\Omega_c/2t) \cdot i_y(t)}_{y_1(t)} + \underbrace{\sqrt{2} \cdot \sin(\Omega_c/2t) \cdot q_y(t)}_{y_2(t)}. \quad (7.53)$$

Since $i_y(t)$ and $q_y(t)$ are real valued signals and each is bandlimited with half the bandwidth of $y(t)$, the equivalent representation of $y(t)$ in terms of the signals $i_y(t)$ and $q_y(t)$ has an effective bandwidth equal to the bandwidth of $y(t)$.

We next show that the signals $y_1(t) = \sqrt{2} \cdot \cos(\Omega_c/2t) \cdot i_y(t)$ and $y_2(t) = \sqrt{2} \cdot \sin(\Omega_c/2t) \cdot q_y(t)$ are orthogonal projections of the signal $y(t)$. Orthogonality is shown by proving that the inner product $\langle y_1(t), y_2(t) \rangle = 0$. Specifically,

$$\begin{aligned} \langle y_1(t), y_2(t) \rangle &= \int_{-\infty}^{\infty} y_1(t) \cdot y_2(t) dt = \\ &= \int_{-\infty}^{\infty} \sqrt{2} \cdot \cos(\Omega_c/2t) \cdot i_y(t) \cdot \sqrt{2} \cdot \sin(\Omega_c/2t) \cdot q_y(t) dt, \end{aligned} \quad (7.54)$$

from which it follows by using Parseval's relation

$$\begin{aligned} \langle y_1(t), y_2(t) \rangle &= 2 \cdot \frac{1}{2\pi} \int_{-\infty}^{\infty} \frac{1}{2} [I_y(\Omega + \Omega_c/2) + I_y(\Omega - \Omega_c/2)] \\ &\quad \cdot \frac{1}{2j} [Q_y(\Omega + \Omega_c/2) - Q_y(\Omega - \Omega_c/2)]^* d\Omega \\ &= \frac{1}{4\pi j} \cdot \left\{ \int_{-\infty}^{\infty} I_y(\Omega + \Omega_c/2) \cdot Q_y^*(\Omega + \Omega_c/2) d\Omega \right. \\ &\quad \left. - \int_{-\infty}^{\infty} I_y(\Omega - \Omega_c/2) \cdot Q_y^*(\Omega - \Omega_c/2) d\Omega \right\} = 0. \end{aligned} \quad (7.55)$$

To show that $y_1(t)$ is a projection of $y(t)$, we note that an alternative representation of $y_1(t)$ in terms of $y(t)$ and $\tilde{y}(t)$ can be obtained by using $i_y(t)$ from (7.52a). Specifically,

$$y_1(t) = \frac{1}{2} [y(t) + \cos(\Omega_c t) y(t) + \sin(\Omega_c t) \tilde{y}(t)], \quad (7.56)$$

or in the frequency domain,

$$Y_1(\Omega) = \frac{1}{2} [Y(\Omega) + Y_-(\Omega - \Omega_c) + Y_+(\Omega + \Omega_c)], \quad (7.57)$$

where

$$Y_-(\Omega) = \begin{cases} Y(\Omega) & -\Omega_c < \Omega < 0 \\ 0 & \text{otherwise} \end{cases}, \quad (7.58)$$

and

$$Y_+(\Omega) = \begin{cases} Y(\Omega) & 0 < \Omega < \Omega_c \\ 0 & \text{otherwise} \end{cases}. \quad (7.59)$$

Then, denoting by $f_1(\cdot)$ the linear transformation from $Y(\Omega)$ to $Y_1(\Omega)$ in (7.57) and applying $f_1(\cdot)$ again on $Y_1(\Omega)$, we obtain $f_1(Y_1(\Omega)) = Y_1(\Omega)$, from which it follows that $y_1(t)$ is an orthogonal projection of $y(t)$. Similar to the representation in (7.57), it is straightforward to show that the Fourier transform $Y_2(\Omega)$ of $y_2(t)$ obeys

$$Y_2(\Omega) = \frac{1}{2} [Y(\Omega) - Y_-(\Omega - \Omega_c) - Y_+(\Omega + \Omega_c)], \quad (7.60)$$

and that $y_2(t)$ is an orthogonal projection of $y(t)$. Figure 7-9 illustrates the decomposition of $Y(\Omega)$ into $Y_1(\Omega)$ and $Y_2(\Omega)$, as implied from (7.57) and (7.60).

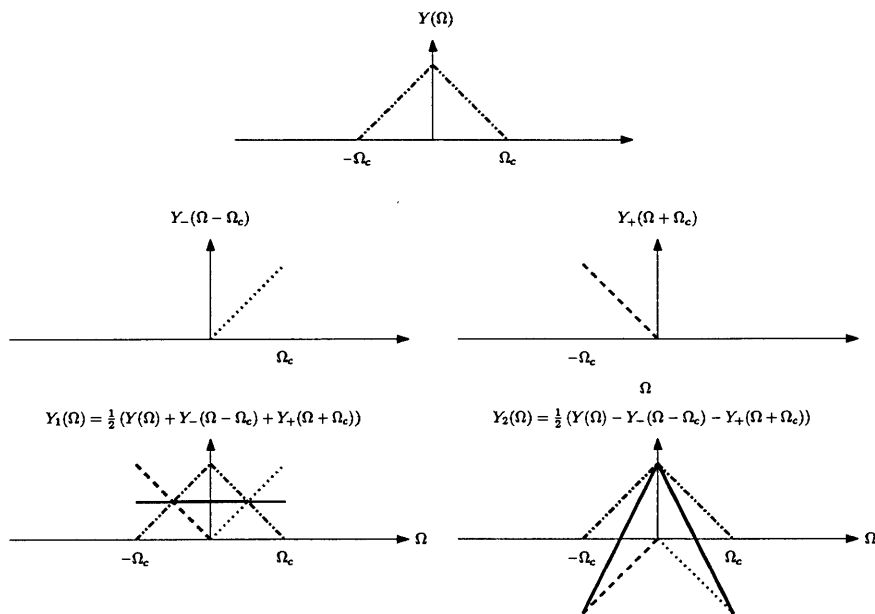


Figure 7-9: Decomposing $Y(\Omega)$ into $Y_1(\Omega)$ and $Y_2(\Omega)$.

The orthogonality in (7.55) between $y_1(t)$ and $y_2(t)$ implies that the energy $E_y = \int_{-\infty}^{\infty} y^2(t) dt$ of $y(t)$ is equal to the sum of the energies E_1 of $y_1(t)$ and E_2 of $y_2(t)$. Using Parseval's relation, it can also be shown that $E_1 = E_i$ and $E_2 = E_q$. Specifically,

$$\begin{aligned} E_1 &= \int_{-\infty}^{\infty} y_1^2(t) dt = \int_{-\infty}^{\infty} \left(i_y(t) \cdot \sqrt{2} \cdot \cos(\Omega_c/2t) \right)^2 dt \\ &= \frac{1}{2} \cdot \frac{1}{2\pi} \int_{-\infty}^{\infty} |I_y(\Omega + \Omega_c/2) + I_y(\Omega - \Omega_c/2)|^2 d\Omega \\ &= \int_{-\infty}^{\infty} i_y^2(t) dt = E_i, \end{aligned} \quad (7.61a)$$

and

$$\begin{aligned} E_2 &= \int_{-\infty}^{\infty} y_2^2(t) dt = \int_{-\infty}^{\infty} \left(q_y(t) \cdot \sqrt{2} \cdot \sin(\Omega_c/2t) \right)^2 dt \\ &= \frac{1}{2} \cdot \frac{1}{2\pi} \int_{-\infty}^{\infty} \left| \frac{1}{j} Q_y(\Omega + \Omega_c) - \frac{1}{j} Q_y(\Omega - \Omega_c) \right|^2 d\Omega \\ &= \int_{-\infty}^{\infty} q_y^2(t) dt = E_q. \end{aligned} \quad (7.61b)$$

Note, however, that the energy E_y of $y(t)$ is not equally distributed between $y_1(t)$ and $y_2(t)$, or alternatively between $i_y(t)$ and $q_y(t)$. Specifically,

$$\begin{aligned} E_1 &= \frac{1}{2} \cdot E_y + \Re \left\{ \frac{1}{2\pi} \int_0^{\Omega_c} Y(\Omega) \cdot Y^*(\Omega - \Omega_c) d\Omega \right\}, \\ E_2 &= \frac{1}{2} \cdot E_y - \Re \left\{ \frac{1}{2\pi} \int_0^{\Omega_c} Y(\Omega) \cdot Y^*(\Omega - \Omega_c) d\Omega \right\}, \end{aligned} \quad (7.62)$$

as follows from (7.57) and (7.60). This property will be exploited in the next section in which we discuss approximation of $y(t)$ in terms of its IQ components.

7.3.2 IQ Anti-aliasing

As an alternative approach to LTI anti-aliasing, the IQ decomposition suggests decomposing the bandlimited signal $y(t)$ into $i_y(t)$ and $q_y(t)$ and then processing these components through LTI selective filters to yield the approximations $\hat{i}_y(t)$ and $\hat{q}_y(t)$ from which we

obtain

$$\hat{y}(t) = \sqrt{2} \cdot \cos(\Omega_c/2t) \cdot \hat{i}_y(t) + \sqrt{2} \cdot \sin(\Omega_c/2t) \cdot \hat{q}_y(t), \quad (7.63)$$

whose effective bandwidth is reduced as compared to that of $y(t)$. Denoting $e_y(t) = y(t) - \hat{y}(t)$ as the error in approximating $y(t)$ with $\hat{y}(t)$, it can be shown by using Parseval's relation that

$$\int_{-\infty}^{\infty} e_y^2(t) dt = \int_{-\infty}^{\infty} e_i^2(t) dt + \int_{-\infty}^{\infty} e_q^2(t) dt, \quad (7.64)$$

where $e_i(t)$ and $e_q(t)$ are the errors corresponding to approximating $i_y(t)$ with $\hat{i}_y(t)$ and $q_y(t)$ with $\hat{q}_y(t)$, respectively. As follows from (7.64), the approximation of $y(t)$ specified in (7.63) is improved as the individual approximations of $i_y(t)$ and $q_y(t)$ are improved.

The orthogonal decomposition in (7.53) can be iteratively applied to the resulting IQ components so that after N iterations the original signal $y(t)$ will be decomposed into 2^N real components, each is bandlimited with a bandwidth which is $1/2^N$ times the bandwidth of the original signal. Figure 7-10 illustrates the decomposition obtained after two iterations, i.e., when $N = 2$.

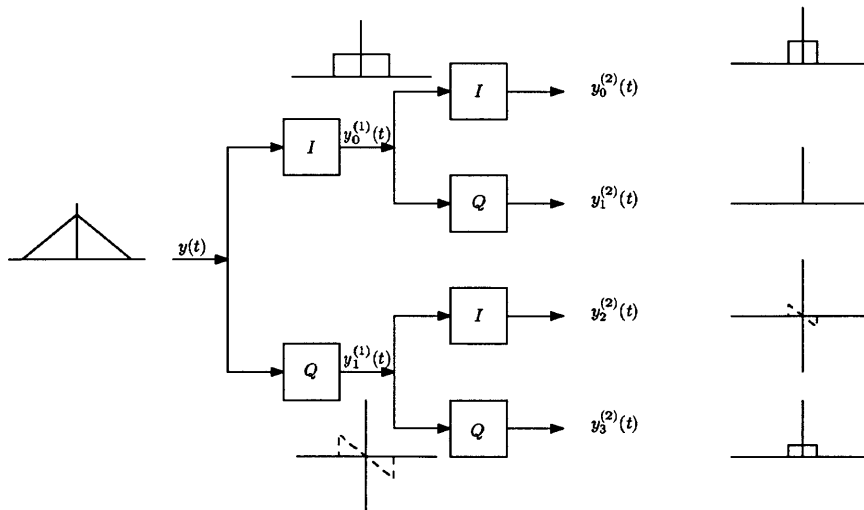


Figure 7-10: Iterative decomposition of $y(t)$ into its inphase and quadrature components after two iterations ($N = 2$).

Clearly, perfect reconstruction of the original signal can be obtained if all IQ components are used. However, if the desired sampling rate is lower than the Nyquist rate of $y(t)$, a reduced bandwidth approximation of the signal is of interest. Reducing the signal's bandwidth can be accomplished by processing the IQ components of the signal through LTI selective filters, or simply by choosing a subset of IQ components for the approximate representation. To minimize the least squares approximation error, the subset should be chosen to contain the components with the highest energy. The approximation $\hat{y}(t)$ obtained from these components will be associated with an error whose energy is equal to the total energy of the IQ components that were filtered out. Since all components have the same bandwidth, which is $1/2^N$ times the bandwidth of $y(t)$, the effective bandwidth of the approximation will be proportional to the number of components used to obtain it.

Figure 7-11 illustrates the two approaches, LTI and IQ anti-aliasing, for approximating a bandlimited signal whose spectrum is triangular with another bandlimited signal with reduced effective bandwidth. As indicated, when the bandwidth of the approximated signal is constrained to 0.3 the bandwidth of the original signal, LTI anti-aliasing filtering achieves poor results as compared to the IQ-based approximation. Specifically, while LTI anti-aliasing achieves zero error in the pass-band region and large error in the stop-band region, the error associated with the IQ-based anti-aliasing is equally spread over the entire spectrum of the signal and its energy is lower. Note also that the effective bandwidth of

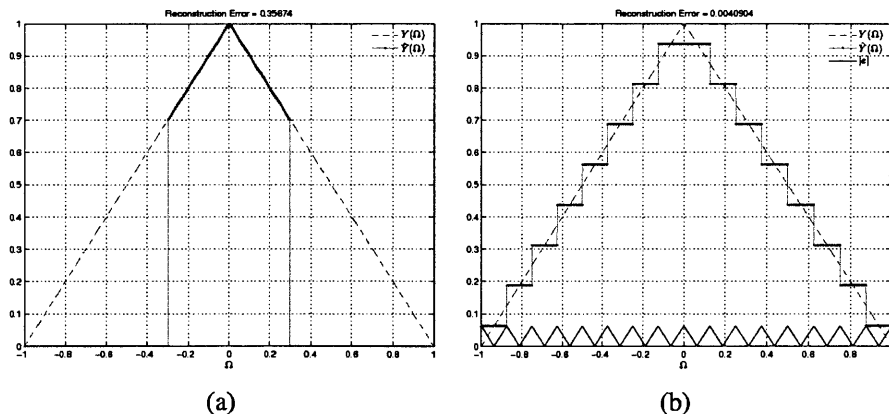


Figure 7-11: A comparison between LTI anti-aliasing filtering and IQ anti-aliasing applied to a signal whose spectrum is triangular to reduce its bandwidth to 0.3 times its original bandwidth. (a) LTI anti-aliasing (original signal dashed). (b) IQ anti-aliasing with $N = 4$ iterations (original signal dashed).

the approximation in both methods is the same; however, the actual bandwidth of the approximation obtained with LTI anti-aliasing filtering is the same as the desired bandwidth, whereas the actual bandwidth of the approximation obtained with IQ anti-aliasing is as large as the bandwidth of the original signal. This is significant in scenarios for which all spectrum regions are equally important and we would rather avoid the use of LTI anti-aliasing filtering, which completely removes components outside its pass-band region. The IQ anti-aliasing method provides us with a way that trades off accuracy in the pass-band with accuracy in the stop-band of the corresponding LTI anti-aliasing filter.

7.3.2.1 IQ Anti-aliasing and Recurrent Nonuniform Sampling

Eqs. (7.57) and (7.60) suggest that the signals $y_1(t)$ and $y_2(t)$ can be obtained as the outputs of the system in Figure 7-12, which consists of sub-Nyquist sampling of $y(t)$ followed by lowpass filtering.

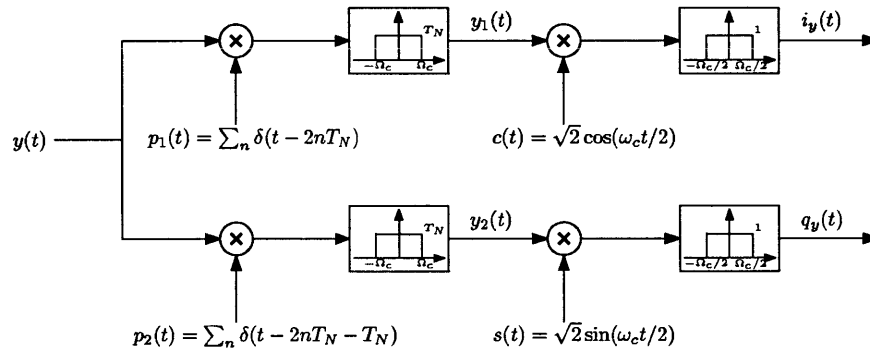


Figure 7-12: Generating $y_1(t)$ and $y_2(t)$ through sub-Nyquist sampling of $y(t)$ followed by lowpass filtering. The Nyquist interval $T_N = \pi/\Omega_c$.

The decomposition of $y(t)$ into its IQ components can be interpreted as a decomposition of a signal into two signals; one which depends only on the odd Nyquist rate samples of $y(t)$ and another which depends only on the even Nyquist rate samples of $y(t)$. Since the IQ anti-aliasing method produces the reduced bandwidth approximation by iteratively decomposing $y(t)$ into its IQ components and eliminating some of them, this method can be shown to correspond in the time-domain to sampling $y(t)$ on a recurrent nonuniform grid.

7.4 Co-sampling

In this section we explore sampling in a multi-input environment and exploit dependencies between signals to reduce their overall sampling rate. Without loss of generality, we will consider here the case of two inputs $y_1(t)$ and $y_2(t)$. The input signals are assumed to be correlated and to satisfy the following set of equations:

$$\begin{aligned} y_1(t) &= h_{11}(t) * x_1(t) + h_{12}(t) * x_2(t), \\ y_2(t) &= h_{22}(t) * x_2(t) + h_{21}(t) * x_1(t), \end{aligned} \quad (7.65)$$

where $x_1(t)$ and $x_2(t)$ are bandlimited to Ω_1 and Ω_2 , respectively, and $\Omega_1 < \Omega_2$. The multi-channel model of eq. (7.65) is shown in Figure 7-13 where $H_{11}(\Omega)$, $H_{12}(\Omega)$, $H_{21}(\Omega)$, $H_{22}(\Omega)$ represent the frequency responses of the LTI systems whose impulse responses are $h_{11}(t)$, $h_{12}(t)$, $h_{21}(t)$, and $h_{22}(t)$, respectively.

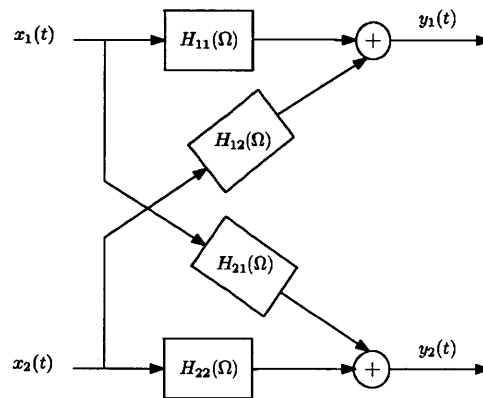


Figure 7-13: The multi-channel model.

According to the Nyquist-Shannon sampling theorem, perfect reconstruction of each of the signals $y_1(t)$ and $y_2(t)$ can be obtained from their corresponding equally-spaced Nyquist rate samples. However, the bandwidth of both signals $y_1(t)$ and $y_2(t)$ is in general the largest bandwidth of $x_1(t)$ and $x_2(t)$. Thus, alias-free reconstruction of $y_1(t)$ and $y_2(t)$ is possible if each is sampled at a rate which meets or exceeds the Nyquist rate $2\Omega_2$.

Utilizing the dependence between $y_1(t)$ and $y_2(t)$, as implied from (7.65), the signals $x_1(t)$ and $x_2(t)$ can be extracted and sampled at their corresponding Nyquist rates. This approach will enable us to reduce the overall sampling rate from $2(\Omega_1 + \Omega_2)$ to $2(\Omega_1 +$

Ω_2). However, each signal will be sampled at a different rate corresponding to its Nyquist rate. There are some advantages in sampling the signals at the same rate. For example, if time-division multiplexing (TDM) of the samples is of interest, the fact that each sequence corresponds to a different sampling rate makes the multiplexing difficult.

The signals $y_1(t)$ and $y_2(t)$ can be alternatively sampled at a unified rate equal to half the average Nyquist rate of $x_1(t)$ and $x_2(t)$, i.e., $\Omega_s = \frac{2\pi}{T_s} = \Omega_1 + \Omega_2$, in which case aliasing will be in general introduced in both channels. This aliasing will be referred to as co-aliasing. As we next show, the co-aliasing can be removed and the signals can be perfectly reconstructed from those samples. With this approach, we reduce the sampling rate of one signal at the expense of increasing the sampling rate of the other, thus achieving the lowest possible overall sampling rate for which perfect reconstruction is possible.

7.4.1 Perfect Reconstruction

For the reconstruction of the signals $x_1(t)$ and $x_2(t)$ from uniform samples of $y_1(t)$ and $y_2(t)$ at half the average Nyquist rate of $x_1(t)$ and $x_2(t)$, i.e., $\Omega_s = \Omega_1 + \Omega_2$, we consider the following multi-channel system

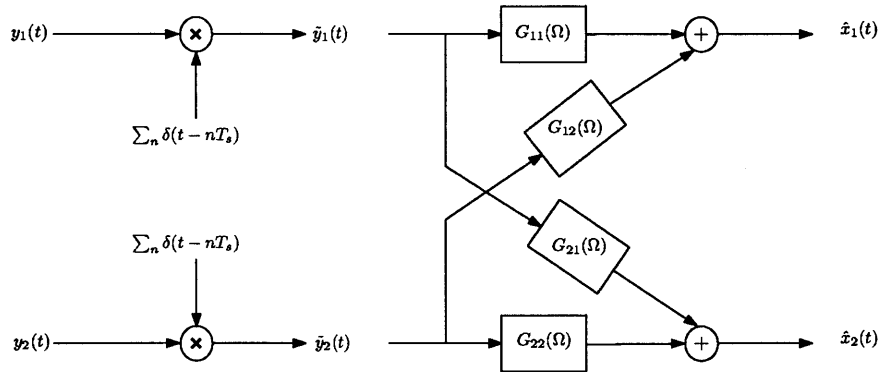


Figure 7-14: Reconstruction of $x_1(t)$ and $x_2(t)$ from uniform samples of $y_1(t)$ and $y_2(t)$.

The Fourier transforms of the outputs $\hat{x}_1(t)$ and $\hat{x}_2(t)$ of the reconstruction system of Figure 7-14 are given by

$$\begin{aligned}\hat{X}_1(\Omega) &= G_{11}(\Omega) \cdot \tilde{Y}_1(\Omega) + G_{12}(\Omega) \cdot \tilde{Y}_2(\Omega), \\ \hat{X}_2(\Omega) &= G_{21}(\Omega) \cdot \tilde{Y}_1(\Omega) + G_{22}(\Omega) \cdot \tilde{Y}_2(\Omega),\end{aligned}\tag{7.66}$$

where $G_{11}(\Omega)$, $G_{12}(\Omega)$, $G_{21}(\Omega)$ and $G_{22}(\Omega)$ are the frequency responses of the LTI reconstruction filters, and $\tilde{Y}_1(\Omega)$ and $\tilde{Y}_2(\Omega)$ represent the Fourier transforms of $\tilde{y}_1(t)$ and $\tilde{y}_2(t)$, which are periodic and given by

$$\begin{aligned}\tilde{Y}_1(\Omega) &= \frac{1}{T_s} [X_1(\Omega) \cdot H_{11}(\Omega) + X_2(\Omega) \cdot H_{12}(\Omega) \\ &+ X_2(\Omega - \Omega_s)H_{12}(\Omega - \Omega_s) + X_2(\Omega + \Omega_s)H_{12}(\Omega + \Omega_s)] \quad |\Omega| < \Omega_s, \quad (7.67)\end{aligned}$$

and

$$\begin{aligned}\tilde{Y}_2(\Omega) &= \frac{1}{T_s} [X_1(\Omega) \cdot H_{21}(\Omega) + X_2(\Omega) \cdot H_{22}(\Omega) \\ &+ X_2(\Omega - \Omega_s)H_{22}(\Omega - \Omega_s) + X_2(\Omega + \Omega_s)H_{22}(\Omega + \Omega_s)] \quad |\Omega| < \Omega_s. \quad (7.68)\end{aligned}$$

Designing the reconstruction filters $G_{11}(\Omega)$, $G_{12}(\Omega)$, $G_{21}(\Omega)$ and $G_{22}(\Omega)$ in the system of Figure 7-14 to cancel the co-aliasing in $\tilde{Y}_1(\Omega)$ and in $\tilde{Y}_2(\Omega)$, and to obtain $\hat{X}_1(\Omega) = X_1(\Omega)$ and $\hat{X}_2(\Omega) = X_2(\Omega)$, results in

$$\begin{bmatrix} G_{11}(\Omega) \\ G_{12}(\Omega) \end{bmatrix} = \begin{bmatrix} H_{11}(\Omega) & H_{21}(\Omega) \\ H_{12}(\Omega) & H_{22}(\Omega) \end{bmatrix}^{-1} \cdot \begin{bmatrix} T_s \\ 0 \end{bmatrix} \quad |\Omega| < \Omega_1, \quad (7.69a)$$

and

$$\begin{aligned}\begin{bmatrix} G_{21}(\Omega) \\ G_{22}(\Omega) \end{bmatrix} &= \begin{bmatrix} H_{11}(\Omega) & H_{21}(\Omega) \\ H_{12}(\Omega) & H_{22}(\Omega) \end{bmatrix}^{-1} \cdot \begin{bmatrix} 0 \\ T_s \end{bmatrix} \quad |\Omega| < \Omega_1 & (7.69b) \\ \begin{bmatrix} G_{21}(\Omega) \\ G_{22}(\Omega) \end{bmatrix} &= \begin{bmatrix} H_{12}(\Omega) & H_{22}(\Omega) \\ H_{12}(\Omega - \Omega_s) & H_{22}(\Omega - \Omega_s) \end{bmatrix}^{-1} \cdot \begin{bmatrix} T_s \\ 0 \end{bmatrix} & \Omega_1 < \Omega < \Omega_2, \\ \begin{bmatrix} G_{21}(\Omega) \\ G_{22}(\Omega) \end{bmatrix} &= \begin{bmatrix} H_{12}(\Omega) & H_{22}(\Omega) \\ H_{12}(\Omega + \Omega_s) & H_{22}(\Omega + \Omega_s) \end{bmatrix}^{-1} \cdot \begin{bmatrix} T_s \\ 0 \end{bmatrix} & -\Omega_2 < \Omega < -\Omega_1,\end{aligned}$$

provided that the inverses involved exist. To reconstruct $y_1(t)$ and $y_2(t)$, we process $\hat{x}_1(t)$

and $\hat{x}_2(t)$ through the multi-channel system of Figure 7-13, i.e.,

$$\begin{aligned}\hat{y}_1(t) &= h_{11}(t) * \hat{x}_1(t) + h_{12}(t) * \hat{x}_2(t), \\ \hat{y}_2(t) &= h_{22}(t) * \hat{x}_2(t) + h_{21}(t) * \hat{x}_1(t).\end{aligned}\tag{7.70}$$

Sampling rate reduction is possible with this approach due to the dependency between the signals and the knowledge of the exact model they satisfy, as specified in (7.65). In section 7.4.2 we discuss the case in which the model for generating the signals $y_1(t)$ and $y_2(t)$ is not fully specified and only partial information is available.

7.4.2 Blind Co-sampling

We now assume that the signals $y_1(t)$ and $y_2(t)$ were generated according to the model

$$\begin{aligned}y_1(t) &= x_1(t) + \sum_{l=0}^{L-1} a_l \cdot x_2(t - \tau_l), \\ y_2(t) &= x_2(t),\end{aligned}\tag{7.71}$$

where $\{a_l, \tau_l\}$ are unknown parameters. This model corresponds to the model in eq. (7.65) where $h_{11}(t) = h_{22}(t) = \delta(t)$, $h_{21}(t) = 0$, and

$$h_{12}(t) = \sum_{l=0}^{L-1} a_l \cdot \delta(t - \tau_l) \triangleq h(t).\tag{7.72}$$

Extracting the signals $x_1(t)$ and $x_2(t)$ from $y_1(t)$ and $y_2(t)$ requires the knowledge of $\{a_l, \tau_l\}_{l=0}^{L-1}$. If these parameters are not known, blind separation techniques may be incorporated prior to sampling to extract these signals. Alternatively, the signals $y_1(t)$ and $y_2(t)$ can be sampled at a unified rate equal to half the average Nyquist rate of $x_1(t)$ and $x_2(t)$, in which case $x_1(t)$ and $x_2(t)$ will be extracted in reconstruction. To extract the signals, we use the reconstruction system of Figure 7-14 whose reconstruction filters are obtained from eqs. (7.69) where $H_{11}(\Omega) = H_{22}(\Omega) = 1$, $H_{21}(\Omega) = 0$, and

$$H_{12}(\Omega) = \sum_{l=0}^{L-1} \hat{a}_l \cdot e^{j\Omega\tau_l} \triangleq \hat{H}(\Omega),\tag{7.73}$$

where $\hat{H}(\Omega)$ is an estimate of $H(\Omega)$. In that case, the Fourier transforms of the outputs $\hat{x}_1(t)$ and $\hat{x}_2(t)$ of the reconstruction system are

$$\hat{X}_1(\Omega) = T_s \cdot (\tilde{Y}_1(\Omega) - \hat{H}(\Omega) \cdot \tilde{Y}_2(\Omega)) \quad |\Omega| < \Omega_1, \quad (7.74)$$

and

$$\hat{X}_2(\Omega) = \begin{cases} T_s \cdot \frac{(\tilde{Y}_1(\Omega) - \hat{H}(\Omega + \Omega_s) \cdot \tilde{Y}_2(\Omega))}{(\hat{H}(\Omega) - \hat{H}(\Omega + \Omega_s))} & -\Omega_2 < \Omega < -\Omega_1, \\ T_s \cdot \tilde{Y}_2(\Omega) & |\Omega| < \Omega_1 \\ T_s \cdot \frac{(\tilde{Y}_1(\Omega) - \hat{H}(\Omega - \Omega_s) \cdot \tilde{Y}_2(\Omega))}{(\hat{H}(\Omega) - \hat{H}(\Omega - \Omega_s))} & \Omega_1 < \Omega < \Omega_2. \end{cases} \quad (7.75)$$

Substituting (7.67) and (7.68) into (7.74) and (7.75), we obtain

$$\hat{X}_1(\Omega) = X_1(\Omega) + (H(\Omega) - \hat{H}(\Omega)) X_2(\Omega), \quad |\Omega| < \Omega_1, \quad (7.76)$$

and

$$\hat{X}_2(\Omega) = \begin{cases} X_2(\Omega) \cdot \frac{(H(\Omega) - \hat{H}(\Omega + \Omega_s))}{(\hat{H}(\Omega) - \hat{H}(\Omega + \Omega_s))} + X_2(\Omega + \Omega_s) \cdot \frac{(H(\Omega + \Omega_s) - \hat{H}(\Omega + \Omega_s))}{(\hat{H}(\Omega) - \hat{H}(\Omega + \Omega_s))} & -\Omega_2 < \Omega < -\Omega_1, \\ X_2(\Omega) & |\Omega| < \Omega_1, \\ X_2(\Omega) \cdot \frac{(H(\Omega) - \hat{H}(\Omega - \Omega_s))}{(\hat{H}(\Omega) - \hat{H}(\Omega - \Omega_s))} + X_2(\Omega - \Omega_s) \cdot \frac{(H(\Omega - \Omega_s) - \hat{H}(\Omega - \Omega_s))}{(\hat{H}(\Omega) - \hat{H}(\Omega - \Omega_s))} & \Omega_1 < \Omega < \Omega_2. \end{cases} \quad (7.77)$$

As expected, when $H(\Omega)$ is known, eqs. (7.76) and (7.77) with $\hat{H}(\Omega) = H(\Omega)$ achieve perfect reconstruction of $x_1(t)$ and $x_2(t)$. Otherwise, assuming that $x_1(t)$ and $x_2(t)$ are orthogonal and choosing \hat{a}_l and \hat{t}_l in $\hat{H}(\Omega)$ to minimize the average power of $\hat{x}_1(t)$ will yield an estimate of $H(\Omega)$, which can be used in $\hat{X}_1(\Omega)$ and $\hat{X}_2(\Omega)$. There is a variety of other methods to estimate these unknown parameters one of which is to decorrelate $\hat{x}_1(t)$ and $\hat{x}_2(t)$.

Appendices

APPENDIX A

OPTIMAL CONSTRAINED RECONSTRUCTION FILTERS

To find the filters $G_m(e^{j\omega})$ which minimize σ_ε^2 in (2.24) under the constraints in (2.8), we use the Lagrange multipliers, where the Lagrangian is defined as

$$L = \sum_{m=0}^{M-1} \sigma_m^2 \cdot |G_m(e^{j\omega})|^2 + \sum_{k=-i}^{L-1-i} \lambda_k^{(i)} \cdot \left(\sum_{m=0}^{M-1} G_m(e^{j\omega}) e^{-j(\omega - \frac{2\pi}{L}k) \frac{\tau_m}{T_N}} - L \cdot \delta[k] \right) \quad \omega \in \Delta\omega_i, \quad i = 0, 1, \dots, L-1. \quad (\text{A-1})$$

Differentiating (A-1) with respect to $G_m^R(e^{j\omega}) = \Re(G_m(e^{j\omega}))$ and $G_m^I(e^{j\omega}) = \Im(G_m(e^{j\omega}))$, we obtain

$$\begin{aligned} \frac{\partial L}{\partial G_m^R(e^{j\omega})} &= 2\sigma_m^2 G_m^R(e^{j\omega}) + \sum_{k=-i}^{L-1-i} \Re(\lambda_k^{(i)}) \cdot \Re\left(e^{-j(\omega - \frac{2\pi}{L}k) \frac{\tau_m}{T_N}}\right) + \Im(\lambda_k^{(i)}) \cdot \Im\left(e^{-j(\omega - \frac{2\pi}{L}k) \frac{\tau_m}{T_N}}\right) \\ \frac{\partial L}{\partial G_m^I(e^{j\omega})} &= 2\sigma_m^2 G_m^I(e^{j\omega}) + \sum_{k=-i}^{L-1-i} -\Re(\lambda_k^{(i)}) \cdot \Im\left(e^{-j(\omega - \frac{2\pi}{L}k) \frac{\tau_m}{T_N}}\right) + \Im(\lambda_k^{(i)}) \cdot \Re\left(e^{-j(\omega - \frac{2\pi}{L}k) \frac{\tau_m}{T_N}}\right), \end{aligned} \quad \omega \in \Delta\omega_i, \quad m = 0, 1, \dots, M-1. \quad (\text{A-2})$$

Solving (A-2) for $G_m(e^{j\omega})$ results in

$$G_m(e^{j\omega}) = 1/\sigma_m^2 \cdot e^{j\omega\tau_m/T_N} \left(\sum_{l=-i}^{L-1-i} \lambda_l^{(i)} \cdot e^{-j2\pi(\tau_m/LT_N)l} \right) \quad \omega \in \Delta\omega_i, \quad i = 0, 1, \dots, L-1, \quad m = 0, 1, \dots, M-1, \quad (\text{A-3})$$

where the values of $\lambda_l^{(i)}$ are determined by the constraints in (2.8), i.e.,

$$\sum_{k=-i}^{L-1-i} \lambda_k^{(i)} \cdot \sum_{m=0}^{M-1} 1/\sigma_m^2 \cdot e^{-j\frac{2\pi}{L}(k-p)\frac{m}{N}} = L \cdot \delta[p] \quad p = -i, -i+1, \dots, L-1-i, \quad i = 0, 1, \dots, L-1. \quad (\text{A-4})$$

APPENDIX B

DERIVATION OF $S_{ee}(e^{j\omega})$

The autocorrelation function of $e_x[n]$ is given by

$$R_{e_x e_x}[n, n-l] = E \left\{ \left(\sum_{m_1=0}^{M-1} \sum_{k_1=-\infty}^{\infty} x_{m_1}[k_1] g_{m_1}[n - k_1 L] - x[n] \right) \cdot \left(\sum_{m_2=0}^{M-1} \sum_{k_2=-\infty}^{\infty} x_{m_2}[k_2] g_{m_2}[n-l - k_2 L] - x[n-l] \right) \right\}. \quad (\text{B-1})$$

To compute the first term in (B-1), we first compute

$$\begin{aligned} E(x_{m_1}[k_1] x_{m_2}[k_2]) &= E(x(k_1 L T_N - \tau_{m_1}) x(k_2 L T_N - \tau_{m_2})) \\ &= R_{xx}((k_1 - k_2) L T_N - \tau_{m_1} + \tau_{m_2}) \\ &= \frac{1}{2\pi} \int_{-\Omega_c}^{\Omega_c} S_{xx}(\Omega) e^{j\Omega[(k_1 - k_2) L T_N - \tau_{m_1} + \tau_{m_2}]} d\Omega, \end{aligned} \quad (\text{B-2})$$

from which it follows

$$\begin{aligned} & E \left\{ \sum_{m_1=0}^{M-1} \sum_{k_1=-\infty}^{\infty} x_{m_1}[k_1] g_{m_1}[n - k_1 L] \cdot \sum_{m_2=0}^{M-1} \sum_{k_2=-\infty}^{\infty} x_{m_2}[k_2] g_{m_2}[n-l - k_2 L] \right\} \\ &= \sum_{m_1=0}^{M-1} \sum_{k_1=-\infty}^{\infty} \sum_{m_2=0}^{M-1} \sum_{k_2=-\infty}^{\infty} g_{m_1}[n - k_1 L] g_{m_2}[n-l - k_2 L] E(x_{m_1}[k_1] x_{m_2}[k_2]) \\ &= \frac{1}{2\pi} \int_{-\Omega_c}^{\Omega_c} S_{xx}(\Omega) \left[\sum_{m_1=0}^{M-1} e^{-j\Omega \tau_{m_1}} \left(\sum_{k_1=-\infty}^{\infty} g_{m_1}[n - k_1 L] e^{j\Omega k_1 L T_N} \right) \right] \\ & \quad \cdot \left[\sum_{m_2=0}^{M-1} e^{j\Omega \tau_{m_2}} \left(\sum_{k_2=-\infty}^{\infty} g_{m_2}[n-l - k_2 L] e^{-j\Omega k_2 L T_N} \right) \right] d\Omega. \end{aligned} \quad (\text{B-3})$$

Note also that

$$\begin{aligned}
\sum_{k_1=-\infty}^{\infty} g_{m_1}[n-k_1L]e^{j\Omega k_1LT_N} &= \sum_{k_1=-\infty}^{\infty} \frac{1}{2\pi} \int_{-\pi}^{\pi} G_{m_1}(e^{j\omega})e^{j\omega(n-k_1L)}d\omega e^{j\Omega k_1LT_N} \\
&= \frac{1}{2\pi} \int_{-\pi}^{\pi} G_{m_1}(e^{j\omega}) \underbrace{\left(\sum_{k_1=-\infty}^{\infty} e^{j(\Omega T_N - \omega)k_1L} \right)}_{\frac{2\pi}{L} \sum_{k_1=-\infty}^{\infty} \delta(\Omega T_N - \omega - \frac{2\pi}{L}k_1)} e^{j\omega n} d\omega \\
&= \frac{1}{L} \sum_{k_1} G_{m_1}\left(e^{j(\Omega T_N - \frac{2\pi}{L}k_1)}\right) e^{j(\Omega T_N - \frac{2\pi}{L}k_1)n}, \quad k_1: \left| \Omega T_N - \frac{2\pi}{L}k_1 \right| \leq \pi
\end{aligned} \tag{B-4}$$

and

$$\begin{aligned}
\sum_{k_2=-\infty}^{\infty} g_{m_2}[n-l-k_2L]e^{-j\Omega k_2LT_N} &= \sum_{k_2=-\infty}^{\infty} \frac{1}{2\pi} \int_{-\pi}^{\pi} G_{m_2}^*(e^{j\omega})e^{-j\omega(n-l-k_2L)}d\omega e^{-j\Omega k_2LT_N} \\
&= \frac{1}{2\pi} \int_{-\pi}^{\pi} G_{m_2}^*(e^{j\omega}) \underbrace{\left(\sum_{k_2=-\infty}^{\infty} e^{-j(\Omega T_N - \omega)k_2L} \right)}_{\frac{2\pi}{L} \sum_{k_2=-\infty}^{\infty} \delta(\Omega T_N - \omega - \frac{2\pi}{L}k_2)} e^{-j\omega(n-l)} d\omega \\
&= \frac{1}{L} \sum_{k_2} G_{m_2}^*\left(e^{j(\Omega T_N - \frac{2\pi}{L}k_2)}\right) e^{-j(\Omega T_N - \frac{2\pi}{L}k_2)(n-l)}, \\
&\quad k_2: \left| \Omega T_N - \frac{2\pi}{L}k_2 \right| \leq \pi
\end{aligned} \tag{B-5}$$

Thus,

$$\begin{aligned}
&E \left\{ \sum_{m_1=0}^{M-1} \sum_{k_1=-\infty}^{\infty} x_{m_1}[k_1]g_{m_1}[n-k_1L] \cdot \sum_{m_2=0}^{M-1} \sum_{k_2=-\infty}^{\infty} x_{m_2}[k_2]g_{m_2}[n-l-k_2L] \right\} \\
&= \frac{1}{2\pi} \int_{-\Omega_c}^{\Omega_c} S_{xx}(\Omega) \left[\sum_{m_1=0}^{M-1} e^{-j\Omega \tau_{m_1}} \frac{1}{L} \sum_{k_1} G_{m_1}\left(e^{j(\Omega T_N - \frac{2\pi}{L}k_1)}\right) e^{j(\Omega T_N - \frac{2\pi}{L}k_1)n} \right] \\
&\quad \cdot \left[\sum_{m_2=0}^{M-1} e^{j\Omega \tau_{m_2}} \frac{1}{L} \sum_{k_2} G_{m_2}^*\left(e^{j(\Omega T_N - \frac{2\pi}{L}k_2)}\right) e^{-j(\Omega T_N - \frac{2\pi}{L}k_2)(n-l)} \right] d\Omega \\
&= \frac{1}{2\pi} \int_{-\Omega_c}^{\Omega_c} S_{xx}(\Omega) \left[\sum_{m_1=0}^{M-1} e^{-j\Omega \tau_{m_1}} \frac{1}{L} \sum_{k_1} G_{m_1}\left(e^{j(\Omega T_N - \frac{2\pi}{L}k_1)}\right) e^{-j\frac{2\pi}{L}k_1 n} \right] \\
&\quad \cdot \left[\sum_{m_2=0}^{M-1} e^{j\Omega \tau_{m_2}} \frac{1}{L} \sum_{k_2} G_{m_2}^*\left(e^{j(\Omega T_N - \frac{2\pi}{L}k_2)}\right) e^{j\frac{2\pi}{L}k_2(n-l)} \right] e^{j\Omega T_N l} d\Omega
\end{aligned} \tag{B-6}$$

To compute the second term of (B-1), we first note that

$$\begin{aligned}
E \{x_{m_1}[k_1]x[n-l]\} &= E(x(k_1LT_N - \tau_{m_1})x((n-l)T_N)) \\
&= R_{xx}((k_1L - n + l)T_N - \tau_{m_1}) = \frac{1}{2\pi} \int_{-\Omega_c}^{\Omega_c} S_{xx}(\Omega) e^{j\Omega((k_1L - n + l)T_N - \tau_{m_1})} d\Omega.
\end{aligned} \tag{B-7}$$

Therefore,

$$\begin{aligned}
&\sum_{m_1=0}^{M-1} \sum_{k_1=-\infty}^{\infty} E \{x_{m_1}[k_1]x[n-l]\} g_{m_1}[n - k_1L] \\
&\sum_{m_1=0}^{M-1} \sum_{k_1=-\infty}^{\infty} \frac{1}{2\pi} \int_{-\Omega_c}^{\Omega_c} S_{xx}(\Omega) e^{j\Omega((k_1L - n + l)T_N - \tau_{m_1})} d\Omega g_{m_1}[n - k_1L] \\
&= \sum_{m_1=0}^{M-1} \frac{1}{2\pi} \int_{-\Omega_c}^{\Omega_c} S_{xx}(\Omega) e^{j\Omega((l-n)T_N - \tau_{m_1})} \left(\sum_{k_1=-\infty}^{\infty} g_{m_1}[n - k_1L] e^{j\Omega k_1LT_N} \right) d\Omega.
\end{aligned} \tag{B-8}$$

Using (B-4) in (B-8), we obtain

$$\begin{aligned}
&\sum_{m_1=0}^{M-1} \sum_{k_1=-\infty}^{\infty} E \{x_{m_1}[k_1]x[n-l]\} g_{m_1}[n - k_1L] \\
&= \sum_{m_1=0}^{M-1} \frac{1}{2\pi} \int_{-\Omega_c}^{\Omega_c} S_{xx}(\Omega) e^{j\Omega((l-n)T_N - \tau_{m_1})} \left(\frac{1}{L} \sum_{k_1} G_{m_1}(e^{j(\Omega T_N - \frac{2\pi}{L}k_1)}) e^{j(\Omega T_N - \frac{2\pi}{L}k_1)n} \right) d\Omega \\
&= \frac{1}{2\pi} \int_{-\Omega_c}^{\Omega_c} S_{xx}(\Omega) e^{j\Omega l T_N} \sum_{m_1=0}^{M-1} e^{-j\Omega \tau_{m_1}} \left(\frac{1}{L} \sum_{k_1} G_{m_1}(e^{j(\Omega T_N - \frac{2\pi}{L}k_1)}) e^{-j\frac{2\pi}{L}k_1 n} \right) d\Omega
\end{aligned} \tag{B-9}$$

Similarly, the third term of (B-1) is shown to be

$$\begin{aligned}
&\sum_{m_2=0}^{M-1} \sum_{k_2=-\infty}^{\infty} E \{x[n]x_{m_2}[k_2]\} g_{m_2}[n - l - k_2L] \\
&\frac{1}{2\pi} \int_{-\Omega_c}^{\Omega_c} S_{xx}(\Omega) e^{j\Omega l T_N} \sum_{m_2=0}^{M-1} e^{j\Omega \tau_{m_2}} \left(\frac{1}{L} \sum_{k_2} G_{m_2}^*(e^{j(\Omega T_N - \frac{2\pi}{L}k_2)}) e^{j\frac{2\pi}{L}k_2 n} \right) d\Omega
\end{aligned} \tag{B-10}$$

To obtain $\sigma_{e_x}^2 = \frac{1}{L} \sum_{n=0}^{L-1} R_{e_x e_x}[n, n]$, i.e., the time and ensemble average of $e_x^2[n]$, we average over time each of the components of $R_{e_x e_x}[n, n]$. Averaging (B-6) over time for $l = 0$, we obtain

$$\begin{aligned}
& \frac{1}{2\pi} \int_{-\Omega_c}^{\Omega_c} S_{xx}(\Omega) \frac{1}{L} \sum_{k_1} \frac{1}{L} \sum_{k_2} \left[\sum_{m_1=0}^{M-1} e^{-j\Omega\tau_{m_1}} G_{m_1}(e^{j(\Omega T_N - \frac{2\pi}{L}k_1)}) \right] \\
& \cdot \left[\sum_{m_2=0}^{M-1} e^{j\Omega\tau_{m_2}} G_{m_2}^*(e^{j(\Omega T_N - \frac{2\pi}{L}k_2)}) \right] \underbrace{\frac{1}{L} \left(\sum_{n=0}^{L-1} e^{j\frac{2\pi}{L}(k_2-k_1)n} \right)}_{\sum_{n=-\infty}^{\infty} \delta[k_2-k_1-nL]} d\Omega \\
& = \frac{1}{2\pi} \int_{-\Omega_c}^{\Omega_c} S_{xx}(\Omega) \sum_k \left| \frac{1}{L} \sum_{m=0}^{M-1} e^{-j\Omega\tau_m} G_m(e^{j(\Omega T_N - \frac{2\pi}{L}k)}) \right|^2 d\Omega \tag{B-11}
\end{aligned}$$

which can be shown to be equivalent to

$$\begin{aligned}
& \sum_{i=0}^{L-1} \frac{1}{2\pi} \int_{\Delta\Omega_i} S_{xx}(\Omega) \left(\frac{1}{L} \right)^{2L-1-i} \sum_{k_1=-i}^{L-1-i} \sum_{k_2=-i}^{L-1-i} \left[\sum_{m_1=0}^{M-1} G_{m_1}(e^{j(\Omega T_N - \frac{2\pi}{L}k_1)}) e^{-j\Omega\tau_{m_1}} \right] \\
& \cdot \left[\sum_{m_2=0}^{M-1} G_{m_2}^*(e^{j(\Omega T_N - \frac{2\pi}{L}k_2)}) e^{j\Omega\tau_{m_2}} \right] \underbrace{\frac{1}{L} \left(\sum_{n=0}^{L-1} e^{j\frac{2\pi}{L}(k_2-k_1)n} \right)}_{\sum_{n=-\infty}^{\infty} \delta[k_2-k_1-nL]} d\Omega \\
& = \sum_{i=0}^{L-1} \frac{1}{2\pi} \int_{\Delta\Omega_i} S_{xx}(\Omega) \sum_{k=-i}^{L-1-i} \left| \frac{1}{L} \sum_{m=0}^{M-1} G_m(e^{j(\Omega T_N - \frac{2\pi}{L}k)}) e^{-j\Omega\tau_m} \right|^2 d\Omega \\
& = \sum_{i=0}^{L-1} \frac{1}{2\pi} \int_{\Delta\omega_i} S_{xx}(\Omega) \sum_{k=-i}^{L-1-i} \left| \frac{1}{L} \sum_{m=0}^{M-1} G_m(e^{j(\Omega T_N - \frac{2\pi}{L}k)}) e^{-j\Omega\tau_m} \right|^2 d\Omega \\
& = \frac{1}{T_N} \sum_{i=0}^{L-1} \frac{1}{2\pi} \int_{\Delta\omega_i} \sum_{k=-i}^{L-1-i} S_{xx} \left(\frac{\omega + \frac{2\pi}{L}k}{T_N} \right) \left| \frac{1}{L} \sum_{m=0}^{M-1} G_m(e^{j\omega}) e^{-j(\omega + \frac{2\pi}{L}k)\tau_m/T_N} \right|^2 d\omega \\
& = \frac{1}{T_N} \frac{1}{2\pi} \int_{-\pi}^{\pi} \sum_{k=-(L-1)}^{L-1} S_{xx} \left(\frac{\omega - \frac{2\pi}{L}k}{T_N} \right) \left| \frac{1}{L} \sum_{m=0}^{M-1} G_m(e^{j\omega}) e^{-j(\omega - \frac{2\pi}{L}k)\tau_m/T_N} \right|^2 d\omega \tag{B-12}
\end{aligned}$$

Similarly, averaging over time (B-8) and (B-10) for $l = 0$ results in

$$\begin{aligned} & \frac{1}{2\pi} \int_{-\Omega_c}^{\Omega_c} S_{xx}(\Omega) \left(\frac{1}{L} \sum_{m_1=0}^{M-1} G_{m_1}(e^{j\Omega T_N}) e^{-j\Omega \tau_{m_1}} \right) d\Omega \\ &= \frac{1}{T_N} \frac{1}{2\pi} \int_{-\pi}^{\pi} S_{xx} \left(\frac{\omega}{T_N} \right) \left(\frac{1}{L} \sum_{m=0}^{M-1} G_m(e^{j\omega}) e^{-j\omega \tau_m/T_N} \right) d\omega \end{aligned} \quad (\text{B-13})$$

and

$$\begin{aligned} & \frac{1}{2\pi} \int_{-\Omega_c}^{\Omega_c} S_{xx}(\Omega) \left(\frac{1}{L} \sum_{m_2=0}^{M-1} G_{m_2}(e^{j\Omega T_N}) e^{-j\Omega \tau_{m_2}} \right)^* d\Omega \\ &= \frac{1}{T_N} \frac{1}{2\pi} \int_{-\pi}^{\pi} S_{xx} \left(\frac{\omega}{T_N} \right) \left(\frac{1}{L} \sum_{m=0}^{M-1} G_m(e^{j\omega}) e^{-j\omega \tau_m/T_N} \right)^* d\omega \end{aligned} \quad (\text{B-14})$$

Thus,

$$\begin{aligned} \sigma_{e_x}^2 &= \frac{1}{2\pi} \int_{-\pi}^{\pi} \sum_{k=-(L-1)}^{L-1} \frac{1}{T_N} S_{xx} \left(\frac{\omega - \frac{2\pi k}{L}}{T_N} \right) \left| \frac{1}{L} \sum_{m=0}^{M-1} G_m(e^{j\omega}) e^{-j(\omega - \frac{2\pi k}{L})\tau_m/T_N} \right|^2 d\omega \\ &\quad - \frac{1}{2\pi} \int_{-\pi}^{\pi} \frac{1}{T_N} S_{xx} \left(\frac{\omega}{T_N} \right) \left(\frac{1}{L} \sum_{m=0}^{M-1} G_m(e^{j\omega}) e^{-j\omega \tau_m/T_N} \right) d\omega \\ &\quad - \frac{1}{2\pi} \int_{-\pi}^{\pi} \frac{1}{T_N} S_{xx} \left(\frac{\omega}{T_N} \right) \left(\frac{1}{L} \sum_{m=0}^{M-1} G_m(e^{j\omega}) e^{-j\omega \tau_m/T_N} \right)^* d\omega \\ &\quad + \frac{1}{2\pi} \int_{-\pi}^{\pi} \frac{1}{T_N} S_{xx} \left(\frac{\omega}{T_N} \right) d\omega \\ &= \frac{1}{2\pi} \int_{-\pi}^{\pi} \sum_{k=-(L-1)}^{L-1} \frac{1}{T_N} S_{xx} \left(\frac{\omega - \frac{2\pi k}{L}}{T_N} \right) \left| \frac{1}{L} \sum_{m=0}^{M-1} G_m(e^{j\omega}) e^{-j(\omega - \frac{2\pi k}{L})\tau_m/T_N} - \delta[k] \right|^2 d\omega \end{aligned} \quad (\text{B-15})$$

and since $\sigma_{e_q}^2 = \frac{1}{2\pi} \int_{-\pi}^{\pi} \sum_{m=0}^{M-1} (\sigma_m^2/L) \cdot |G_m(e^{j\omega})|^2 d\omega$, we obtain

$$\begin{aligned} S_{ee}(e^{j\omega}) &= \sum_{k=-(L-1)}^{L-1} \frac{1}{T_N} S_{xx} \left(\frac{\omega - \frac{2\pi k}{L}}{T_N} \right) \left| \frac{1}{L} \sum_{m=0}^{M-1} G_m(e^{j\omega}) e^{-j(\omega - \frac{2\pi k}{L})\tau_m/T_N} - \delta[k] \right|^2 \\ &\quad + \sum_{m=0}^{M-1} (\sigma_m^2/L) \cdot |G_m(e^{j\omega})|^2 \end{aligned} \quad (\text{B-16})$$

APPENDIX C

OPTIMAL MMSE RECONSTRUCTION FILTERS

Taking the derivative of $S_{ee}(e^{j\omega})$ from (3.8) with respect to $G_m^R(e^{j\omega}) = \Re \{G_m(e^{j\omega})\}$ and $G_m^I(e^{j\omega}) = \Im \{G_m(e^{j\omega})\}$, we obtain

$$\begin{aligned} \frac{\partial S_{ee}(e^{j\omega})}{\partial G_l^R(e^{j\omega})} &= \sum_{k=-(L-1)}^{L-1} \frac{1}{T_N} S_{xx} \left(\frac{\omega - \frac{2\pi}{L}k}{T_N} \right) \cdot \left\{ \left(\frac{1}{L} \sum_{m=0}^{M-1} G_m(e^{j\omega}) e^{-j(\omega - \frac{2\pi}{L}k)\tau_m/T_N} - \delta[k] \right) \frac{1}{L} e^{j(\omega - \frac{2\pi}{L}k)\tau_l/T_N} \right. \\ &\quad \left. + \frac{1}{L} e^{-j(\omega - \frac{2\pi}{L}k)\tau_l/T_N} \left(\frac{1}{L} \sum_{m=0}^{M-1} G_m^*(e^{j\omega}) e^{j(\omega - \frac{2\pi}{L}k)\tau_m/T_N} - \delta[k] \right) \right\} + 2 \frac{\sigma_l^2}{L} G_l^R(e^{j\omega}) = 0, \\ & l = 0, 1, \dots, M-1, \quad \omega \in [-\pi, \pi] \end{aligned} \tag{C-1}$$

and

$$\begin{aligned} \frac{\partial \sigma_e^2}{\partial G_l^I(e^{j\omega})} &= \sum_{k=-(L-1)}^{L-1} \frac{1}{T_N} S_{xx} \left(\frac{\omega - \frac{2\pi}{L}k}{T_N} \right) \left\{ \left(\frac{1}{L} \sum_{m=0}^{M-1} G_m(e^{j\omega}) e^{-j(\omega - \frac{2\pi}{L}k)\tau_m/T_N} - \delta[k] \right) (-j) \frac{1}{L} e^{j(\omega - \frac{2\pi}{L}k)\tau_l/T_N} \right. \\ &\quad \left. + j \frac{1}{L} e^{-j(\omega - \frac{2\pi}{L}k)\tau_l/T_N} \left(\frac{1}{L} \sum_{m=0}^{M-1} G_m^*(e^{j\omega}) e^{j(\omega - \frac{2\pi}{L}k)\tau_m/T_N} - \delta[k] \right) \right\} + 2 \frac{\sigma_l^2}{L} G_l^I(e^{j\omega}) = 0, \\ & l = 0, 1, \dots, M-1, \quad \omega \in [-\pi, \pi], \end{aligned} \tag{C-2}$$

from which it follows that

$$\begin{aligned} & \sum_{k=-(L-1)}^{L-1} \frac{1}{T_N} S_{xx} \left(\frac{\omega - \frac{2\pi}{L}k}{T_N} \right) \left\{ \left(\frac{1}{L} \sum_{m=0}^{M-1} G_m(e^{j\omega}) e^{-j(\omega - \frac{2\pi}{L}k)\tau_m/T_N} - \delta[k] \right) e^{j(\omega - \frac{2\pi}{L}k)\tau_l/T_N} \right\} \\ & + \sigma_l^2 G_l(e^{j\omega}) = 0, \quad l = 0, 1, \dots, M-1, \quad \omega \in [-\pi, \pi]. \end{aligned} \tag{C-3}$$

Rearranging eq. (C-3) results in the following set of equations

$$\begin{aligned}
& \sum_{m=0}^{M-1} G_m(e^{j\omega}) \left\{ \left(\frac{1}{L} \sum_{k=-(L-1)}^{L-1} \frac{1}{T_N} S_{xx} \left(\frac{\omega - \frac{2\pi}{L}k}{T_N} \right) e^{j\frac{2\pi}{L}k(\tau_m - \tau_l)/T_N} \right) e^{-j\omega(\tau_m - \tau_l)/T_N} + \sigma_l^2 \delta[m-l] \right\} \\
& = \frac{1}{T_N} S_{xx} \left(\frac{\omega}{T_N} \right) e^{j\omega\tau_l/T_N}, \quad l = 0, 1, \dots, M-1, \quad \omega \in [-\pi, \pi], \tag{C-4}
\end{aligned}$$

from which the optimal reconstruction filters can be obtained.

APPENDIX D

RANDOMIZED SINC INTERPOLATION - MSE DERIVATION

The autocorrelation function of $\hat{x}(t) = \sum_{n=-\infty}^{\infty} x[n]\tilde{h}(t - \tilde{t}_n)$ is

$$R_{\hat{x}\hat{x}}(t, t - \tau) = E \left\{ \sum_n x(nT + \xi_n) \tilde{h}(t - nT - \zeta_n) \cdot \sum_k x(kT + \xi_k) \tilde{h}(t - \tau - kT - \zeta_k) \right\} \quad (\text{D-1})$$

where $\tilde{h}(t) = T/T_N \cdot h(t)$. Using iterated expectation and representing $R_{xx}(t)$ and $\tilde{h}(t)$ in terms of their corresponding Fourier transforms $S_{xx}(\Omega)$ and $\tilde{H}(\Omega)$, we obtain

$$R_{\hat{x}\hat{x}}(t, t - \tau) = \frac{1}{2\pi} \int_{-\Omega_c}^{\Omega_c} \frac{1}{T^2} |\tilde{H}(\Omega)|^2 \cdot S_{xx}(\Omega) \cdot |\Phi_{\xi\zeta}(\Omega, -\Omega)|^2 e^{j\Omega\tau} d\Omega + \frac{1}{2\pi} \int_{-\Omega_c}^{\Omega_c} \frac{1}{T} |\tilde{H}(\Omega)|^2 \cdot \left[R_{xx}(0) - \frac{1}{2\pi} \int_{-\Omega_c}^{\Omega_c} S_{xx}(\Omega_1) \cdot |\Phi_{\xi\zeta}(\Omega_1, -\Omega)|^2 d\Omega_1 \right] \cdot e^{j\Omega\tau} d\Omega. \quad (\text{D-2})$$

Similarly, the cross correlation of $\hat{x}(t)$ and $x(t)$ can be expressed as

$$R_{\hat{x}x}(t, t - \tau) = E \left\{ \sum_n x(nT + \xi_n) \tilde{h}(t - nT - \zeta_n) \cdot x(t - \tau) \right\} = \frac{1}{2\pi} \int_{-\Omega_c}^{\Omega_c} \frac{1}{T} S_{xx}(\Omega) \tilde{H}(\Omega) \cdot \Phi_{\xi\zeta}(\Omega, -\Omega) e^{j\Omega\tau} d\Omega. \quad (\text{D-3})$$

Taking the Fourier transform of (D-2) and (D-3) with respect to τ results in

$$S_{\hat{x}\hat{x}}(\Omega) = S_{xx}(\Omega) \cdot |\Phi_{\xi\zeta}(\Omega, -\Omega)|^2 + \frac{T}{2\pi} \int_{-\Omega_c}^{\Omega_c} S_{xx}(\Omega_1) \cdot [1 - |\Phi_{\xi\zeta}(\Omega_1, -\Omega)|^2] d\Omega_1 \quad |\Omega| < \Omega_c \quad (\text{D-4})$$

and

$$S_{\hat{x}x}(\Omega) = S_{xx}(\Omega) \cdot \Phi_{\xi\zeta}(\Omega, -\Omega) \quad |\Omega| < \Omega_c, \quad (\text{D-5})$$

from which the second-order statistics model of Figure (4-2) clearly follows. The power spectrum of the reconstruction error $e^R(t) = \hat{x}(t) - x(t)$ is

$$S_{e^R e^R}(\Omega) = S_{\hat{x}\hat{x}}(\Omega) - S_{\hat{x}x}(\Omega) - S_{x\hat{x}}(\Omega) + S_{xx}(\Omega) \quad (\text{D-6})$$

where $S_{\hat{x}\hat{x}}(\Omega)$ and $S_{\hat{x}x}(\Omega)$ are given in (D-4) and (D-5) respectively, and $S_{x\hat{x}}(\Omega) = S_{\hat{x}x}^*(\Omega)$. Consequently,

$$S_{e^R e^R}(\Omega) = S_{xx}(\Omega) \cdot |1 - \Phi_{\xi\zeta}(\Omega, -\Omega)|^2 + \frac{T}{2\pi} \int_{-\Omega_c}^{\Omega_c} S_{xx}(\Omega_1) \cdot [1 - |\Phi_{\xi\zeta}(\Omega_1, -\Omega)|^2] d\Omega_1 \quad |\Omega| < \Omega_c.$$

Integrating the power spectrum over frequency, we obtain the MSE

$$\begin{aligned} E(\{e^R(t)\}^2) &= \frac{1}{2\pi} \int_{-\Omega_c}^{\Omega_c} S_{e^R e^R}(\Omega) d\Omega = \\ &= \frac{1}{2\pi} \int_{-\Omega_c}^{\Omega_c} S_{xx}(\Omega) \cdot |1 - \Phi_{\xi\zeta}(\Omega, -\Omega)|^2 d\Omega + \\ &+ \frac{T}{T_N} \cdot \frac{1}{2\pi} \int_{-\Omega_c}^{\Omega_c} S_{xx}(\Omega) \cdot \left[1 - \frac{1}{2\Omega_c} \int_{-\Omega_c}^{\Omega_c} |\Phi_{\xi\zeta}(\Omega, -\Omega_1)|^2 d\Omega_1 \right] d\Omega. \end{aligned} \quad (\text{D-7})$$

APPENDIX E

THE AUTOCORRELATION FUNCTION OF A BANDLIMITED SIGNAL

The autocorrelation function $R_{xx}(\tau)$ of a bandlimited signal $x(t)$ whose spectrum $S_{xx}(\Omega) = 0$ for all $\Omega \geq \pi/T_N$ satisfies the following properties:

1. Non-negativity -

$$R_{xx}(\tau) > 0 \quad \forall |\tau| < T_N/2,$$

2. For all ζ_0

$$R_{xx}(\tau) \geq \frac{1}{2} (R_{xx}(\tau - \zeta_0) + R_{xx}(\tau + \zeta_0)) \quad \forall |\tau| < T_N/2$$

where in general equality is achieved if and only if $\zeta_0 = 0$,

3. Strictly concave in the region $(-T_N/2, T_N/2)$.

To prove the first property we first use symmetry and real arguments of the power spectrum which results in

$$R_{xx}(\tau) = \frac{1}{2\pi} \int_{-\pi/T_N}^{\pi/T_N} S_{xx}(\Omega) \cos(\Omega\tau) d\Omega. \quad (\text{E-1})$$

We then note that in the interval of integration $\cos(\Omega\tau) > 0$ for all $|\tau| < T_N/2$, which completes the proof since $S_{xx}(\Omega) \geq 0$ for all Ω .

The second property follows by noting that

$$\frac{1}{2}(R_{xx}(\tau - \zeta_0) + R_{xx}(\tau + \zeta_0)) = \frac{1}{2\pi} \int_{-\pi/T_N}^{\pi/T_N} S_{xx}(\Omega) \cos(\Omega \zeta_0) \cos(\Omega \tau) d\Omega, \quad (\text{E-2})$$

and that for every $|\tau| < T_N/2$,

$$\frac{1}{2\pi} \int_{-\pi/T_N}^{\pi/T_N} S_{xx}(\Omega) \cos(\Omega \zeta_0) \cos(\Omega \tau) d\Omega \leq \frac{1}{2\pi} \int_{-\pi/T_N}^{\pi/T_N} S_{xx}(\Omega) \cos(\Omega \tau) d\Omega. \quad (\text{E-3})$$

To show concavity, we differentiate twice eq. (E-1) with respect to τ , i.e.

$$R_{xx}''(\tau) = -\frac{1}{2\pi} \int_{-\pi/T_N}^{\pi/T_N} \Omega^2 S_{xx}(\Omega) \cos(\Omega \tau) d\Omega \quad (\text{E-4})$$

and note that $R_{xx}''(\tau)$ is negative for all $|\tau| < T_N/2$, excluding the degenerate case where $S_{xx}(\Omega) = 2\pi R_{xx}(0) \delta(\Omega)$ in which $R_{xx}''(\tau) = 0$.

Properties (1)-(3) are not limited to autocorrelation functions of bandlimited signals and hold for any function whose Fourier transform pair is real, non-negative, symmetric, and has bounded support, e.g. the characteristic function of a symmetric pdf whose support is bounded.

APPENDIX F

TIME JITTER IN DISCRETE-TIME PROCESSING OF CONTINUOUS-TIME SIGNALS

The cross-correlation function between $y(t)$ and $x(t)$ can be expressed as

$$R_{yx}(t, t - \tau) = E \left(\sum_{n=-\infty}^{\infty} \left(\sum_{l=-\infty}^{\infty} x((n-l)T + \xi_{n-l}) \cdot g[l] \right) \cdot h(t - nT - \zeta_n) \cdot x(t - \tau) \right) \quad (\text{F-1})$$

where $h(t) = \text{sinc}\left(\frac{\pi}{T}t\right)$. Using iterated expectation and representing $R_{xx}(t)$ and $h(t)$ in terms of their corresponding Fourier transforms $S_{xx}(\Omega)$ and $H(\Omega)$, we obtain

$$\begin{aligned} R_{yx}(t, t - \tau) &= \sum_{n=-\infty}^{\infty} \sum_{l=-\infty}^{\infty} E(R_{xx}((n-l)T + \xi_{n-l} - t + \tau) \cdot g[l] \cdot h(t - nT - \zeta_n)) \\ &= \left(\frac{1}{2\pi}\right)^2 \int_{-\pi/T}^{\pi/T} \int_{-\pi/T}^{\pi/T} S_{xx}(\Omega_1) \Phi_{\xi}(\Omega_1) e^{j\Omega_1(-t+\tau)} H(\Omega_2) \Phi_{\zeta}(-\Omega_2) e^{j\Omega_2 t} \\ &\quad \cdot \left(\sum_{n=-\infty}^{\infty} e^{j(\Omega_1 - \Omega_2)nT} \right) \cdot \left(\sum_{l=-\infty}^{\infty} g[l] e^{-j(\Omega_1 T)l} \right) d\Omega_1 d\Omega_2 = \\ &= \frac{1}{2\pi} \int_{-\pi/T}^{\pi/T} S_{xx}(\Omega) \Phi_{\xi}(\Omega) G(e^{j\Omega T}) e^{j\Omega \tau} d\Omega. \end{aligned} \quad (\text{F-2})$$

The autocorrelation function of $y(t)$ can be expressed as

$$\begin{aligned}
R_{yy}(t, t - \tau) &= E \left(\sum_{n=-\infty}^{\infty} y[n]h(t - nT - \zeta_n) \sum_{m=-\infty}^{\infty} y[m]h(t - \tau - mT - \zeta_m) \right) = \\
&E \left(\sum_{n=-\infty}^{\infty} \sum_{l=-\infty}^{\infty} x(lT + \xi_l)g[n-l]h(t - nT - \zeta_n) \cdot \sum_{m=-\infty}^{\infty} \sum_{p=-\infty}^{\infty} x(pT + \xi_p)g[m-p]h(t - \tau - mT - \zeta_m) \right) \\
&\sum_{n=-\infty}^{\infty} \sum_{l=-\infty}^{\infty} \sum_{m=-\infty}^{\infty} \sum_{p=-\infty}^{\infty} g[n-l]g[m-p] \cdot E(R_{xx}((l-p)T + \xi_l - \xi_p)h(t - nT - \zeta_n)h(t - \tau - mT - \zeta_m)).
\end{aligned} \tag{F-}$$

Expressing $R_{xx}(t)$, $h(t)$ and $g[n]$ in terms of their corresponding Fourier transforms $S_{xx}(\Omega)$, $H(\Omega)$ and $G(e^{j\omega})$, we obtain

$$\begin{aligned}
R_{yy}(t, t - \tau) &= \left(\frac{1}{2\pi} \right)^5 \int_{-\pi/T}^{\pi/T} \int_{-\pi/T}^{\pi/T} \int_{-\pi/T}^{\pi/T} \int_{-\pi}^{\pi} \int_{-\pi}^{\pi} S_{xx}(\Omega)H(\Omega_1)H^*(\Omega_2)e^{j\Omega_1 t}e^{-j\Omega_2(t-\tau)} \cdot \\
&G(e^{j\omega_1})G^*(e^{j\omega_2}) \left(\sum_{l=-\infty}^{\infty} \sum_{p=-\infty}^{\infty} e^{j(\Omega T)(l-p)} E(e^{j\Omega(\xi_l - \xi_p)})e^{j(\omega_2 p - \omega_1 l)} \right) \cdot \\
&\left(\sum_{n=-\infty}^{\infty} \sum_{m=-\infty}^{\infty} e^{j(\Omega_2 m - \Omega_1 n)T} E(e^{j(\Omega_2 \zeta_m - \Omega_1 \zeta_n)})e^{j(\omega_1 n - \omega_2 m)} \right) dw_1 dw_2 d\Omega_1 d\Omega_2 d\Omega,
\end{aligned} \tag{F-4}$$

where

$$\begin{aligned}
&\sum_{l=-\infty}^{\infty} \sum_{p=-\infty}^{\infty} e^{j(\Omega T)(l-p)} E(e^{j\Omega(\xi_l - \xi_p)})e^{j(\omega_2 p - \omega_1 l)} = \\
&|\Phi_{\xi}(\Omega)|^2 \left(\sum_{l=-\infty}^{\infty} e^{j(\Omega T - \omega_1)l} \right) \left(\sum_{p=-\infty}^{\infty} e^{j(\omega_2 - \Omega T)p} \right) + (1 - |\Phi_{\xi}(\Omega)|^2) \left(\sum_{l=-\infty}^{\infty} e^{j(\omega_2 - \omega_1)l} \right)
\end{aligned} \tag{F-5}$$

and

$$\begin{aligned}
& \sum_{n=-\infty}^{\infty} \sum_{m=-\infty}^{\infty} e^{j(\Omega_2 m - \Omega_1 n)T} E(e^{j(\Omega_2 \zeta_m - \Omega_1 \zeta_n)}) e^{j(\omega_1 n - \omega_2 m)} = \\
& \Phi_{\zeta}(-\Omega_1) \Phi_{\zeta}(\Omega_2) \left(\sum_{n=-\infty}^{\infty} e^{j(\omega_1 - \Omega_1 T)n} \right) \left(\sum_{m=-\infty}^{\infty} e^{j(\Omega_2 T - \omega_2)m} \right) + \\
& + \left(\Phi_{\zeta}(\Omega_2 - \Omega_1) - \Phi_{\zeta}(-\Omega_1) \Phi_{\zeta}(\Omega_2) \right) \left(\sum_{n=-\infty}^{\infty} e^{j((\Omega_2 - \Omega_1)T + \omega_1 - \omega_2)n} \right). \quad (\text{F-6})
\end{aligned}$$

Thus,

$$\begin{aligned}
R_{yy}(t, t - \tau) &= \frac{1}{2\pi} \int_{-\pi/T}^{\pi/T} S_{xx}(\Omega) \cdot |\Phi_{\xi}(\Omega)|^2 |\Phi_{\zeta}(\Omega)|^2 |G(e^{j\Omega T})|^2 e^{j\Omega\tau} d\Omega + \\
& \frac{1}{2\pi} \int_{-\pi/T}^{\pi/T} T \left(1 - |\Phi_{\zeta}(\Omega_1)|^2 \right) e^{j\Omega_1\tau} d\Omega_1 \cdot \frac{1}{2\pi} \int_{-\pi/T}^{\pi/T} S_{xx}(\Omega) |\Phi_{\xi}(\Omega)|^2 |G(e^{j\Omega T})|^2 d\Omega + \\
& \frac{T}{2\pi} \int_{-\pi/T}^{\pi/T} S_{xx}(\Omega) \left(1 - |\Phi_{\xi}(\Omega)|^2 \right) d\Omega \cdot \frac{1}{2\pi} \int_{-\pi/T}^{\pi/T} |\Phi_{\zeta}(\Omega_1)|^2 |G(e^{j\Omega_1 T})|^2 e^{j\Omega_1\tau} d\Omega_1 + \\
& \frac{1}{2\pi} \int_{-\pi/T}^{\pi/T} S_{xx}(\Omega) \left(1 - |\Phi_{\xi}(\Omega)|^2 \right) d\Omega \cdot \frac{1}{2\pi} \int_{-\pi/T}^{\pi/T} T \left(1 - |\Phi_{\zeta}(\Omega_1)|^2 \right) e^{j\Omega_1\tau} d\Omega_1 \cdot \frac{1}{2\pi} \int_{-\pi}^{\pi} |G(e^{j\omega_1})|^2 d\alpha \quad (\text{F-}
\end{aligned}$$

Applying the Fourier transform to $R_{yx}(\tau)$ in (F-2) and to $R_{yy}(\tau)$ in (F-7) results in $S_{yx}(\Omega)$ and $S_{yy}(\Omega)$.

APPENDIX G

RANDOMIZED SINC INTERPOLATION - SUB-NYQUIST SAMPLING

The autocorrelation function of $\hat{x}(t) = \sum_{n=-\infty}^{\infty} x(t_n)h_T(t - \tilde{t}_n)$ is

$$\begin{aligned}
 R_{\hat{x}\hat{x}}(t, t - \tau) &= E \left(\sum_{n=-\infty}^{\infty} x(nT + \xi_n)h_T(t - nT - \zeta_n) \sum_{k=-\infty}^{\infty} x(kT + \xi_k)h_T(t - \tau - kT - \zeta_k) \right) \\
 &= R_{xx}(0)E \left(\sum_{n=-\infty}^{\infty} h_T(t - nT - \zeta_n)h_T(t - \tau - nT - \zeta_n) \right) \\
 &\quad + \sum_{n \neq k} E(R_{xx}((n-k)T + \xi_n - \xi_k)h_T(t - nT - \zeta_n)h_T(t - \tau - kT - \zeta_k)) \quad (G-1)
 \end{aligned}$$

where $h_T(t) = \text{sinc}(\frac{\pi}{T}t)$. Representing $R_{xx}(t)$ and $h_T(t)$ in terms of $S_{xx}(\Omega)$ and $H_T(\Omega)$, we obtain

$$E \left(\sum_{n=-\infty}^{\infty} h_T(t - nT - \xi_n)h_T(t - \tau - nT - \xi_n) \right) = h_T(\tau) \quad (G-2)$$

and

$$\begin{aligned}
 &\sum_{n \neq k} E(R_{xx}((n-k)T + \xi_n - \xi_k)h_T(t - nT - \zeta_n)h_T(t - \tau - kT - \zeta_k)) = \\
 &= \frac{1}{2\pi} \int_{-\frac{\pi}{T}}^{\frac{\pi}{T}} \sum_{n=-\infty}^{\infty} S_{xx}(\Omega - \frac{2\pi}{T}n) \cdot |\Phi_{\xi\xi}(\Omega - \frac{2\pi}{T}n, -\Omega)|^2 e^{j\Omega\tau} d\Omega \\
 &\quad + \frac{1}{2\pi} \int_{-\frac{\pi}{T}}^{\frac{\pi}{T}} \frac{T}{2\pi} \int_{-\Omega_c}^{\Omega_c} S_{xx}(\Omega) |\Phi_{\xi\xi}(\Omega, -\Omega_1)|^2 d\Omega e^{j\Omega_1\tau} d\Omega_1. \quad (G-3)
 \end{aligned}$$

Substituting (G-2) and (G-3) into (G-1) and taking the Fourier transform with respect

to τ , we obtain

$$\begin{aligned}
S_{\hat{x}\hat{x}}(\Omega) &= \sum_{n=-\infty}^{\infty} S_{xx}\left(\Omega - \frac{2\pi}{T}n\right) |\Phi_{\xi\zeta}\left(\Omega - \frac{2\pi}{T}n, -\Omega\right)|^2 \\
&+ \frac{T}{2\pi} \int_{-\Omega_c}^{\Omega_c} S_{xx}(\Omega_1) (1 - |\Phi_{\xi\zeta}(\Omega_1, -\Omega)|^2) d\Omega_1 \quad |\Omega| < \frac{\pi}{T}. \quad (\text{G-4})
\end{aligned}$$

The cross-correlation of $\hat{x}(t)$ and $x(t)$ is

$$\begin{aligned}
R_{\hat{x}x}(t, t - \tau) &= E \left(\sum_{n=-\infty}^{\infty} x(nT + \xi_n) h_T(t - nT - \zeta_n) x(t - \tau) \right) \\
&= \sum_{n=-\infty}^{\infty} E (R_{xx}(nT + \xi_n + \tau - t) h_T(t - nT - \zeta_n)) \quad (\text{G-5})
\end{aligned}$$

where, again, by representing $R_{xx}(t)$ and $h_T(t)$ in terms of $S_{xx}(\Omega)$ and $H_T(\Omega)$, we obtain

$$R_{\hat{x}x}(t, t - \tau) = \frac{1}{2\pi} \int_{-\pi/T}^{\pi/T} \sum_{n=-\infty}^{\infty} \left(S_{xx}\left(\Omega - \frac{2\pi}{T}n\right) \Phi_{\xi\zeta}\left(\Omega - \frac{2\pi}{T}n, -\Omega\right) e^{j\frac{2\pi}{T}n(t-\tau)} \right) e^{j\Omega\tau} d\Omega. \quad (\text{G-6})$$

An alternative representation is obtained by representing $S_{xx}(\Omega)$ and $\Phi_{\xi\zeta}(\Omega_1, \Omega_2)$ in terms of $R_{xx}(t)$ and $f_{\xi\zeta}(\xi, \zeta)$, i.e.,

$$R_{\hat{x}x}(t, t - \tau) = \int_{-\infty}^{\infty} R_{xx}(t_1) \cdot \sum_{n=-\infty}^{\infty} \left[f_{\xi\zeta}(t_1 + t - nT - \tau, \zeta) * h_T\left(\frac{\pi}{T}\zeta\right) \right] |_{\zeta=t-nT} dt_1. \quad (\text{G-7})$$

Bibliography

- [1] R. Amirtharajah, J. Collier, J. Siebert, B. Zhou, and A. Chandrakasan. Dsp's for energy harvesting sensors: applications and architectures. *IEEE Pervasive Computing*, 4(3):72–79, July 2005.
- [2] A. V. Balakrishnan. A note on the sampling principle for continuous signals. *IRE Trans. Information Theory*, 3(2):143–146, 1957.
- [3] A. V. Balakrishnan. On the problem of time jitter in sampling. *IRE Trans. Inform. Theory*, 8:226–236, 1962.
- [4] W.R. Bennett. Spectra of quantized signals. *Bell System Technical J.*, 27:446–472, 1948.
- [5] F. J. Beutler. Error-free recovery of signals from irregularly spaced samples. *SIAM Rev.*, 8(3):328–335, 1966.
- [6] A. Björck. *Numerical methods for least squares problems*. SIAM, Philadelphia, 1996.
- [7] H. S. Black. *Modulation Theory*. D. Van Nostrand Co., Inc., New York, N.Y.
- [8] R. P. Boas. *Entire Functions*. Academic Press, Inc., New York, N. Y., 1954.
- [9] F. E. Bond and C. R. Cahn. On sampling the zeroes of bandwidth limited signals. *IRE Trans. Inform. Theory*, IT-4:110–113, 1958.
- [10] C. De Boor. On calculating with b-splines. *J. Approximat. Theory*, 6:50–62, 1970.
- [11] William M. Brown. Sampling with random jitter. *Journal of the Society for Industrial and Applied Mathematics*, 11(2):460–473, 1963.
- [12] J. L. Brown, Jr. On the error in reconstructing a nonband-limited function by means of the band pass sampling theorem. *J. Math. Anal. Appl.*, 18:75–84, 1967.
- [13] J. L. Brown, Jr. Uniform linear prediction of bandlimited processes from past samples. *IEEE Trans. Inform. Theory*, IT-18, 1972.
- [14] P. L. Butzer, W. Splettstosser, and R. L. Stens. The sampling theorem and linear prediction in signal analysis. *Jber. d. Dt. Math. Verein.*, 90:1–70, 1988.

- [15] J.C. Candy and G.C. Temes. *Oversampling Delta-Sigma Data Converters*. IEEE Press New York, NY, 1992.
- [16] A. L. Cauchy. Memoire sur diverse formulaes de analyse. *Compt. Rend. Paris*, 12:283–298, 1841.
- [17] J. J. Clark, M. R. Palmer, and P. D. Lawrence. A transformation method for the reconstruction of functions from nonuniformly spaced samples. *IEEE Trans. Acoust., Speech, Signal Processing*, ASSP-33(4):1151–1165, October 1985.
- [18] Robert L. Cook. Stochastic sampling in computer graphics. *ACM Transactions on Graphics*, 5(1):51–72, January 1986.
- [19] R. E. Crochiere, S. A. Webber, and J. L. Flanagan. Digital coding of speech in sub-bands. *Bell System Technical Journal*, 55(8):1069–1085, 1976.
- [20] C. C. Cutler. Differential quantization for communication signals. *U.S. Patent 2,605,361*, July 29, 1952.
- [21] Vijay Divi and Gregory W. Wornell. Blind calibration of timing skew in time-interleaved analog-to-digital converters. *IEEE Journal of Selected Topics in Signal Processing*, 3(3):509, 2009.
- [22] J. Elbornsson, F. Gustafsson, and J.-E. Eklund. Blind adaptive equalization of mismatch errors in time-interleaved A/D converter system. *IEEE Trans. Circuits Syst.*, 51(1):151–158, 2004.
- [23] Y. C. Eldar and A. V. Oppenheim. Filterbank reconstruction of bandlimited signals from nonuniform and generalized samples. *IEEE Trans. Signal Processing*, 48(10):2864–2875, 2000.
- [24] P. Elias. Predictive coding. *IRE Trans. on Information Theory*, pages 16–33, 1955.
- [25] H. G. Feichtinger and K. Grochenig. Irregular sampling theorems and series expansions of band-limited functions. *J. Math. Anal. and Appl.*, 167:530–556, 1992.
- [26] H. G. Feichtinger, K. Grochenig, and T. Strohmer. Efficient numerical methods in non-uniform sampling theory. *Numerische Mathematik*, 69(4):423–440, July 1995.
- [27] L. Fogel. A note on the sampling theorem. *IRE Trans.*, 1:47–48, 1955.
- [28] D. Gabor. Theory of communication. *J. IEE*, 93:429–457, 1946.
- [29] W. A. Gardner. A sampling theorem for nonstationary random processes. *IEEE Trans. Inform. Theory*, IT-18:808–809, 1972.
- [30] K. Grochenig. Reconstruction algorithms in irregular sampling. *Math. Comp.*, 59(199):181–194, July 1992.

- [31] H. D. Helms and J. B. Thomas. Truncation error of sampling theorem expansion. *Proc. IRE*, 50:179–184, 1962.
- [32] J. R. Higgins. Five short stories about the cardinal series. *Bull. Amer. Math. Soc.*, 12:45–89, 1985.
- [33] J. R. Higgins. *Sampling Theory in Fourier and Signal Analysis: Foundations*. Oxford Science Publications, Clarendon Press, Oxford, 1996.
- [34] E.M. Hofstetter. Construction of time-limited functions with specified autocorrelation functions. *IEEE Trans. Information Theory*, 10(2):119–126, 1964.
- [35] H. Horiuchi. Sampling principle for continuous signals with time-varying bands. *Inform. Contr.*, 13:53–61, 1968.
- [36] S. Huang and B. C. Levy. Adaptive blind calibration of timing offset and gain mismatch for two-channel time-interleaved ADCs. *IEEE Trans. Circuits Syst.*, 53(6):1278–1288, 2006.
- [37] S. Huang and B. C. Levy. Blind calibration of timing offsets for four channel time-interleaved ADCs. *IEEE Trans. Circuits Syst.*, 54(4):863–876, 2007.
- [38] Robert J. Marks II. *Introduction to Shannon Sampling and Interpolation Theory*. Springer-Verlag New York Inc., 1991.
- [39] D. L. Jagerman and L. Fogel. Some general aspects of the sampling theorem. *IRE Trans. Inform. Theory*, IT-2:139–146, 1956.
- [40] N.S. Jayant and Peter Noll. *Digital Coding of Waveforms: Principles and Applications to Speech and Video*. Prentice Hall, 1984.
- [41] Y. C. Jenq. Digital spectra of nonuniformly sampled signals: a robust sampling time offset estimation algorithm for ultra high-speed waveform digitizers using interleaving. *IEEE Trans. Instrum. Meas.*, 39(1):71–75, 1990.
- [42] A. J. Jerri. *Integral and Discrete Transforms with Applications and Error Analysis*. Marcel Dekker publ., New York, 1992.
- [43] Abdul J. Jerri. The Shannon sampling theorem-its various extensions and applications: A tutorial review. *Proceedings of the IEEE*, 65(11):1565–1596, 1977.
- [44] H. Jin and E. K. F. Lee. A digital-background calibration technique for minimizing timing-error effects in time-interleaved ADCs. *IEEE Trans. Circuits Syst.*, 47(4):603–613, 2000.
- [45] R.P. Boas Jr. and M. Kac. Inequalities for Fourier transforms of positive functions. *Duke Math. J.*, 12(1):189–206, 1945.
- [46] W. C. Black Jr. and D. A. Hodges. Time interleaved converter arrays. *IEEE J. Solid-State Circuits*, SC-15:1022–1029, Dec 1980.

- [47] Ramin Khoini-Poorfard and David A. Johns. Time-interleaved oversampling converters. *Electronics Letters*, 29(19):1673 – 1674, 2002.
- [48] Ramin Khoini-Poorfard, Lysander B. Lim, and David A. Johns. Time-interleaved oversampling A/D converters: Theory and practice. *IEEE Trans. Circuits and Systems*, 44(8):634–645, 1997.
- [49] A. Kohlenberg. Exact interpolation of band-limited functions. *J. Appl. Physics*, 24:1432–1436, 1953.
- [50] V. A. Kotel'nikov. On the transmission capacity of ether and wire in electrocommunications. *Izd. Red. Upr. Svyazi RKKA*, 1933.
- [51] H.J. Landau. Sampling, data transmission, and the Nyquist rate. *Proceedings of the IEEE*, 55(10):1701 – 1706, 1967.
- [52] O. A. Z. Leneman and J. B. Lewis. Random sampling of random processes: Mean-square comparison of various interpolators. *IEEE Transactions on Automatic Control*, 11(3):396–403, July 1966.
- [53] Norman Levinson. *Gap and Density Theorems*. American Mathematical Society, 1940.
- [54] D. A. Linden. A discussion of sampling theorems. *Proc. IRE*, 47:1219–1226, 1959.
- [55] D. A. Linden and N. M. Abramson. A generalization of the sampling theorem. *Inform. Contr.*, 3:26–31, 1960.
- [56] S. P. Lloyd. A sampling theorem for stationary (wide sense) stochastic process. *Trans. Am. Math. Soc.*, 92:1–12, 1959.
- [57] N. Macon and A. Spitzbart. Inverses of vandermonde matrices. *The American Mathematical Monthly*, 65(2):95–100, 1958.
- [58] F. Marvasti. *Nonuniform Sampling*. Kluwer Academic, New York, 2001.
- [59] P. Marziliano and Martin Vetterli. Reconstruction of irregularly sampled discrete-time bandlimited signal with unknown sampling locations. *IEEE Trans. Signal Processing*, 48(12):3462–3471, 2000.
- [60] Shay Maymon and Alan V. Oppenheim. Randomized sinc interpolation of nonuniform samples. *EUSIPCO 2009, 17th European Signal Processing Conference*, August 2009.
- [61] Shay Maymon and Alan V. Oppenheim. Quantization and compensation in sampled interleaved multi-channel systems. *ICASSP 2010, IEEE International Conference on Acoustics, Speech and Signal Processing*, March 2010.

- [62] J. G. McMichael. Trade-off between timing offsets and quantization error in interleaved multi-channel measurements. Master's thesis, Massachusetts Institute of Technology, Cambridge, MA, June 2011.
- [63] R. Mersereau. The processing of hexagonally sampled two dimensional signals. *Proc. IEEE*, 67:930–949, 1979.
- [64] R. Mersereau and T. Speake. The processing of periodically sampled multidimensional signals. *IEEE Trans. Acoust. Speech Signal Process.*, ASSP-31:188–194, 1983.
- [65] Don P. Mitchell. Generating antialiased images at low sampling densities. *International Conference on Computer Graphics and Interactive Techniques*, 5(1):65–72, January 1987.
- [66] H. Miyakawa. Sampling theorem of stationary stochastic variables in multidimensional space. *J. Inst. Elec. Commun. Engrs., Japan*, 42:421–427, 1959.
- [67] H. Nyquist. Certain topics in telegraph transmission theory. *AIEE Trans.*, 47:617–644, 1928.
- [68] B.M. Oliver. Efficient coding. *Bell System Technical J.*, pages 724–756, 1952.
- [69] Alan V. Oppenheim and Ronald W. Schaffer. *Discrete-Time Signal Processing*. Prentice Hall, 2010.
- [70] A. Papoulis. Error analysis in sampling theory. *Proceedings of the IEEE*, 54(7):947–955, July 1966.
- [71] A. Papoulis. Generalized sampling expansion. *IEEE Trans. Circuits and Systems*, CAS-24(11):652–654, 1977.
- [72] E. Parzen. A simple proof and some extensions of sampling theorems. *Stanford University, Stanford, CA, Tech. Rep.*, (7), 1956.
- [73] Welch PD. The use of fast fourier transform for the estimation of power spectra: A method based on time averaging over short, modified periodograms. *IEEE Transactions on Audio Electroacoustics*, AU-15:7073, 1967.
- [74] D. P. Petersen and D. Middleton. Sampling and reconstruction of wave number-limited function in n-dimensional euclidean spaces. *Informat. Contr.*, 5:279–323, 1962.
- [75] Z. A. Pirnashvili. On the problem of interpolation of random processes. *Theory Prob. Appl.*, 12:647–657, 1967.
- [76] Lawrence Rabiner and Ronald Schaffer. *Theory and Applications of Digital Speech Processing*. Prentice Hall, 2010.

- [77] J. Selva. Functionally weighted Lagrange interpolation of band-limited signals from nonuniform samples. *Trans. Sig. Proc.*, 57(1), January 2009.
- [78] M. Seo, M. J. W. Rodwell, and U. Madhow. Blind correction of gain and timing mismatches for a two-channel time-interleaved analog-to digital converter. *Proc. 39th Asilomar Conf. Signals, Syst.*, page 11211125, 2005.
- [79] C. E. Shannon. Communications in the presence of noise. *Proc. IRE*, 37:10–21, 1949.
- [80] H. S. Shapiro and R. A. Silverman. Alias-free sampling of random noise. *Journal of the Society for Industrial and Applied Mathematics*, 8(2):225–248, 1960.
- [81] Anekal B. Sripad and Donald L. Snyder. A necessary and sufficient condition for quantization errors to be uniform and white. *IEEE Trans. Acoustics, Speech, and Signal Processing*, ASSP-25(5):442–448, 1977.
- [82] T. Strohmer and J. Tanner. Fast reconstruction methods for bandlimited functions from periodic nonuniform sampling. *SIAM J. Numer. Anal.*, 44(3):1073–1094, 2006.
- [83] T. Strohmer and J. Xu. Fast algorithms for blind calibration in time interleaved analog-to-digital converters. *Proc. IEEE ICASSP*, page 12251228, 2007.
- [84] A. Tarczynski. Fir filters for systems with input clock jitter. *Circuits and Systems, 2001. Iscas2001*, 2:617–620, 2001.
- [85] Nguyen T. Thao and Martin Vetterli. Lower bound on the mean-squared error in oversampled quantization of periodic signals using vector quantization analysis. *IEEE Trans. Information Theory*, 42(2):469–479, 1996.
- [86] E. C. Titchmarsh. *The Theory of Functions*. Oxford University Press, New York, N. Y., 1939.
- [87] B. S. Tsybakov and V. P. Iakovlev. On the accuracy of reconstructing a function with a finite number of terms of kotel’nikov series. *Radio Eng. Electron.*, 4(3):274, 1959.
- [88] Michael Unser. Sampling - 50 years after Shannon. *Proceedings of the IEEE*, 88(4):569–587, April 2000.
- [89] M. Vetterli, J. Kovačević, and V. K. Goyal. *Fourier and Wavelet Signal Processing*. 2011. Release $\alpha 2.0$ available online at <http://FourierAndWavelets.org>.
- [90] C. Vogel. A frequency domain method for blind identification of timing mismatches in time-interleaved ADCs. *Proc. Norchip Conf.*, pages 45–48, 2006.
- [91] P. Weiss. An estimation of the error arising from misapplication of the sampling theorem. *Amer. Math. Soc. Notices*, 10:351, 1963.
- [92] E. T. Whittaker. On the functions which are represented by the expansion of interpolating theory. *Proc. Roy. Soc. Edinburgh*, 35:181–194, 1915.

- [93] J. M. Whittaker. The fourier theory of the cardinal functions. *Proc. Math. Soc. Edinburgh*, 1:169–176, 1929.
- [94] J. M. Whittaker. *Interpolatory Function Theory*. Number 33. Cambridge, U.K.: Cambridge Univ. Press (Cambridge Tracts in Mathematics and Mathematical Physics), 1935.
- [95] Bernard Widrow, Istvan Kollar, and Ming Chang Liu. Statistical theory of quantization. *IEEE Trans. Instrumentation and Measurement*, 45(2):353–361, 1996.
- [96] Bernard Widrow and Istvn Kollr. *Quantization Noise: Roundoff Error in Digital Computation, Signal Processing, Control, and Communications*. Cambridge University Press, 2008.
- [97] Max A. Woodbury. Inverting modified matrices. *Memorandum Rept. 42, Statistical Research Group, Princeton University, Princeton, NJ*, 1950.
- [98] Kung Yao and John B. Thomas. On some stability and interpolatory properties of nonuniform sampling expansions. *IEEE Trans. Circuit Theory*, CT-14(4):404–408, 1967.
- [99] Kung Yao and John B. Thomas. On a class of nonuniform sampling representation. *Symp. Signal Trans. Processing*, pages 69–75, 1968.
- [100] J. L. Yen. On nonuniform sampling of bandwidth-limited signals. *IRE Trans. Circuit Theory*, 3(4):251–257, 1956.
- [101] M. Zakai. Band-limited functions and the sampling theorem. *Inform. Contr.*, 8:143–158, 1965.
- [102] Ahmed I. Zayed. *Advances in Shannon’s Sampling Theory*. CRC Press, Inc., 1993.
- [103] Y. Y. Zeevi and E. Shlomot. Nonuniform sampling and antialiasing in image representation. *IEEE Trans. Signal Processing*, 41(3):1223–1236, March 1993.